AD

REPORT NO. RG-TR-72-14

SUBOPTIMAL ESTIMATION OF INERTIAL SYSTEM ERROR STATES USING RADAR AREA CORRELATION AND ALTIMETER POSITION MEASUREMENTS

by

Harold L. Pastrick

6 June 1972

Approved for public release; distribution unlimited

U.S. ARMY MISSILE COMMAND
Redstone Arsenal, Alabama

170

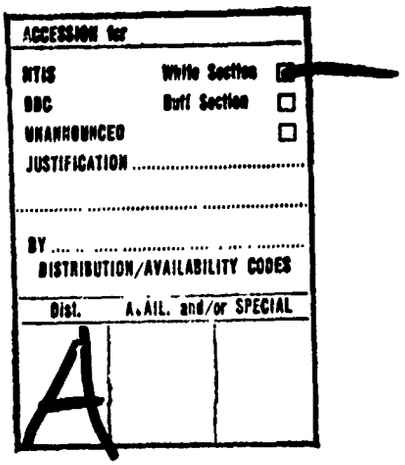

DISPOSITION INSTRUCTIONS

Destroy this report when it is no longer needed. Do not return it to the originator.

DISCLAIMER

The findings in this report are not to be construed as an official Department of the Army position unless so designated by other authorized documents.

UNCLASSIFIED
Security Classification

DOCUMENT CONTROL DATA - R & D

(Security classification of title, body of abstract and indexing annotation must be entered when the overall report is classified)

1. ORIGINATING ACTIVITY (Corporate author) Guidance and Control Directorate Directorate for Res, Dev, Eng and Msl Sys Lab U.S. Army Missile Command, Redstone Arsenal, Ala. 35809	2a. REPORT SECURITY CLASSIFICATION Unclassified 2b. GROUP

3. REPORT TITLE

SUBOPTIMAL ESTIMATION OF INERTIAL SYSTEM ERROR STATES USING RADAR AREA CORRELATION AND ALTIMETER POSITION MEASUREMENTS

4. DESCRIPTIVE NOTES (Type of report and inclusive dates)

5. AUTHOR(S) (First name, middle initial, last name)

Harold L. Pastrick

6. REPORT DATE 6 June 1972	7a. TOTAL NO. OF PAGES 171	7b. NO. OF REFS 27
8a. CONTRACT OR GRANT NO. b. PROJECT NO. (DA) 1X263306.D073 c. AMC Management Structure Code No. 5913.21.20100 d.	9a. ORIGINATOR'S REPORT NUMBER(S) RG-TR-72-14 9b. OTHER REPORT NO(S) (Any other numbers that may be assigned this report) AD_____	

10. DISTRIBUTION STATEMENT

Approved for public release, distribution unlimited

11. SUPPLEMENTARY NOTES	12. SPONSORING MILITARY ACTIVITY Same as No. 1

13. ABSTRACT

This research describes one of several alternatives being explored to establish advanced guidance techniques for the Army's long range tactical missile, the PERSHING. The analysis is given for estimating the inertial measurement unit's error states in an aided terminal guidance mode. Position observations measured by a radar area correlation system and a radar altimeter are processed in an extended Kalman filter to yield the suboptimal estimates of the inertial measurement unit's errors.

The dynamics of the inertial system are modeled in four coordinate systems to allow the choice of the least complex mechanization. To minimize on-board computer requirements, an analysis of the filter's performance is made by comparing the optimal filter gains with a filter formulated with fixed gains chosen a posteriori from those computed optimally.

Several variations of the problem are simulated. The observations are modeled as discrete time measurements obtained once per second and then once every two seconds in the terminal guidance phase of the flight. Also, conditions are varied to simulate optimistic as well as realistic radar imagery processing time and its effect on the accuracy of the filter.

Results indicating filter error and root mean square values of the state estimates obtained in a Monte Carlo computer simulation are shown graphically to validate the conclusions.

DD FORM 1 NOV 68 1473 REPLACES DD FORM 1473, 1 JAN 64, WHICH IS OBSOLETE FOR ARMY USE.

UNCLASSIFIED
Security Classification

14. KEY WORDS	LINK A		LINK B		LINK C	
	ROLE	WT	ROLE	WT	ROLE	WT
PERSHING						
Advanced guidance techniques						
Inertial measurement unit's errors						
Mathematical modeling						
Computer simulation						

6 June 1972

Report No. RG-TR-72-14

SUBOPTIMAL ESTIMATION OF INERTIAL SYSTEM ERROR STATES USING RADAR AREA CORRELATION AND ALTIMETER POSITION MEASUREMENTS

by

Harold L. Pastrick

DA Project No. 1X263306D073
AMC Management Structure Code No. 5913.21.20100

Guidance and Control Directorate
Directorate for Research, Development, Engineering
and Missile Systems Laboratory
U.S. Army Missile Command
Redstone Arsenal, Alabama 35809

ic

ABSTRACT

This research describes one of several alternatives being explored to establish advanced guidance techniques for the Army's long range tactical missile, the PERSHING. The analysis is given for estimating the inertial measurement unit's error states in an aided terminal guidance mode. Position observations measured by a radar area correlation system and a radar altimeter are processed in an extended Kalman filter to yield the suboptimal estimates of the inertial measurement unit's errors.

The dynamics of the inertial system are modeled in four coordinate systems to allow the choice of the least complex mechanization. To minimize on-board computer requirements, an analysis of the filter's performance is made by comparing the optimal filter gains with a filter formulated with fixed gains chosen a posteriori from those computed optimally.

Several variations of the problem are simulated. The observations are modeled as discrete time measurements obtained once per second and then once every two seconds in the terminal guidance phase of the flight. Also, conditions are varied to simulate optimistic as well as realistic radar imagery processing time and its effect on the accuracy of the filter.

Results indicating filter error and root mean square values of the state estimates obtained in a Monte Carlo computer simulation are shown graphically to validate the conclusions.

ACKNOWLEDGMENT

This research was performed while the author attended Stanford University under the sponsorship of the Army Missile Command's Graduate Long Term Training Program. Grateful acknowledgment is made to Jess B. Huff, Director of the Guidance and Control Directorate, who stimulated the desire for the knowledge obtainable in a graduate engineering curriculum and who with Dr. John L. McDaniel, Director of Research, Development, Engineering and Missile Systems Laboratory, provided the opportunity and support to bring it to fruition.

The author is indebted to his advisor, Professor Daniel B. DeBra, for guiding and critizing this research, for supplying his intuitive skills in bringing classroom theory to real world application, and most of all for genuinely being concerned about the well being of his student and advisee. He acknowledges the contribution of Professor Bejamin O. Lange who, through his teaching, developed the foundation for much of the theory displayed in this manuscript. He also extends appreciation to Dr. W. Earl Hall, Jr., Dr. Paul G. Kaminski, Carl Granstrom, Donald Reed, Michael Tashker, and other classmates and associates at Stanford University who contributed suggestions and assistance.

Finally, he expresses profound gratitude to his wife, Vivienne, whose contributions to this research and to the success of his graduate studies were made through her continuing encouragement, patience, understanding, and devotion.

TABLE OF CONTENTS

TABLE OF CONTENTS (Cont)

TABLE OF CONTENTS (Cont)

FIGURES

TABLE OF CONTENTS (Cont)

FIGURES

TABLE OF CONTENTS (Cont)

FIGURES

TABLE OF CONTENTS (Cont)

FIGURES

TABLE OF CONTENTS (Cont)

FIGURES

TABLES

CHAPTER I. INTRODUCTION

1.1 BACKGROUND

Studies are being conducted by various elements of the U.S. Army Missile Command and teams of radar and guidance contractors to establish advanced guidance and reentry techniques for the Army's tactical ballistic missile, the PERSHING. These wide ranging studies are considering the feasibility of modifying the reentry body configuration and guidance trajectories, updating the inertial sensors, digitizing the control system, changing the vehicle's aerodynamic characteristics, and augmenting the guidance system. The objective of these studies and follow-up development work is to improve the missile's basic figure of merit which is the target miss distance at impact.

This report summarizes a study of only one of those alternatives, in particular, the analysis and simulation is performed for an inertial guidance system augmented by a radar area correlation device. Aiding an inertial measurement unit (IMU) with position and velocity measuring devices is not a new idea. The literature abounds with techniques and methods of maintaining inertial equipment within acceptable error bounds. Papers by Broxmeyer [1], Duncan [2], Dworetsky and Edwards [3], and Friedman [4] are only a few which are representative of the early work in this area. However, the use of additional external measurements, optimal in a sense, is much more recent and has never been applied to the PERSHING.

1.2 PREVIOUS INVESTIGATIONS

Of the many attempts to improve inertial system performance by using external information, one of the earliest was that of damping the 84-minute and 24-hour natural periods of the vertical and gyrocompass heading loops, respectively. The primary purpose of damping the inertial system was to reduce the amplitude of the oscillations caused by offsets and gyro drifts, or at worst, to reduce the oscillations to a fixed constant value. Attention was focused on various damping configurations or equalizers which led to concepts such as second-order (velocity) and third-order (acceleration) tuning [3]. The need for an external source in damping the IMU was apparent when it was observed that errors caused by vehicle motion would result if only information from the inertial system were used [5]. However, if external speed information was properly introduced into the inertial system, there would be no error caused by the vehicular induced motion provided that the external information which was used matched the inertially derived information in accuracy.

Another way of using external information to obviate inertial errors was found not in the literature but in practice. In that method external measurements were used directly to update the inertial system rather than implement a damping scheme. Inertial system position indication was changed to agree with the results of a position fix and inertial system velocity indication was changed to agree with the results of a velocity measurement update. Although it may have been expedient, this approach ignored the fact that the inertial

system errors were primarily caused by random time varying inertial sensor errors and that the external measurements also contained random errors which may have been significant compared to the inertial system errors.

The use, by practicing navigators, of measurement updates in this manner, however, led systems designers to consider more viable alternatives in using the external fix information when it became available. Consequently, within the framework of inertial systems analysis, the problem evolved of finding the optimal estimate of the system error (a random variable) when a linear function of that variable was corrupted by additive noise.

The earliest published study of this class of problems (1809) was Gauss's Theoria Motes Corporum Coelestium in which astronomical parameters were estimated. Legendre independently invented the method of least squares estimation and published it in 1806. (According to Sorenson [6], Gauss claimed to have invented the method of least squares in 1795 but did not publish it until 1809.) R. A. Fisher introduced the maximum likelihood method in 1912. In 1942, Kolomogorov and Weiner independently developed a linear minimum mean-square estimation technique. The key result of these studies was an integral equation called the Weiner-Hopf equation in the U.S. The solution of this equation was a weighting function which, when convolved with the corrupted linear measurement, produced the unbiased minimum variance estimate of the random signal. The application was limited initially to statistically stationary processes and provided optimum estimates

only in the steady state. Kolomogorov and Weiner's work was expanded during the next 20 years to include discrete, nonstationary, and multi-port systems, but in a way which required cumbersome calculations. In the 1950's, the idea of generating least-squares estimates recursively was introduced by several investigators: Carlton and Follin; Swerling; Blum, Robbins, and Mundo; and Kiefer and Wolfowitz, all noted in Sorensen's paper [6]. Kalman [7] (1960) and Kalman and Bucy [8] (1961) generalized the results of Weiner and Kolomogorov to nonstationary random processes and developed the problem based on a state-space and time-domain formulation. The recursive nature of the filter developed by Kalman made it ideally suitable for solutions on the digital computer.

Since then, there has been a veritable explosion of investigations applying the estimation technique, commonly called the Kalman filter, to a host of aerospace oriented problems. The study by Gelb and Sutherland [9] alone lists over 40 such references. Yet, in all of this literature, there was interestingly enough no unclassified reference to the particular optimal combination of systems described in this report, i.e., radar area correlation and inertial guidance systems.

1.3 PROBLEM MOTIVATION

In this application, the IMU on the PERSHING must perform two functions: (1) provide data to allow the missile to be guided during boost accurately enough to reach a terminal acquisition basket during reentry and (2) provide the attitude reference for the terminal

guidance device. Prior to the terminal guidance phase, the reentry body follows a ballistic trajectory determined by the launch-phase guidance system. At a particular altitude, in the case of PERSHING 30,000 feet, the reentry body must be in a specified position if the terminal guidance scheme is to be of any value. Without terminal guidance the reentry body would continue on its ballistic path into impact with a miss distance representing the accumulation of all errors of the launch phase, mid-course phase, and terminal phase of the flight. This covers the entire range of possible error sources including atmospheric perturbations on the intended trajectory, errors in the guidance and propulsion systems, false targeting, etc. To minimize the effects of these errors and consequently the miss distance, use of a radar area correlation terminal guidance system will be studied.

The map-matching function, as it is sometimes known, is to determine the difference between the desired position and actual position of the vehicle at various altitudes by use of radar correlation detectors. Knowledge of position error is sufficient to determine the necessary trajectory correction because the velocity vector of the reentry body, within certain bounds, is precisely known (as determined by the IMU). To obtain the position error, an image of an area near or ideally including the target, is obtained at a specified altitude using a side-looking airborne radar. This area is mapped by a beam scan. The radar image obrained is compared with previously stored reference imagery to determine the position error. To accomplish this objective, in the

presence of errors in the image formation and radar noise, the images are matched for that displacement which results in the highest correlation between radar and reference:

Conceptually, this external data could be used to update the inertial system because the position and velocity indicated by the IMU would be in error. Unfortunately, these data are too imperfect to be used directly because of measurement errors and other effects such as intensity quantizing errors, scale factor errors, resolution effects, etc. Thus the discussion returns to the general class of problems described earlier, i.e., given measurements Z_1, Z_2, ...Z_n, determine the best estimate of the states X_1, X_2, ...X_n. With certain restrictions, criteria that define the optimal state estimate introduce the formulation commonly referred to as the Kalman filter.

1.4 PROBLEM STATEMENT

The problem is to optimally estimate the inertial guidance system errors using the position measurements obtained from a radar area correlation system and a radar altimeter during the terminal phase of the PERSHING missile flight and to consider suboptimal mechanizations which would simplify the hardware.

1.5 OBJECTIVES

There are several objectives to be fulfilled in the course of seeking a solution to the problem. Representation or modeling of the inertial system will require a decision on the mechanization to be used, i.e., wandering azimuth, local level north-east, tangent plane or space-fixed tangent plane mechanizations.

There is time enough in the terminal guidance phase to permit as few as 5 or as many as 15 observations of position. The second objective will be to determine the optimum number of measurement observations to be made by the radar system and their spatial timing.

It is conceivable that an on-board digital computer will be utilized to do a variety of command and control tasks. To simplify its computational burden, the third objective will be to discard systematically error variables from the complete mathematical model for a minimum Kalman filter mechanization.

The optimal gains applied to the updating of the state variable estimate are typically time varying. The fourth objective, consistent with reducing the computation burden, will be to determine the extent fixed gains or other simplifications such as programmed gains can be utilized in the model.

The fifth objective is to define a set of specifications on the IMU and radar systems suitable for real world system synthesis.

CHAPTER II. DYNAMICS OF THE INERTIAL SYSTEM

2.1 GENERAL

Detailed descriptions of inertial sensors and systems are available in standard texts by O'Donnell [10], Pitman [11], and Fernandez and Macomber [12]. It is assumed that the reader is generally knowledgeable with their works. For completeness however, the following paragraph summarizes the essentials.

The inertial guidance system consists of sensors that measure specific force (the accelerometers) and sensors that measure angular motion in a coordinate system fixed in the IMU (the gyros). The gimballed platform, shown schematically in Fig. 2.1. is typical of those that have been used on the PERSHING. It permits isolation of the instruments from the angular motion of the vehicle by using the gyros as sensors of orientation change. Through gimbal servos, the platform is returned to its proper attitude permitting the accelerometers to measure changes in specific force. To obtain velocity, position, and attitude information from the instruments and the platform, sets of equations are mechanized in the computer. Additionally, the mechanization equations provide the information for torques needed to precess the gyros.

In the sections which follow, mechanization equations will first be developed in ideal invariant vector form. Because system-state

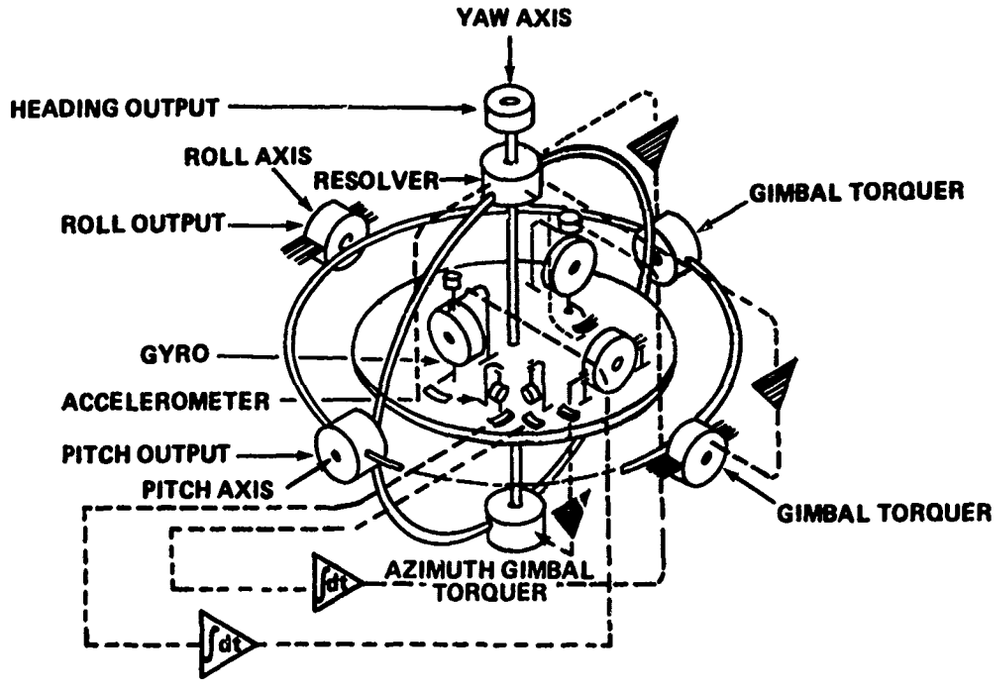

FIG. 2.1. SCHEMATIC DIAGRAM OF A THREE GIMBALLED INERTIAL GUIDANCE SYSTEM'S IMU

variables are sought for use in the estimation problem, inertial system error equations will be developed as well as a comment on their applicability in the problem.

2.2 INVARIANT VECTOR FORMULATION OF THE IMU MECHANIZATION EQUATIONS

It is meaningful at this point to briefly explain the differences among the various coordinate bases which will be used in the development and indicate why one may be preferred over the other. In deriving the ideal mechanization equations in text (and the error equations in the appendices), the following bases are important:

(I) - The inertial basis defined as fixed in "space" and nonmoving

(E) - The earth fixed basis which rotates with respect to the inertial basis at earth's angular velocity

(L) - The local basis defined by the true position on the earth

(C) - The computer basis defined to be the same as the local basis except it also is defined by the indicated position

(P) - The platform basis defined as equal to the computer basis but rotated from it by some small angle.

It is desirable to derive the equations in the local basis because navigation is done in the basis which is defined by the true position of the vehicle on the earth. In the historical development of the art of dead reckoning navigation, the local level or "plumb bob" level (described later) was the most easily realizable vertical. Thus the local basis, in many cases, tends to be similary mechanized, i.e., locally level. That practice will be followed in the sequel.

The computer basis, used in the development of the error equations, is the basis in which the navigation variables are computed and output. Thus, this is the basis in which indicated position is given. It is also convenient to think of it as the realizable mechanization of the local basis.

The platform basis, used in the error equations, is the basis in which the inertial instruments are considered fixed. It is in error with the computer basis in an amount contributed by the gyro and accelerometer instrument errors as well as several other error sources.

These bases are shown in Fig. 2.2 which defines their relative orientations. The mass center of the earth, represented by O, is also the center of the inertially fixed basis, $\vec{X}_I$, $\vec{Y}_I$, $\vec{Z}_I$. The subscripts E and L refer to unit vectors fixed in the rotating earth's basis and local basis, respectively*.

*J. R. Streeter discusses using the center of the earth rather than the sun as the origin of coordinates fixed in inertial space in O'Donnell's book [10].

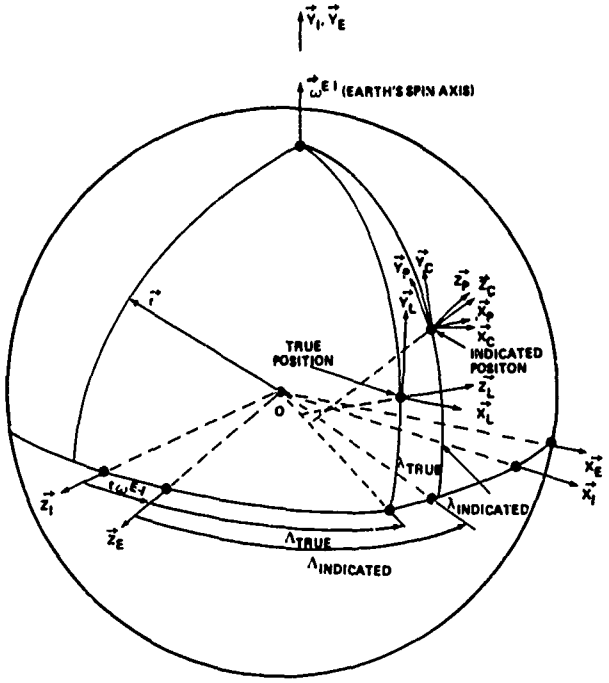

FIG. 2.2. COORDINATE SYSTEM ORIENTATIONS

The following notations are in the development which follow:

$\vec{r} \triangleq$ vector expressing position from earth's center of mass to the vehicle

$\left.\frac{d(\vec{r})}{dt}\right|_E \triangleq \overset{E}{\vec{r}} \triangleq$ vector expressing velocity of vehicle with respect to earth fixed basis

$\left.\frac{d(\vec{r})}{dt}\right|_I \triangleq \overset{I}{\vec{r}} \triangleq$ vector expressing velocity of vehicle with respect to an inertially fixed basis which is nominally time invariant

$\left.\frac{d(\vec{r})}{dt}\right|_L \triangleq \overset{L}{\vec{r}} \triangleq$ vector expressing velocity of vehicle with respect to a local basis.

Also let

$$\vec{V} \triangleq \overset{E}{\vec{r}}$$

and

$$\vec{U} \triangleq \overset{I}{\vec{r}} = \vec{V} + \vec{\omega}^{E-I} \times \vec{r} \quad .$$

By the Coriolis law,

$$\overset{L}{\vec{r}} = \overset{E}{\vec{r}} + \vec{\omega}^{E-L} \times \vec{r}$$

$$= \vec{V} + \vec{\omega}^{E-L} \times \vec{r} \quad . \tag{2.1}$$

Also,

$$\overset{I}{\vec{r}} = \overset{E}{\vec{r}} + \vec{\omega}^{E-I} \times \vec{r}$$

$$= V + \omega^{E-I} \times \vec{r} \quad . \tag{2.2}$$

The specific force meter (SFM), as described by Markey and Hovorka [13], can be idealized as follows:

$$\overset{II}{\vec{r}} = \vec{f} + \vec{G} \quad , \tag{2.3}$$

where

$\vec{f} \triangleq$ specific force

$\vec{G} \triangleq$ gravitational field intensity vector at the center of mass of the SFM mass element

$\overset{II}{\vec{r}} = \left.\dfrac{d^2(r)}{dt}\right|_I \triangleq$ vector expressing the acceleration of the specific force meter's case with respect to the inertial basis.

The left side of Eq. (2.3) is given as

$$\overset{II}{\vec{r}} = \overset{I}{\vec{U}} \quad , \tag{2.4}$$

Substituting Eq. (2.2) into Eq. (2.3) and noting $\vec{\omega}^{E-I}$, the earth's spin rate, is a constant for practical purposes,

$$\vec{f} + \vec{G} = \frac{d^I}{dt}\left(\vec{V} + \vec{\omega}^{E\text{-}I} \times \vec{r}\right)$$

$$= \overset{I\cdot}{\vec{V}} + \vec{\omega}^{E\text{-}I} \times \overset{I}{\vec{r}}$$

$$= \overset{I}{\vec{V}} + \vec{\omega}^{E\text{-}I} \times \vec{u}$$

$$= \overset{L}{\vec{V}} + \vec{\omega}^{L\text{-}I} \times \vec{V} + \vec{\omega}^{E\text{-}I} \times \vec{u} \qquad (2.5)$$

Substituting Eq. (2.2) into Eq. (2.5) for $\vec{u}$ gives

$$\vec{f} + \vec{G} = \overset{L}{\vec{V}} + \vec{\omega}^{L\text{-}I} \times \vec{V} + \vec{\omega}^{E\text{-}I} \times \left(\vec{V} + \vec{\omega}^{E\text{-}I} \times \vec{r}\right) \quad . \qquad (2.6)$$

Combining and rearranging yields

$$\overset{L}{\vec{V}} = \vec{f} + \vec{G} - \left(\vec{\omega}^{E\text{-}I} + \vec{\omega}^{L\text{-}I}\right) \times \vec{V} - \vec{\omega}^{E\text{-}I} \times \left(\vec{\omega}^{E\text{-}I} \times \vec{r}\right) \quad , \qquad (2.7)$$

where the gravity field intensity vector can now be defined as

$$\vec{g} \triangleq \vec{G} - \vec{\omega}^{E\text{-}I} \times \left(\vec{\omega}^{E\text{-}I} \times \vec{r}\right) \quad .$$

This is the vector which is the vector sum of the gravitational field intensity vector and the centrifugal acceleration vector caused by the earth's rotation relative to an inertial basis. More commonly, it is the apparent specific force caused by gravity which acts along a plumb

bob suspended to the point considered (Fig. 2.3). This is an important consideration because most of the tactical maps in use today are based on the concept of a local, plumb bob level. Even though more and more use is made of cartographic satellites which map earth's imagery relative to the $\vec{G}$ gravity, the former is still more commonly used by the Army. Thus, Eq. (2.7) simplifies to the following ideal invariant vector form:

$$\boxed{\overset{L}{\vec{V}} = \vec{f} + \vec{g} - \left(\vec{\omega}^{E-I} + \vec{\omega}^{L-I}\right) \times \vec{V}} \tag{2.8a}$$

Rewriting Eq. (2.1) for completeness,

$$\boxed{\overset{L}{\vec{r}} = \vec{V} + \vec{\omega}^{E-L} \times \vec{r}} \tag{2.8b}$$

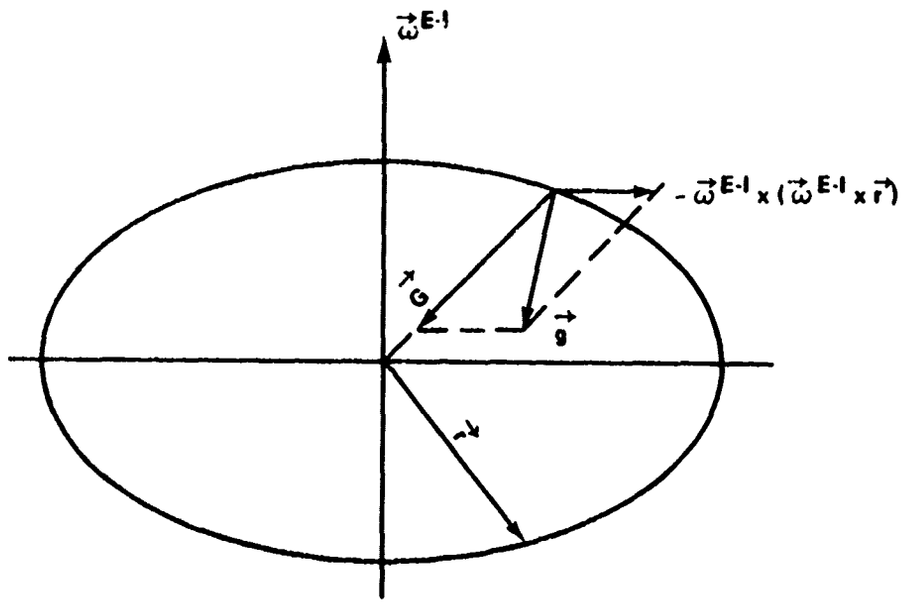

FIG. 2.3. GEOCENTRIC AND MASS ATTRACTION PARAMETERS

Equations (2.8a) and (2.8b) are the ideal position state equations in convenient form for hardware implementation. The left side of Eq. (2.8a) is the derivative of velocity relative to a local basis oriented near the earth's surface. The term $\vec{f}$, the specific force, is provided directly by the accelerometers, and the last two terms are calculated from knowledge of position and the angular velocity of the local basis which are instrumented and computed on-board the vehicle. It remains to choose the local basis for coordinatizing Eq. (2.8a) explicitly. Several are common, including the wander azimuth, local level north-east, tangent plane, space-fixed tangent plane, free azimuth, latitude longitude, and relocated pole latitude longitude. These various mechanizations differ basically in the way the vector $\vec{\omega}^{L-I}$ is prescribed.

For purposes of this study, the free azimuth, the tangent plane, the space-fixed tangent plane, and the local level north-east mechanizations will be investigated.

2.3 THE IMU ERROR EQUATIONS

Ideally, Eq. (2.8a) may be implemented in any of the coordinate systems previously mentioned. Realistically however, it is impossible to instrument the equations without errors because of such factors as gyro drift, erroneous gyro and accelerometer scale factors, accelerometer bias, etc. Consequently for reasons that will be discussed later, the ideal equations will not be used in the filter. Instead, standard perturbation techniques will be applied so that the effects of the

errors on the navigation computations can be determined. The inertial system errors are estimated in the filter and not the states of the vehicle nor of the navigation problem directly.

The inertial system errors are described by the following error vector differential equations:

$$\overset{L}{\vec{\psi}} = -\vec{\omega}^{L-I} \times \vec{\psi} + \vec{\vec{K}}_g \cdot \vec{\omega}^{L-I} + \vec{\epsilon} \quad \text{(platform error)} \qquad (2.9)$$

and

$$\overset{II}{\delta\vec{r}} + \omega_s^2 \left(\vec{\vec{1}} - 3\, \hat{r}\hat{r} \right) \cdot \delta\vec{r} = \vec{\vec{K}}_f \cdot \vec{f} + \vec{b} - \vec{\psi} \times \vec{f} \quad \text{(position error)} \qquad (2.10)$$

where

$\vec{\psi}$ $\triangleq$ vector representing the small angular misalignment between a basis fixed in the computer and a basis fixed in the platform (Fig. 2.4)

ω_s $\triangleq$ Schuler angular frequency given by $\sqrt{K/r^3}$

$\vec{\vec{K}}_g$ $\triangleq$ tensor representing the gyro scale factor errors on the principal diagonal and misalignments on the off-diagonal

$\vec{\vec{K}}_f$ $\triangleq$ tensor representing the SFM scale factor errors on the principal diagonal and misalignments on the off-diagonal

$\vec{\epsilon}$ $\triangleq$ vector representing gyro-drift rate as an error

$\vec{b}$ $\triangleq$ vector representing SFM bias as an error

$\hat{r}\hat{r}$ $\triangleq$ dyad of unit vectors in the $\vec{r}$ direction.

Equations (2.9) and (2.10) are derived in Appendix A in a manner following that of Lange [14]. It differs from derivations shown in the standard texts mentioned earlier.

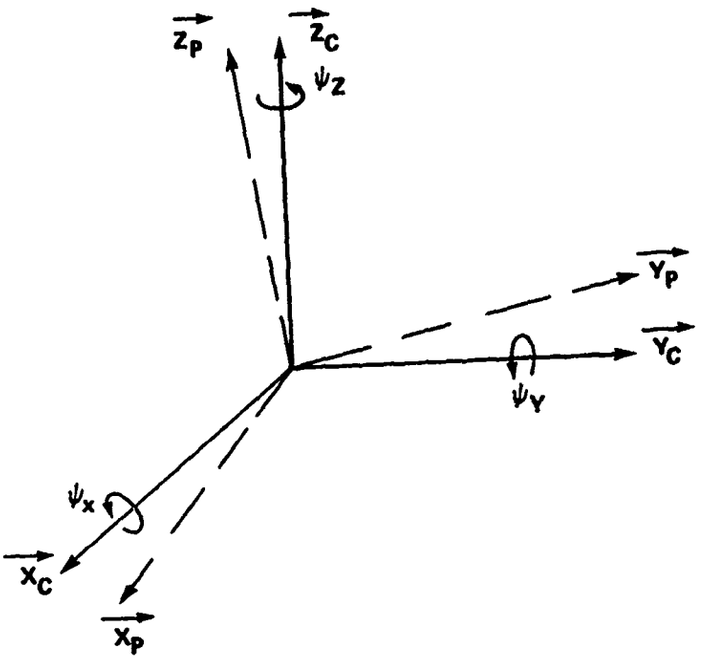

FIG. 2.4. EULER ANGLE ROTATIONS OF PLATFORM ERROR ANGLES, $\vec{\psi}$

Expanding Eq. (2.10) by the Coriolis Law yields

$$\overset{I}{\vec{\delta r}} = \overset{L}{\vec{\delta r}} + \vec{\omega}^{L-I} \times \vec{\delta r} \tag{2.11}$$

and

$$\overset{II}{\vec{\delta r}} = \overset{LL}{\vec{\delta r}} + \vec{\omega}^{L-I} \times \overset{L}{\vec{\delta r}} + \overset{L}{\vec{\omega}}^{L-I} \times \vec{\delta r}$$

$$+ \vec{\omega}^{L-I} \times \left(\overset{L}{\vec{\delta r}} + \vec{\omega}^{L-I} \times \vec{\delta r} \right) . \tag{2.12}$$

Substituting Eq. (2.12) into Eq. (2.10) for $\overset{II}{\vec{\delta r}}$ gives

$$\overset{LL}{\vec{\delta r}} = -2\vec{\omega}^{L-I} \times \overset{L}{\vec{\delta r}} - \overset{L}{\vec{\omega}}^{L-I} \times \vec{\delta r} - \vec{\omega}^{L-I} \times \left(\vec{\omega}^{L-I} \times \vec{\delta r} \right)$$

$$- \omega_s^2 \left[\vec{\vec{1}} - 3 \hat{r} \hat{r} \right] \cdot \vec{\delta r} + \vec{\vec{K}}_f \cdot \vec{f} + \vec{b} - \vec{\psi}^{P-C} \times \vec{f} \quad . \tag{2.13}$$

The results shown in Eqs. (2.9) and (2.13) are important. They imply that if $\vec{\psi}$ is used as a basic characterization of platform angles, a differential equation exists for $\vec{\psi}$ which is independent of position errors. Thus, the decoupled $\vec{\psi}$ equation, Eq. (2.9), can be solved independently and the result used as driving variables in the position error equation, Eq. (2.13).

Now coordinatize the two sets of equations into a local basis (L-basis). Beginning with Eq. (2.9) and noting vector and dyadic operators,

$$\dot{\underset{L}{\psi}} = \begin{bmatrix} \dot{\psi}_x \\ \dot{\psi}_y \\ \dot{\psi}_z \end{bmatrix} , \tag{2.14}$$

$$\underset{L}{\omega}^{L-I} \times \underset{L}{\psi} = \begin{bmatrix} - & - & - \\ \omega_x & \omega_y & \omega_z \\ \psi_x & \psi_y & \psi_z \end{bmatrix} , \tag{2.15}$$

$$\underset{L}{K_g} = \begin{bmatrix} \Delta K_{g1} & m_{12} & m_{13} \\ m_{21} & \Delta K_{g2} & m_{23} \\ m_{31} & m_{32} & \Delta K_{g3} \end{bmatrix} , \tag{2.16}$$

$$\underset{L}{K_g} \cdot \underset{L}{\omega}^{L-I} = \begin{bmatrix} \Delta K_{g1} & m_{12} & m_{13} \\ m_{21} & \Delta K_{g2} & m_{23} \\ m_{31} & m_{32} & \Delta K_{g3} \end{bmatrix} \begin{bmatrix} \omega_x \\ \omega_y \\ \omega_z \end{bmatrix} \tag{2.17}$$

and

$$\underset{L}{\epsilon} = \begin{bmatrix} \epsilon_x \\ \epsilon_y \\ \epsilon_z \end{bmatrix} . \tag{2.18}$$

Thus Eq. (2.9), the platform error angles, coordinatized in the local basis is given by

$$\begin{bmatrix} \dot{\psi}_x \\ \dot{\psi}_y \\ \dot{\psi}_z \end{bmatrix} = - \begin{bmatrix} (\omega_y \psi_z - \omega_z \psi_y) \\ (\omega_z \psi_x - \omega_x \psi_z) \\ (\omega_x \psi_y - \omega_y \psi_x) \end{bmatrix} + \begin{bmatrix} (\Delta K_{g1} \omega_x + m_{12} \omega_y + m_{13} \omega_z) \\ (m_{21} \omega_x + \Delta K_{g2} \omega_y + m_{23} \omega_z) \\ (m_{31} \omega_x + m_{32} \omega_y + \Delta K_{g3} \omega_z) \end{bmatrix} \begin{bmatrix} \epsilon_x \\ \epsilon_y \\ \epsilon_z \end{bmatrix} . \tag{2.19}$$

Coordinatizing Eq. (2.13) in the local basis gives

$$\underset{L}{\delta r} = \begin{bmatrix} \delta x \\ \delta y \\ \delta z \end{bmatrix} , \quad \underset{L}{\delta \dot{r}} = \begin{bmatrix} \delta \dot{x} \\ \delta \dot{y} \\ \delta \dot{z} \end{bmatrix} , \quad \underset{L}{\delta \ddot{r}} = \begin{bmatrix} \delta \ddot{x} \\ \delta \ddot{y} \\ \delta \ddot{z} \end{bmatrix} , \tag{2.20}$$

$$\underset{L}{\omega}^{L-I} \times \underset{L}{\delta \dot{r}} = \begin{bmatrix} - & - & - \\ \omega_x & \omega_y & \omega_z \\ \delta \dot{x} & \delta \dot{y} & \delta \dot{z} \end{bmatrix} , \tag{2.21}$$

$$\underset{L}{\omega}^{L-I} \times \left(\underset{L}{\omega}^{L-I} \times \underset{L}{\delta r} \right) = \begin{bmatrix} - & - & - \\ \omega_x & \omega_y & \omega_z \\ \omega_y \delta z - \omega_z \delta y & \omega_z \delta x - \omega_x \delta z & \omega_x \delta y - \omega_y \delta x \end{bmatrix} , \tag{2.22}$$

$$\left[\underset{L}{\overset{\rightrightarrows}{1}} - 3\hat{r}\hat{r}\right] \cdot \underset{L}{\delta r} = \left\{\begin{bmatrix}1 & 0 & 0\\ 0 & 1 & 0\\ 0 & 0 & 1\end{bmatrix} - 3\begin{bmatrix}0\\0\\1\end{bmatrix}\begin{bmatrix}0 & 0 & 1\end{bmatrix}\right\}\begin{bmatrix}\delta x\\ \delta y\\ \delta z\end{bmatrix}, \quad (2.23)$$

$$\underset{L}{b} = \begin{bmatrix}b_x\\ b_y\\ b_z\end{bmatrix}, \quad (2.24)$$

and

$$\underset{L}{\psi} \times \underset{L}{f} = \begin{bmatrix}- & - & -\\ \psi_x & \psi_y & \psi_z\\ f_x & f_y & f_z\end{bmatrix} . \quad (2.25)$$

Carrying out the indicated operations and substituting into Eq. (2.13) yields the following position error equations coordinatized in the L-basis:

$$\begin{bmatrix}\ddot{\delta x}\\ \ddot{\delta y}\\ \ddot{\delta z}\end{bmatrix} = -2\begin{bmatrix}\left(\omega_y\dot{\delta z} - \omega_z\dot{\delta y}\right)\\ \left(\omega_z\dot{\delta x} - \omega_x\dot{\delta z}\right)\\ \left(\omega_x\dot{\delta y} - \omega_y\dot{\delta x}\right)\end{bmatrix} - \begin{bmatrix}\left(\dot{\omega}_y\delta z - \dot{\omega}_z\delta y\right)\\ \left(\dot{\omega}_z\delta x - \dot{\omega}_x\delta z\right)\\ \left(\dot{\omega}_x\delta y - \dot{\omega}_y\delta x\right)\end{bmatrix}$$

$$- \begin{bmatrix}\left(-\left(\omega_y^2 + \omega_z^2\right)\delta x + \omega_x\omega_y\delta y + \omega_x\omega_z\delta z\right)\\ \left(-\left(\omega_x^2 + \omega_z^2\right)\delta y + \omega_y\omega_z\delta z + \omega_x\omega_y\delta x\right)\\ \left(\omega_x\omega_z\delta x + \omega_y\omega_z\delta y - \left(\omega_x^2 + \omega_y^2\right)\delta z\right)\end{bmatrix}$$

$$
- \omega_s^2 \begin{bmatrix} \delta x \\ \delta y \\ -2\delta z \end{bmatrix} + \begin{bmatrix} \left(\Delta K_{f1} f_x + m_{12} f_y + m_{13} f_z\right) \\ \left(m_{21} f_x + \Delta K_{f2} f_y + m_{23} f_z\right) \\ \left(m_{31} f_x + m_{32} f_y + \Delta K_{f3} f_z\right) \end{bmatrix}
$$

$$
+ \begin{bmatrix} b_x \\ b_y \\ b_z \end{bmatrix} - \begin{bmatrix} \psi_y f_z - \psi_z f_y \\ \psi_z f_x - \psi_x f_z \\ \psi_x f_y - \psi_y f_x \end{bmatrix} \quad . \tag{2.26}
$$

2.4 THE SCALAR FORM OF THE TORQUING EQUATIONS

2.4.1 Coordinatization of Vector $\vec{\omega}$ in the Tangent Plane Mechanization

The IMU equations of error angle between the platform and computer, Eq. (2.19), and the position error, Eq. (2.26) can be made more explicit through one more expansion on the vector $\vec{\omega}$. Recall, that $\vec{\omega}$ is the angular rate at which the platform is torqued or rotated, relative to inertial space, about its nominal X, Y, and Z axes. Regarding the local basis, L, as the true or computer basis, C, (the basis in which the computations are performed to update velocity, position and angular velocity terms) the vector $\vec{\omega}$ can be coordinatized in any of the bases previously mentioned. If the tangent plane mechanization is chosen, the platform angular rates are constant rather than time varying as in all of the others. Thus, the platform is held fixed relative to the fixed point on the earth, regardless of the vehicle position. Fig. 2.5 displays the geometry and shows the tangent plane

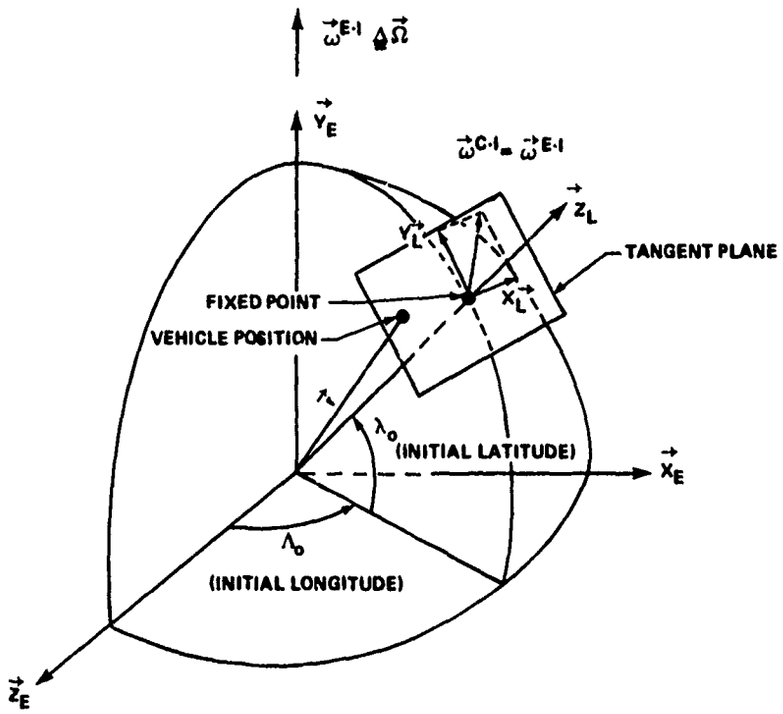

FIG. 2.5. TANGENT PLANE MECHANIZATION GEOMETRY

eminating from the fixed point passing through the launch site. By inspection, the components of the gyro torquing signals $\omega_C^{C\text{-}I}$ in the computer basis are given by

$$\omega_C^{C\text{-}I} = \begin{bmatrix} \omega_x \\ \omega_y \\ \omega_z \end{bmatrix} = \begin{bmatrix} 0 \\ \Omega \cos \lambda_o \\ \Omega \sin \lambda_o \end{bmatrix} \quad . \tag{2.27}$$

The following analysis is performed as a check. The coordinatization begins with

$$\omega_C^{C\text{-}I} = \omega_C^{C\text{-}E} + \omega_C^{E\text{-}I} \quad . \tag{2.28}$$

To keep the requirement that only constant gyro torques are mechanized,

$$\underset{C}{\omega}^{C-E} = 0 \quad . \tag{2.29}$$

Now $\vec{\omega}^{E-I}$ is best coordinatized in the earth's fixed basis in which it is known and nominally constant, i.e.,

$$\underset{E}{\omega}^{E-I} = \begin{bmatrix} 0 \\ \Omega \\ 0 \end{bmatrix} \quad . \tag{2.30}$$

Thus, to express Eq. (2.28) in the common basis given, a transformation is required on Eq. (2.30),

$$\underset{C}{\omega}^{E-I} = T_{C/E} \underset{E}{\omega}^{E-I} \quad , \tag{2.31}$$

where $T_{C/E}$ is defined as the direction cosine matrix representing the coordinate transformation from the earth's basis (E) to the computer's basis (C).

The summary of the transformation is shown in Table 2.1.

Table 2.1

TRANSFORMATION SUMMARY

Transformation	Angle of Rotation	Axis of Rotation	Basis Name
$T_{C/E}$			Earth
	Λ_o	$\vec{Y}_E$	E'
	λ_o	$-\vec{X}_e$	Computer

This results in the following:

$$T_{C/E} = \begin{bmatrix} 1 & 0 & 0 \\ 0 & \cos\lambda_o & -\sin\lambda_o \\ 0 & \sin\lambda_o & \cos\lambda_o \end{bmatrix} \begin{bmatrix} \cos\Lambda_o & 0 & -\sin\Lambda_o \\ 0 & 1 & 0 \\ \sin\Lambda_o & 0 & \cos\Lambda_o \end{bmatrix}, \quad (2.32)$$

because

$$\omega_C^{C-I} = \begin{bmatrix} \omega_x \\ \omega_y \\ w_z \end{bmatrix}, \quad (2.33)$$

then

$$\begin{bmatrix} \omega_x \\ \omega_y \\ \omega_z \end{bmatrix} = \begin{bmatrix} 0 \\ \Omega\cos\lambda_o \\ \Omega\sin\lambda_o \end{bmatrix} \quad \text{(tangent plane mechanization).} \quad (2.34)$$

In this case, the base point or fixed point latitude, λ_o, is used throughout the mission and the torquing rates applied to the gyros are shown in Eq. (2.34).

2.4.2 Coordinatization of Vector $\vec{\omega}$ in the Space Fixed Tangent Plane Mechanization

For completeness, the following discussion concerns another mechanization scheme that is simple enough to be competitive with the tangent plane mechanization. For lack of a more widely accepted terminology, it is called the space-fixed tangent plane

mechanization. It was, in fact, used on some versions of the PERSHING guidance system. The local level is established via IMU mounted pendulums or precision accelerometers and there is no torquing of the azimuth gyro. This mechanization is identical to the tangent plane scheme described in detail earlier. However, in the space-fixed tangent plane mechanization, the computation of earth's rate is terminated immediately before launch so that the horizontal and vertical components of earth rate torquing to the level gyros are also zero. That is, in this mechanization

$$\begin{bmatrix} \omega_x \\ \omega_y \\ \omega_z \end{bmatrix} = \begin{bmatrix} 0 \\ 0 \\ 0 \end{bmatrix} \quad \text{(space fixed tangent plane mechanization).} \qquad (2.35)$$

The obvious advantage to mechanizing a scheme that does not torque the gyros is more than a simplification in the on-board computer. The entire inertial instrumentation package is made at least an order of magnitude less precise in terms of manufacturing tolerances. Torquer linearity, precision pickoffs, voltage and current supplies, and pulse and analog circuits benefit from this consideration.

The burden of the simplified on-board hardware, in the case of PERSHING, is placed on the ground based level and alignment hardware. Though the earth's rate components are not calculated nor used to torque the two level gyros, a set of firing tables are required to offset the missile's trajectory to the primary target to compensate for the Coriolis acceleration. (The laws of nature still remain fixed

regardless of the mechanization chosen.) Consequently, it is a matter of choice, based on the preceding alternatives, as to which of the two simplest mechanizations one is willing to instrument. For purposes of this study, the more self-contained version, the true tangent plane mechanization will be used. In the simulation results which are presented later, there is practically no difference in using this choice other than replacing by zero the constants in the system's F matrix.

2.4.3 Coordinatization of Vector $\vec{\omega}$ in the Free Azimuth Mechanization

The utility of using a northern reference, per se, is susceptible to questioning in the case of a missile terminal guidance scheme. That it is of fundamental importance in terrestial navigation or terrestrial dead reckoning is, however, gospel. This derivation of a mechanization scheme and the next two that follow are north referenced because they are considered in the framework of a navigation problem. That is, the missile terminal guidance scheme is based upon maps that have been generated in the context of local earth coordinates which include a precise reference to north. Anticipating the results however, makes the argument somewhat academic because the additional state variables required to define a north reference preclude these mechanizations on economic grounds. These arguments are discussed more fully in later chapters.

This mechanization eliminates the torquing error associated with the Z-gyro, i.e., the gyro with its input axis vertical, because it does not provide a torquing command about the vertical axis. Instead,

the indicated north direction is computed by calculating the angle between the north given in a level plane and the level platform axes. The angle, α, shown in Fig. 2.6 is the angle between the horizontal platform Y axis and the true north.

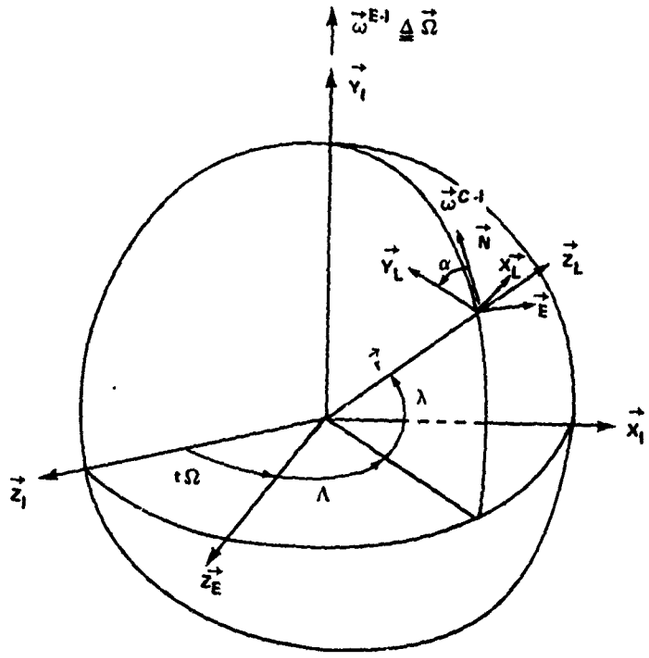

FIG. 2.6. FREE AZIMUTH MECHANIZATION GEOMETRY

As in the previous case, the local basis (L) is considered to be the computer or true basis. Equation (2.28) is repeated for convenience,

$$\omega_C^{C-I} = \omega_C^{C-E} + \omega_C^{E-I} \quad .$$

Again the argument for a transformation on the earth's rate is valid, i.e.,

$$\omega_C^{E-I} = T^*_{C/E}\, \omega_E^{E-I} \quad . \tag{2.36}$$

However, this direction cosine matrix, $T^*_{C/E}$, differs from $T_{C/E}$ of the tangent plane mechanization. It is summarized in Table 2.2.

Table 2.2

TRANSFORMATION SUMMARY

Transformation	Angle of Rotation	Axis of Rotation	Basis Name
$T^*_{C/E}$			Earth
	Λ	$\vec{Y}_I$	E'
	λ	$-\vec{X}_I$	E''
	α	$\vec{Z}_L$	Computer

$$T^*_{C/E} = \begin{bmatrix} \cos\alpha & \sin\alpha & 0 \\ -\sin\alpha & \cos\alpha & 0 \\ 0 & 0 & 1 \end{bmatrix} \begin{bmatrix} 1 & 0 & 0 \\ 0 & \cos\lambda & -\sin\lambda \\ 0 & \sin\lambda & \cos\lambda \end{bmatrix} \begin{bmatrix} \cos\Lambda & 0 & -\sin\Lambda \\ 0 & 1 & 0 \\ \sin\Lambda & 0 & \cos\Lambda \end{bmatrix} . \tag{2.37}$$

As before

$$\omega^{E-I}_{E} = \begin{bmatrix} 0 \\ \Omega \\ 0 \end{bmatrix} ,$$

so that Eq. (2.36) may be expanded to yield

$$\omega^{E-I}_{C} = \begin{bmatrix} \Omega \sin\alpha \cos\lambda \\ \Omega \cos\alpha \cos\lambda \\ \Omega \sin\lambda \end{bmatrix} . \tag{2.38}$$

Unlike the previous case, where it was considered zero,

$$\vec{\omega}^{C-E} = \dot{\alpha}\,\vec{Z}_L + \dot{\lambda}\,\vec{Z}_E + \dot{\Lambda}\,\vec{Y}_E \quad . \tag{2.39}$$

Here, $\vec{Z}_L$ is the unit vector about the Z axis of the platform, and $\vec{Z}_E$ and $\vec{Y}_E$ are the unit vectors, respectively, about which small rotations of angles λ and Λ are made in the intermediate Euler sequence. To coordinatize all the vectors into the computer basis, the $\dot{\alpha}$ rotation needs no transformation, the $\dot{\lambda}$ term is transformed through the angle α to determine its components in the computer basis, and the $\dot{\Lambda}$ term is transformed into the computer axes through the angles α and λ. The coordinatization is given by

$$\omega_C^{C-E} = \begin{bmatrix} 0 \\ 0 \\ \dot{\alpha} \end{bmatrix} + T_{C/Z_E} \begin{bmatrix} -\dot{\lambda} \\ 0 \\ 0 \end{bmatrix} + T^{**}_{C/E} \begin{bmatrix} 0 \\ \dot{\Lambda} \\ 0 \end{bmatrix} \quad . \tag{2.40}$$

The minus sign on $\dot{\lambda}$ indicates that the platform is maintained locally level by torquing the X-gyro to produce the precession rate $-\dot{\lambda}$ [15].

The transformation $T^{**}_{C/E}$ is summarized in Table 2.3.

Table 2.3

TRANSFORMATION SUMMARY

Transformation	Angle of Rotation	Axis of Rotation	Basis Name
$T^{**}_{C/E}$			Earth
	λ	$-\vec{X}_E$	E'
	α	$\vec{Z}_L$	
			Computer

The result is

$$T^{**}_{C/E} = \begin{bmatrix} \cos\alpha & \sin\alpha & 0 \\ -\sin\alpha & \cos\alpha & 0 \\ 0 & 0 & 1 \end{bmatrix} \begin{bmatrix} 1 & 0 & 0 \\ 0 & \cos\lambda & -\sin\lambda \\ 0 & \sin\lambda & \cos\lambda \end{bmatrix} . \quad (2.41)$$

T_{C/Z_E} is a simple transformation resulting from a small rotation of angle α about the $\vec{Z}_L$ axis. Thus,

$$T_{C/Z_E} = \begin{bmatrix} \cos\alpha & \sin\alpha & 0 \\ -\sin\alpha & \cos\alpha & 0 \\ 0 & 0 & 1 \end{bmatrix} . \quad (2.42)$$

Substituting Eqs. (2.41) and (2.42) into Eq. (2.40) yields

$$\omega_C^{C-E} = \begin{bmatrix} -\dot{\lambda}\cos\alpha + \dot{\Lambda}\sin\alpha\cos\lambda \\ \dot{\lambda}\sin\alpha + \dot{\Lambda}\cos\alpha\cos\lambda \\ \dot{\alpha} + \dot{\Lambda}\sin\lambda \end{bmatrix} . \quad (2.43)$$

Substituting Eqs. (2.38) and (2.43) into Eq. (2.28) gives the following coordinatization result:

$$\begin{bmatrix} \omega_x \\ \omega_y \\ \omega_z \end{bmatrix} = \begin{bmatrix} (\Omega + \dot{\Lambda})\sin\alpha\cos\lambda - \dot{\lambda}\cos\alpha \\ (\Omega + \dot{\Lambda})\cos\alpha\cos\lambda + \dot{\lambda}\sin\alpha \\ (\Omega + \dot{\Lambda})\sin\lambda + \dot{\alpha} \end{bmatrix} . \quad (2.44)$$

As previously mentioned, one of the main advantages of the free azimuth mechanization results in not having to torque the azimuth or Z-gyro, i.e., it is free to rotate. (Another similar mechanization,

called the wander azimuth mechanization, results when the Z component of $\vec{\omega}^{C-E}$ is constrained to equal the Z component of $\vec{\Omega}^{E-I}$.) Thus, ω_z is made zero by forcing

$$\dot{\alpha} = -(\Omega + \dot{\Lambda}) \sin \alpha \tag{2.45}$$

which results in

$$\begin{bmatrix} \omega_x \\ \omega_y \\ \omega_z \end{bmatrix} = \begin{bmatrix} (\Omega + \dot{\Lambda}) \sin \Omega \cos \lambda - \dot{\lambda} \cos \alpha \\ (\Omega + \dot{\Lambda}) \cos \alpha \cos \lambda + \dot{\lambda} \sin \alpha \\ 0 \end{bmatrix} \quad \begin{matrix} \text{(free azimuth} \\ \text{mechanization)} \end{matrix} \tag{2.46}$$

2.4.4 Coordinatization of Vector $\vec{\omega}$ in the Local Level, North-East Mechanization

Another coordinate mechanization widely used for navigation which has potential for this application is the local level, north-east system. The usefulness of this system is important when the system's outputs are desired corresponding to map data or when an explicit vertical is desired to drive auxiliary equipment. This basis is also observable in Fig. 2.7, but with the angle, α, now kept constant at the value of zero.

The platform torquing rate is again repeated

$$\omega_C^{C-I} = \omega_C^{C-E} + \omega_C^{E-I} \quad .$$

Now

$$\omega_C^{E-I} = T_{C/E}^{***} \omega_E^{E-I} \quad , \tag{2.47}$$

where $T^{***}_{C/E}$ is of the same form as the transformation $T_{C/E}$ of Eq. (2.32) i.e.,

$$T^{***}_{C/E} = \begin{bmatrix} 1 & 0 & 0 \\ 0 & \cos\lambda & -\sin\lambda \\ 0 & \sin\lambda & \cos\lambda \end{bmatrix} \begin{bmatrix} \cos\Lambda & 0 & \sin\Lambda \\ 0 & 1 & 0 \\ \sin\Lambda & 0 & \cos\Lambda \end{bmatrix} . \quad (2.48)$$

Again, the earth rate components are

$$\omega^{E-I}_{E} = \begin{bmatrix} 0 \\ \Omega \\ 0 \end{bmatrix} , \quad (2.49)$$

so that

$$\omega^{E-I}_{C} = \begin{bmatrix} 0 \\ \Omega\cos\lambda \\ \Omega\sin\lambda \end{bmatrix} . \quad (2.49)$$

The term ω^{C-E}_{C} is similar to its counterpart in the free azimuth system; only here it is less complex, i.e.,

$$\omega^{C-E}_{C} = T_{C/E} \begin{bmatrix} 0 \\ \dot{\Lambda} \\ 0 \end{bmatrix} + \begin{bmatrix} -\dot{\lambda} \\ 0 \\ 0 \end{bmatrix} , \quad (2.50)$$

$$\omega^{C-E}_{C} = \begin{bmatrix} 1 & 0 & 0 \\ 0 & \cos\lambda & \sin\lambda \\ 0 & -\sin\lambda & \cos\lambda \end{bmatrix} \begin{bmatrix} 0 \\ \dot{\Lambda} \\ 0 \end{bmatrix} + \begin{bmatrix} -\dot{\lambda} \\ 0 \\ 0 \end{bmatrix} . \quad (2.51)$$

Adding Eqs. (2.49) and (2.51) gives the final result

$$\begin{bmatrix} \omega_x \\ \omega_y \\ \omega_z \end{bmatrix} = \begin{bmatrix} -\dot{\lambda} \\ (\Omega + \dot{\Lambda}) \cos \lambda \\ (\Omega + \dot{\Lambda}) \sin \lambda \end{bmatrix} \quad \text{(local level north-east mechanization)} \quad . \quad (2.52)$$

Notice that it is a special case of the free azimuth mechanization given by Eq. (2.46) but with α set equal to zero in this case.

Sufficient analysis has been performed to display the coordinatization of the IMU's rate of rotation or torque rate, $\vec{\omega}$, in four mechanizations. The rationale for the specific choice best suited to this application is discussed in more detail in Chapter III.

CHAPTER III. MATHEMATICAL MODELING OF THE SYSTEM

3.1 IDENTIFICATION OF THE INERTIAL SYSTEM MECHANIZATION

The first step in applying the Kalman-Bucy theory is to identify the system on which the filter is to be based. In the case of improving the guidance of a reentry vehicle, it may seem that the most direct choice would be a system that estimated the desired parameters of the vehicle. The filter would then be based on the equations that describe the motions of the vehicle itself. This approach is functionally visualized in Fig. 3.1. Though appealing for an orbiting spacecraft guidance problem where the position and velocity could be predicted for any future time with accuracy, it is not easily implemented for a rapidly varying dynamic system.

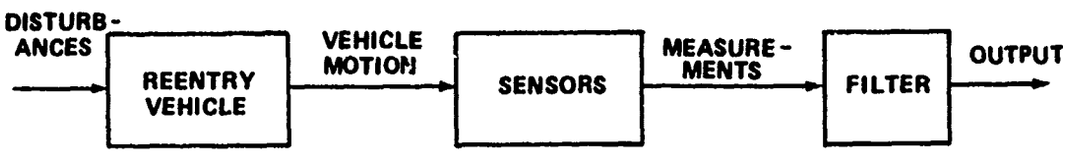

FIG. 3.1. FUNCTIONAL DIAGRAM OF A DIRECT FILTER

Instead, an indirect filter is implemented based on kinematic considerations. It is worthwhile to diverge at this point for a brief discussion relating the notions of dynamics, kinematics, and measurements in the context of this problem.

Dynamics is expressed by some as the study of the motion of a particle (system of particles) from the knowledge of the external

forces acting on it. Kinematics is sometimes expressed as the study of the motion of a particle (system of particles) disregarding the forces associated with the motion. Simply, it is the study of the geometry of the motion relating time, displacement, velocity, acceleration, etc., both translational and rotational.

Confusion may arise because control engineers use the terminology "dynamic systems" to describe a plant by equations which vary as a function of time. This is often done to emphasize that the system under discussion is not static. An analytical dynamicist, however, uses the terminology "dynamic equations" to define the set of equations describing motion of a particle acted on by forces as previously summarized. Thus to a dynamicist, the Euler equations of rigid body mechanics, for example, are dynamic expressions while the equations relating angular velocity among reference bases are kinematic expressions.

Measurements can be thought of as one of the three types of inputs for a Kalman-Bucy filter. In a navigation or guidance problem, the measurement may be a doppler radar measuring velocity components, it may be a Loran receiver measuring time differences in radio wave propagation, or it may be a radar area correlator as in this problem. The second input is the driving noise associated with gyro drift, SFM bias, etc. The third input is the main forcing variable of the differential equation which may be a torque, a force, or other driving function. Thus, in the expression for a plant given by

$$\dot{x}(t) = F(t)\ x(t) + G(t)\ u(t) + w(t) \quad ,$$

with a measurement given by

$$Z(t) = H(t)\, x(t) + v(t) \quad .$$

The variable u(t) is the forcing variable, the variable w(t) is the driving noise, Z(t) is the measurement of x(t) with a corruption of additive noise v(t).

In a direct filter formulated for a vehicle carrying an IMU, the dynamic system (control's sense) on which the filter is based is the system of equations that describe the motions of the vehicle itself (dynamicists' sense). The filter would use all measurements, including those of the IMU, to produce estimates of the position and velocity of the vehicle directly. The dynamic equations describing the system requires a statistical dynamic model for the vehicle to be included in the state space formulation [16]. However, the model used to describe these random motions is difficult to obtain for a vehicle rapidly varying in velocity and position as a function of time. In fact, measurements of vehicle acceleration and angular velocity are much better data to process than to model the disturbances or forces which cause them.

The indirect filter is a completely different way of formulating the navigation problem which avoids most of the practical problems of the previous method if in addition to the inertial navigation system there is included some other source of navigation data. Instead of estimating the state of the vehicle directly, the filter is used to estimate the <u>error state</u> of an inertial navigation system. The

inertial system follows the high frequency motions of the vehicle very accurately but has low-frequency errors which grow with time. The dynamic system on which the filter is based is the set of error equations for the inertial system which are relatively well known, well behaved, low frequency, and essentially linear. The sample period can range from several seconds up to a minute without greatly influencing the effectiveness of the filter. For these reasons, this method is used for virtually every practical terrestrial referenced IMU Kalman filter mechanization. In the particular case of navigating the reentry body, the time of flight under this condition is so short that the indirect scheme can be functionally implemented, as shown in Fig. 3.2.

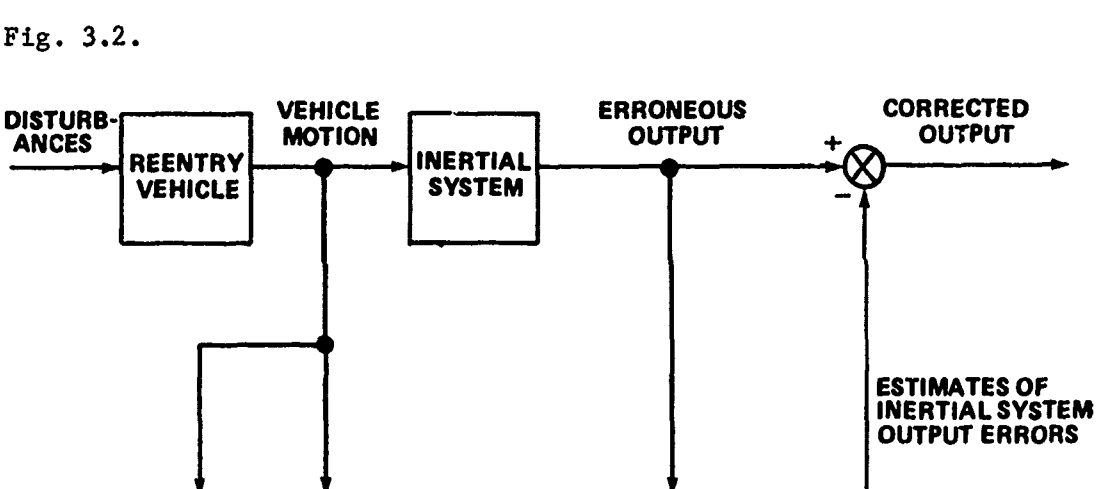

FIG. 3.2. FUNCTIONAL DIAGRAM OF AN INDIRECT FILTER

Note that the outputs from the inertial system are not the measurements in the Kalman-Bucy theory. Rather, they are the forcing

function or driving input in the dynamical equations describing the system. The radar area correlation system and the radar altimeter are the measurement kinematics as far as this estimation problem is concerned.

The error equations in inertial systems position and velocity, given as Eqs. (2.19) and (2.26) are logical choices for the inertial system states. Rewriting them in a manner more amenable to manipulation as state variables follows. From Eq. (2.26),

$$\begin{aligned}\delta\ddot{x} &= \delta x\left[\left(\omega_y^2 + \omega_z^2\right) - \omega_s^2\right] + \delta y\left[\dot{\omega}_z - \omega_x\omega_y\right] + \delta z\left[-\dot{\omega}_y - \omega_x\omega_z\right] \\ &+ \delta\dot{y}\left[2\omega_z\right] + \delta\dot{z}\left[-2\omega_y\right] + b_x - \psi_y f_z + \psi_z f_y \\ &+ \Delta K_{f1} f_x + m_{12} f_y + m_{13} f_z \quad , \end{aligned} \tag{3.1}$$

$$\begin{aligned}\delta\ddot{y} &= \delta x\left[-\dot{\omega}_z - \omega_x\omega_y\right] + \delta y\left[\omega_x^2 + \omega_z^2 - \omega_s^2\right] + \delta z\left[\dot{\omega}_x - \omega_y\omega_z\right] \\ &+ \delta\dot{x}\left[-2\omega_z\right] + \delta\dot{z}\left[2\omega_x\right] + b_y + \psi_x f_z - \psi_z f_x \\ &+ m_{12} f_x + \Delta K_{f2} f_y + m_{23} f_z \quad , \end{aligned} \tag{3.2}$$

$$\begin{aligned}\delta\ddot{z} &= \delta x\left[\dot{\omega}_y - \omega_x\omega_z\right] + \delta y\left[-\dot{\omega}_x - \omega_y\omega_z\right] + \delta z\left[\left(\omega_x^2 + \omega_y^2\right) + 2\omega_s^2\right] \\ &+ \delta\dot{x}\left[2\omega_y\right] + \delta\dot{y}\left[-2\omega_x\right] + b_z - \psi_x f_z + \psi_z f_x \\ &+ m_{31} f_x + m_{32} f_y + \Delta K_{f3} f_z \quad . \end{aligned} \tag{3.3}$$

From Eq. (2.19),

$$\dot{\psi}_x = \psi_y\omega_z - \psi_z\omega_y + \Delta K_{g1}\omega_x + m_{12}\omega_y + m_{13}\omega_z + \epsilon_x \quad , \qquad (3.4)$$

$$\dot{\psi}_y = -\psi_x\omega_z + \psi_z\omega_x + m_{12}\omega_x + \Delta K_{g2}\omega_y + m_{23}\omega_z + \epsilon_y \quad , \qquad (3.5)$$

and

$$\dot{\psi}_z = \psi_x\omega_y - \psi_y\omega_x + m_{31}\omega_x + m_{32}\omega_y + \Delta K_{g3}\omega_z + \epsilon_z \quad . \qquad (3.6)$$

3.1.1 State Vector for the Tangent Plane Mechanization

From Eqs. (3.1) through (3.6), part of the state vector is chosen to be

$$X^T = \left[\delta x,\ \delta y,\ \delta z,\ \delta V_x,\ \delta V_y,\ \delta V_z,\ \psi_x,\ \psi_y,\ \psi_z\right] , \qquad (3.7)$$

where

$$\delta\dot{x} = \delta V_x \triangleq \text{error in IMU x-velocity}$$

$$\delta\dot{y} = \delta V_y \triangleq \text{error in IMU y-velocity}$$

$$\delta\dot{z} = \delta V_z \triangleq \text{error in IMU z-velocity,}$$

and other variables are as previously defined.

The gyro torquing rates ω_x, ω_y, and ω_z implicit in Eq. (3.7) were shown to differ according to the mechanization scheme. The tangent plane mechanization torquing rates are constants given by

$$\omega_x = 0$$

$$\omega_y = \Omega \cos\lambda_o$$

$$\omega_z = \Omega \sin\lambda_o \quad . \qquad (3.8)$$

Because there are no additional states required to define the torquing rates for this mechanization, the state vector would remain as given by Eq. (3.7).

3.1.2 State Vector for the Space-Fixed Tangent Plane Mechanization

The torquing rates in the space-fixed tangent plane mechanization are equally as simple and also constant. To be exact, the constant is zero. However for the reasons previously described, the space-fixed tangent plane mechanization is rejected in favor of the true tangent plane mechanization.

3.1.3 State Vector for the Free Azimuth Mechanization

The free azimuth torquing rates as described in Eq. (2.46) are complicated by the additional explicit dependence on latitude and longitude rates, $\dot{\lambda}$ and $\dot{\Lambda}$, respectively. Also the wander angle, α, is seen as an independent variable. For consistency then, the error in these three variables must be derived and included in the state vector. The perturbation in these variables may be rationalized as follows. Until now the assumption was used that the local basis (L) was equal to the computer or true basis (C). Generally, the possibility exists that the computer is in error by some small amount in its calculation of the actual position as given in the local basis. The development which follows depicts the effect by way of perturbations on the ideal equations.

Refer to Fig. 2.6 to visualize the ideal, errorless rates given by

$$\dot{\vec{\lambda}} = \frac{\vec{V}_N}{\vec{r}} \triangleq \frac{\vec{V}_N}{R_N + h} \quad , \tag{3.9}$$

or

$$\dot{\lambda} = \frac{V_x \sin\alpha + V_x \cos\alpha}{R_N + h} \quad . \tag{3.10}$$

Also,

$$\dot{\vec{\Lambda}} = \frac{\vec{V}_E}{\vec{r}} \triangleq \frac{\vec{V}_E}{\left(R_E + h\right) \cos \lambda} \tag{3.11}$$

and

$$\dot{\Lambda} = \frac{V_x \cos \alpha - V_y \sin \alpha}{\left(R_E + h\right) \cos \lambda} \quad , \tag{3.12}$$

where:

$V_N \triangleq$ vector representing velocity in northerly direction

$V_E \triangleq$ vector representing velocity easterly direction

$h \triangleq$ altitude above the reference ellipsoid

$R_E \triangleq$ radius of curvature of reference ellipsoid in easterly direction

$R_N \triangleq$ radius of curvature of reference ellipsoid in northerly direction

$V_x \triangleq$ component of velocity along platform's x-axis

$V_y \triangleq$ component of velocity along platform's y-axis .

A perturbation on the latitude and longitude rate equations yields the differential equations for the latitude and longitude errors. Thus, from Eq. (3.10)

$$\frac{d}{dt}(\lambda + \delta\lambda) = \frac{\left(V_x + \delta V_x\right) \sin\ (\alpha + \delta\alpha) + \left(V_y + \delta V_y\right) \cos\ (\alpha + \delta\alpha)}{R_N + h} \quad . \tag{3.13}$$

Noting that

$$\cos \delta\alpha \approx 1 \quad , \tag{3.14}$$

$$\sin \delta\alpha \approx \delta\alpha \quad , \tag{3.15}$$

and expanding the sine and cosine functions by their trigonometric identity results in

$$\dot{\delta\lambda} = \frac{V_x \cos\alpha\delta\alpha + \delta V_x \sin\alpha - V_y \sin\alpha\delta\alpha + \delta V_y \cos\alpha}{R_N + h} \quad . \tag{3.16}$$

Similarly, from Eq. (3.12)

$$\frac{d}{dt}(\Lambda + \delta\Lambda) = \frac{\left(V_x + \delta V_x\right) \cos(\alpha + \delta\alpha) - \left(V_y + \delta V_y\right) \sin(\alpha + \delta\alpha)}{\left(R_E + h\right) \cos(\lambda + \delta\lambda)} \quad . \tag{3.17}$$

This result is

$$\dot{\delta\Lambda} = \frac{-V_x \sin\alpha\delta\alpha + \delta V_x \cos\alpha - V_y \cos\alpha\delta\alpha - \delta V_y \sin\alpha}{\left(R_E + h\right) \sin\lambda\delta\lambda} \quad . \tag{3.18}$$

The variation in the wander angle, α, is obtained from Eq. (2.45) viz,

$$\dot{\alpha} = -(\Omega + \dot{\Lambda}) \sin\lambda \quad . \tag{3.19}$$

Again, to first order

$$\dot{\delta\alpha} = (\Omega + \dot{\Lambda}) \cos\lambda\delta\lambda - \sin\lambda\dot{\delta\Lambda} \quad . \tag{3.20}$$

Substituting Eq. (3.12) into Eq. (3.20) yields

$$\dot{\delta\alpha} = -\left(\Omega + \frac{\delta x \cos\alpha - \delta y \sin\alpha}{\left(R_E + h\right) \cos\lambda}\right) \cos\lambda\delta\lambda - \sin\lambda\dot{\delta\Lambda} \quad . \tag{3.21}$$

These three error differential equations, required to extend the state vector when they appeared in the torquing equations, have in turn generated the requirement for the inclusion of the true or idealized

velocity components V_x and V_y. Both are obtained from Eq. (2.8a) but must be coordinatized in the free azimuth basis. That is, nominally

$$\dot{V}_L = \begin{bmatrix} \dot{V}_x \\ \dot{V}_y \\ \dot{V}_z \end{bmatrix} \tag{3.22}$$

and from Eq. (2.8b)

$$\dot{r}_L = \begin{bmatrix} \dot{r}_x \\ \dot{r}_y \\ \dot{r}_z \end{bmatrix} \quad . \tag{3.23}$$

For this mechanization, the state vector would be

$$X^T = \left[\delta x,\ \delta y,\ \delta z,\ \delta V_x,\ \delta V_y,\ \delta V_z,\ \psi_x,\ \psi_y,\ \psi_z,\ \delta\lambda,\ \delta\Lambda,\ \delta\alpha\right] \tag{3.24}$$

The increased number of states required to mechanize this scheme is evidence by comparing this state vector with the state vector described by Eq. (3.7).

3.1.4 State Vector for the Local Level North-East Mechanization

The local level north-east mechanization would have gyro torquing rates given by Eq. (2.52),

$$\omega_x = -\dot{\lambda}$$
$$\omega_y = (\Omega + \dot{\Lambda}) \cos\lambda$$
$$\omega_z = (\Omega + \dot{\Lambda}) \sin\lambda \quad .$$

Again, there is a need for the error differential equation describing λ and Λ. However, without the need for α, the state vector is simplified by one state over the previous mechanization as

$$X^T = \left[\delta x,\ \delta y,\ \delta z,\ \delta V_x,\ \delta V_y,\ \delta V_z,\ \psi_x,\ \psi_y,\ \psi_z,\ \delta\lambda,\ \delta\Lambda\right] \qquad (3.25)$$

3.1.5 State Vector Augmentation

In addition, there is a possibility that gyro and accelerometer errors are correlated requiring six more augmented states to be included by addition to each model mechanized, i.e.,

$$X_A^T = \left[\epsilon_x,\ \epsilon_y,\ \epsilon_z,\ A_x,\ A_y,\ A_z\right] \quad .$$

Therefore, a fully mechanized inertial system, with 6 augmented gyro and accelerometer states a possibility, can be modeled with as few as 15 states in the tangent plane or as many as 18 states in the free azimuth. The local level north-east mechanization is a compromise requiring 17 states. It is therefore reasonable to choose a mechanization based on the constraint that the airborne computer will have only limited capability to accommodate the filter implementation. Because the optimal filter requires computation of the Riccati error covariance equation, it alone requires $n(n+1)/2$ equations based on n number of states. The minimum number of equations that must be solved, including the number of states required to model only the inertial system, are seen in Table 3.1.

Table 3.1

COMPARISON OF MECHANIZATION COMPLEXITY

Mechanization	No. of Equations
Tangent Plan	135
Space-Fixed Tangent Plane	135
Local Level North-East	153
Free Azimuth	171

To obtain a torque-free azimuth gyro in the free azimuth mechanization, a 27 percent increase in computer capability compared to the tangent plane is required. The tangent plane mechanization requires 12 percent less computer capability than does the local level north-east. For this initial analysis, the tangent plane mechanization is chosen and the first objective of this study is met.

3.2 CHOICE OF THE MODEL'S TRAJECTORY

Additional considerations simplify the state space description of the total system even more. For purposes of this report, the PERSHING trajectory can be represented as a parabolic arc with the baseline reaching a maximum of 400 nautical miles and a maximum height of 120 miles from the earth's surface. Results of previous studies have dictated that the terminal guidance phase be initiated at an altitude of 30,000 feet above the earth's surface. The trajectory is shown in Fig. 3.3 in the IMU X-Z plane. The velocity of the reentry body at the 30,000-foot level is approximately 3000 feet per second in the negative Z direction (down). Also, the velocity is almost constant from this altitude to impact. Actually, it will vary according to the vehicle's ballistic drag coefficient, air density, exact altitude of the target, specific reentry angle of attack, etc. However, the model is simplified by not including the vehicle's aerodynamic characteristics. Previous flights have shown the time to impact from this altitude varies from approximately 7 to 12 seconds. For convenience, a flight time of 10 seconds is used in the model's simulation.

An additional comment is necessary concerning the simulation of the trajectory. Although a constant velocity of -3000 feet per second

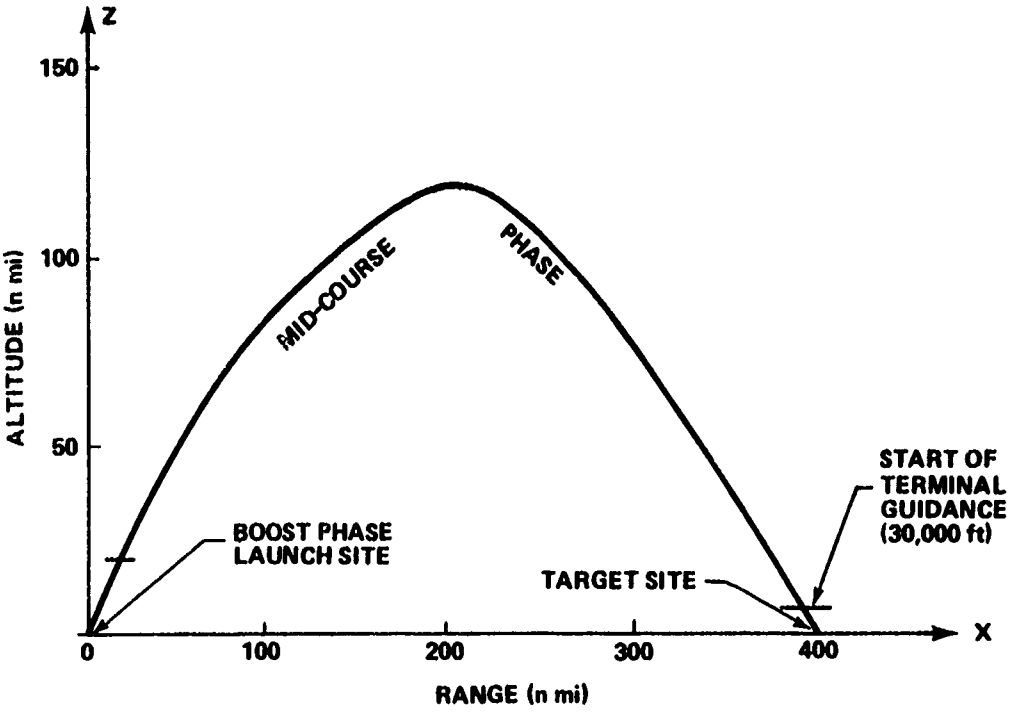

FIG. 3.3. TYPICAL PERSHING FLIGHT PROFILE

in the Z direction is reasonable, there could be an additional Y or X component. To eliminate one state the trajectory is constrained to the X-Z plane, with no loss in generality, because the Y component could be eliminated choice of axes. Thus, the f_z and f_x specific force terms in the IMU mechanizations are initialized at zero because their corresponding velocities are constant. As will been seen, however, this is only of academic interest because additional simplifications eliminate even those terms. The result is a free trajectory, i.e., there is no state modeled representing actual vehicle position, velocity, or acceleration as was discussed previously. The system states are IMU errors in these domains and are driven by IMU error inputs. When the specific force terms are neglected there is no physically meaningful trajectory generated, not to imply that it cannot be done. However, in this model, there is ample justification to neglect them.

3.3 FORMULATION OF THE IMU ERROR MODEL

The terminal guidance phase is only 10-seconds long for the application in which the filter will be implemented. The effect of correcting the gyro and accelerometer errors, which propagate with an 84-minute period, is negligible over this short time span. In addition, their effect on system error buildup is known from extensive flight test and analytic data (Martin-Marietta Report [17]).

Instead of modeling error sources which propagate at negligibly low frequency, i.e., the platform tilts, $\vec{\psi}$, and the gyro and accelerometer scale factor errors, $\Delta\vec{\vec{K}}_g$, and $\Delta\vec{\vec{K}}_f$, respectively, their random errors, $\vec{c}$, and the accelerometer bias, $\vec{b}$, their effects on the system are included as driving noise in the IMU error equations. Because gyro or accelerometer errors are not modeled, the six states can be eliminated, as given in Eq. (3.26). Three more states are eliminated by not modeling the tilt equations. It should be noted that to assume $\dot{\vec{\psi}}$ is zero is not exactly true. The argument is that $\vec{\psi}$ and $\dot{\vec{\psi}}$ are zero because the effect of the tilts on IMU performance at initiation of the terminal guidance phase can be included as a forcing term in the IMU error equations; i.e., the total $\vec{\psi}$ error accrued during the flight is mechanized in the filter as an initial condition. Its buildup and additional contribution to the IMU error is considered negligible in this application during the 10-second period. Longer flights, even in the order of minutes in other applications for example, and in cases where the data are not available to permit this alternative treatment would invalidate the simplification.

With $\vec{\psi}$ and $\vec{\dot{\psi}}$ zero, Eqs. (3.1) through (3.6) simplify to the degree of excluding the specific force terms f_x, f_y, and f_z, as was alluded to previously. With no other means to propagate a physical trajectory, the IMU error equations are seen in a free trajectory for 10 seconds in which the accumulated system errors to that point drive the system as initial conditions.

The δV_y state is excluded because the model is constrained to the X-Z plane for this analysis. This is not to imply that because δy is initialized equal to zero, δV_y can be neglected. The converse is true. There is every reason to believe that the error state pairs δx and δy as well as δV_x and δV_y will be nearly equal for this application. However, to save computer memory and operating time, only one of the velocities will be estimated, in this case δV_x. The results, shown later, should be interpreted to mean that the estimates for δV_x are equally likely to be representative of δV_y.

With so much emphasis on eliminating state variables, it is almost incongruous to justify keeping two states that are most often eliminated. The δz and δV_z states are, in every reference source, shown to be in a divergent or unstable mechanization and are thus not instrumented. In most terrestrial navigators, the Z accelerometer is not even physically mounted on the IMU. It was observed by Kayton [18] that the error in the altitude channel grows exponentially and doubles in the amplitude in approximately 28 minutes. However, the total PERSHING flight is less than 7 minutes and the terminal guidance phase is almost two orders of magnitude smaller than that. Consequently, the Z-channel

instability will not cause a catastrophically larger error in this case, given reasonable initial conditions. Because the Z-channel information is very desirable for on-board functions such as arming, safing, and fuzing, and because it could be useful in scheduling imagery and gains in one configuration of a suboptimal filter, it is included in the IMU error mechanization equations.

As a consequence of these decisions, the IMU is modeled as follows:

$$\begin{bmatrix} \delta\dot{x} \\ \delta\dot{y} \\ \delta\dot{z} \\ \delta\dot{V}_x \\ \delta\dot{V}_z \end{bmatrix} = \begin{bmatrix} 0 & 0 & 0 & 1 & 0 \\ 0 & 0 & 0 & 0 & 0 \\ 0 & 0 & 0 & 0 & 1 \\ F41 & F42 & F43 & 0 & -2\omega_y \\ F51 & F52 & F53 & 2\omega_y & 0 \end{bmatrix} \begin{bmatrix} \delta x \\ \delta y \\ \delta z \\ \delta V_x \\ \delta V_z \end{bmatrix} , \qquad (3.27)$$

where:

$$F41 = -\omega_s + \omega_y^2 + \omega_z^2$$

$$F42 = -\omega_x\omega_y$$

$$F43 = -\omega_x\omega_z$$

$$F51 = -\omega_x\omega_z$$

$$F52 = -\omega_y\omega_z$$

$$F53 = 2\omega_s + \omega_x^2 + \omega_y^2 \quad ,$$

and

$$\omega_x = 0$$

$$\omega_y = \Omega \cos \lambda$$

$$\omega_z = \Omega \sin \lambda \quad ,$$

with

Ω = constant (earth's rate of rotation)

λ = constant (launch site latitude),

so that $\dot{\vec{\omega}} = 0$ and is thus omitted from the F-matrix.

3.4 FORMULATION OF THE RADAR AREA CORRELATION SYSTEM

The description of the radar area correlation system application to terminal guidance is discussed in Appendix B. The radar system is used as an additional external measurement device (external to the IMU) to measure position in the X-Y plane defined by the IMU. The observations or measurements for the Kalman filter are actually differences between system-indicated and externally measured information. As is common practice [9], the measurement errors are attributed to inaccuracies in the external indications only. Thus, by forming the difference between the externally indicated and inertially indicated positions

$$\begin{aligned} Z &= P_{ind}\ (\text{external}) - P_{ind}\ (\text{IMU}) \\ &= \left(P_{true} + e_p\right) - (P_{true} + \delta P) \\ &= e_p - \delta P \quad , \end{aligned} \tag{3.28}$$

where

P_{ind} = position indicated

P_{true} = true position or errorless position

δP = inertial position error

e_p = external device position error .

Equation (3.28) is equivalent to expressing the observation equation as

$$Z(t) = H\ x(t) + v(t) \tag{3.29}$$

$$Z(t) = \begin{bmatrix} -1 & 0 \end{bmatrix} \begin{bmatrix} \delta P(t) \\ \delta V(t) \end{bmatrix} + e_p(t) \quad , \tag{3.30}$$

where δP and δV are inertial errors in position and velocity for this exploratory example.

The available unclassified information on radar area correlators did not delve into the possible statistical correlation in position errors from fix to fix. Although the fix to fix correlation seems a distinct possibility, the first cut at a model excluded that consideration. In terms of the state variables defined for the IMU, the radar area correlation system's observation is modeled as

$$Z(t) = \begin{bmatrix} 1 & 0 & 0 & 0 & 0 \\ 0 & 1 & 0 & 0 & 0 \end{bmatrix} \begin{bmatrix} \delta x \\ \delta y \\ \delta z \\ \delta V_x \\ \delta V_z \end{bmatrix} + \begin{bmatrix} v_x(t) \\ v_y(t) \end{bmatrix} \quad . \tag{3.31}$$

The values for the radar system errors are chosen as typical state-of-the-art. Stauffer [19] considers that to be planar resolution or, for this model, $v_x = v_y = 50$ feet RMS.

Another consideration for the radar position measurement model is the effect of processing time on the filter's performance. It was learned that the time delay, as it may be considered, in matching the reference imagery to the radar's projected real time imagery is

approximately 0.2 second. This indicates that by the time a position fix has been processed by the typical radar system, the information is 0.2-second old, i.e., the vehicle has moved on. In the case of the PERSHING, reentry at 3000 feet per second the radar processing time alone will require a 600-foot measurement compensation in the filter mechanization. Intuition suggests that such an error would eventually be a source of filter divergence if not properly addressed.

This problem was treated in the model in two ways. First it was neglected. This is not as startling a choice as might first appear. There is very little mention of this delay phenomenon in the literature and its effect on filter performance. It is often mentioned as an existing problem but is quickly discarded with the statement that future studies will be conducted in that area. The best justification for not implementing it in this filter application is that the time duration is so short (10 seconds) that filter divergence will not accrue a meaningful error. The results seem to verify this, at least in the case where optimal gains are used.

Meaningful fixes to this problem have been proposed. DeBra [20] has suggested that the measurement model incorporate the time delay as a nonlinear exponential function with a time constant comparable to the best guess at the time delay. For example, instead of the linear measurement in the variables δx and δy given by Eq. (3.31), a model in the frequency domain is given by

$$Z_1(s) = e^{-sT}\,\delta x(s) + v_x(s)$$

$$Z_2(s) = e^{-sT}\,\delta y(s) + v_y(s) \quad , \qquad (3.32)$$

where the time delay is chosen by the value T. In the time domain, two additional state variables are required, one to define the time delay for each channel. Thus, the F-matrix would require a two-state augmentation.

Bryson [21] has suggested the following methods, particularly applicable when the time delay is not well known:

a) Increase the magnitude of appropriate variance elements in the covariance error equations

b) Increase the amplitude of the measurement noise

c) Combination of a) and b).

The effect is to decrease the knowledge of the system from the filter's point of view.

The model for the reentry vehicle was simulated alternatively in the manner of Bryson. The 600-foot error was caused by processing time was included as additional error in the measurement error covariance matrix R. Its effect was, therefore, directly observable in the calculation for the optimal filter gains. These results are described in Chapter IV.

3.5 FORMULATION OF THE RADAR ALTIMETER MODEL

The radar altimeter carried on the PERSHING will be used to obtain vertical position measurements above the earth's surface. It is mechanized in the Kalman filter formulation in exactly the same way as the radar area correlator, i.e.,

$$Z = \delta P_z + e_{Pz} \quad . \tag{3.33}$$

Thus, the radar altimeter is modeled as the 2-channel observation

$$Z(t) = [0 \quad 0 \quad 1 \quad 0 \quad 0] \begin{bmatrix} \delta x \\ \delta y \\ \delta z \\ \delta V_x \\ \delta V_z \end{bmatrix} + v_z(t) \quad . \qquad (3.34)$$

From data on previous PERSHING flights, the radar altimeter error is known to be approximately 10 percent of altitude indication. So that an additional state would not be required, it was considered for several cases in this study to be constant at 100 feet and for several cases, constant at 1200 feet. The effect of the change is discussed in Chapter IV.

3.6 A FILTER MECHANIZATION FOR NONLINEAR SYSTEMS

The filter equations developed by Kalman and Bucy and an extension to correlated input--measurement noise (derived in Appendix C) were developed under the assumption that the system disturbances and the measurement errors were random variables described by Gaussian statistics, zero means, and that the plant was describable by linear equations. The resulting filter then was shown to give the optimal estimate of the states. Numerous researchers in this area have expanded the ideas to the more useful and practical case of systems described by nonlinear dynamical equations. For example, Bryson and Ho [22], in addition to their own contributions, have a rich bibliography on these and related topics.

The filter equations used in this model are of the form most applicable to the navigation problem at hand, i.e., a mixture of discrete and continuous equations. The discrete form is used at a time when a new measurement is introduced and the continuous form is used to extrapolate between measurements. Also, the equations are a mixture of linear and nonlinear expressions. The nonlinear describe the system, i.e., the navigation system error equations, and the linearized equations are used for the covariance error propagation. These equations are linearized about the current estimate because in a navigator, in general, and in this model, in particular, there is no convenient nominal path about which to linearize. These equations, developed in Section 12.6 of Bryson and Ho [22] are summarized in Table 3.2.

3.7 EQUATIONS USED IN THE DIGITAL COMPUTER SIMULATION

This section summarizes the equations in the model which were used in the Monte Carlo simulation. The inertial system is modeled by five error states; the observation matrix (H), models the IMU position error in three coordinates as measured by a radar area correlation system (δx, δy); and a radar altimeter (δz). The initial conditions, error covariances and constants are summarized in Tables 3.3 through 3.5.

Table 3.2

EXTENDED KALMAN FILTER FOR NONLINEAR SYSTEMS MODELED IN CONTINUOUS - DISCRETE FORM

Message model (nonlinear)	$\dot{x}(t) = f(x, u, t)$
Observation model (nonlinear)	$z(t) = h(x, t) + v(t)$
Linearization about the current estimate	$F(t) = \left.\frac{\partial f}{\partial x}\right\|_{x=\dot{x}}$, $G(t) = \left.\frac{\partial f}{\partial u}\right\|_{x=\hat{x}}$, $H(t) = \left.\frac{\partial h}{\partial x}\right\|_{x=\hat{x}}$
A priori statistics	$E\{u(t)\} = 0$ $E\{u(t), u^T(\tau)\} = Q\delta(t-\tau)$ } Process noise $E\{v(t)\} = 0$ $E\{v(t), v^T(\tau)\} = R\delta(t-\tau)$ } Measurement noise $E\{u(t), v(\tau)\} = 0$ } Correlated process and measurement noise
Filter algorithm between measurements	$\dot{\hat{x}}(t) = f(\hat{x}, t)$
Error variance algorithm between measurements	$\dot{P}(t) = F(t)\,P(t) + P(t)\,F^T(t) + G(t)\,Q(t)\,G^T(t)$
Filter algorithm at a measurement update	$\hat{x}_+(t) = \hat{x}_-(t) + K(t)\left[z(t) - h(\hat{x}_-, t)\right]$
Error variance algorithm at a measurement update	$P_+(t) = [I - K(t)\,H(t)]\,P_-(t)$
Optimal gain algorithm at a measurement update	$K(t) = P_-(t)\,H^T(t)\left[H(t)\,P_-(t)\,H^T(t) + R(t)\right]^{-1}$
Initial conditions	$\hat{x}(o) = E\{\hat{x}(t_o)\} = \mu_x(o)$ $P(o) = E\left[x(t_o) - \dot{x}(t_o)\right]\left[x(t_o) - \hat{x}(t_o)\right] = \sigma_x(o)$ $x(o) = x(t_o)$

Table 3.3

SYSTEM MODEL: $\dot{x}(t) = Fx(t) + Gu(t)$

$$\begin{bmatrix} \delta\dot{x} \\ \delta\dot{y} \\ \delta\dot{z} \\ \delta\dot{V}_x \\ \delta\dot{V}_z \end{bmatrix} = \begin{bmatrix} 0 & 0 & 0 & 1 & 0 \\ 0 & 0 & 0 & 0 & 0 \\ 0 & 0 & 0 & 0 & 1 \\ F41 & F42 & F43 & 0 & -2\omega_y \\ F51 & F52 & F53 & 2\omega_y & 0 \end{bmatrix} \begin{bmatrix} \delta x \\ \delta y \\ \delta z \\ \delta V_x \\ \delta V_z \end{bmatrix} + \begin{bmatrix} 1 & 0 & 0 & 0 & 0 \\ 0 & 1 & 0 & 0 & 0 \\ 0 & 0 & 1 & 0 & 0 \\ 0 & 0 & 0 & 0 & 0 \\ 0 & 0 & 0 & 0 & 0 \end{bmatrix} \begin{bmatrix} u_x \\ u_y \\ u_z \\ u_{Vx} \\ u_{Vz} \end{bmatrix}$$

$F41 = -\omega_s + \omega_y^2 + \omega_z^2$, $F51 = -\omega_x\omega_z$

$F42 = -\omega_x\omega_y$, $F52 = -\omega_y\omega_z$

$F43 = -\omega_x\omega_z$, $F53 = 2\omega_s + \omega_x^2 + \omega_y^2$

$\omega_x = 0$, $\omega_s = \sqrt{G_e/R_e}$

$\omega_y = \Omega \cos \lambda$

$\omega_z = \Omega \sin \lambda$

$\Omega = 15.04107$ degrees/hour, $G_e = 32.1724$ feet/second^2

$\lambda = 45$ degrees north latitude, $R_e = (6{,}378{,}388$ meters$)(3.281$ feet/meter$)$

$u_x = 1253$ feet , $u_{Vx} = 1.2$ feet/second

$u_y = 1317$ feet , $u_{Vz} = 1.4$ feet/second

$u_z = 1500$ feet

$\delta x(0) = 1253$ feet , $\delta V_x(0) = 10$ feet/second

$\delta y(0) = 1317$ feet , $\delta V_z(0) = 10$ feet/second

$\delta z(0) = 1500$ feet

Table 3.4

OBSERVATION MODEL: $z(t) = Hx(t) + v$

$$\begin{bmatrix} z_1 \\ z_2 \\ z_3 \end{bmatrix} = \begin{bmatrix} 1 & 0 & 0 & 0 & 0 \\ 0 & 1 & 0 & 0 & 0 \\ 0 & 0 & 1 & 0 & 0 \end{bmatrix} \begin{bmatrix} \delta x \\ \delta y \\ \delta z \\ \delta V_x \\ \delta V_z \end{bmatrix} + \begin{bmatrix} v_x \\ v_y \\ v_z \end{bmatrix}$$

Case 1 (1σ)	Case 2 (1σ)
v_x = 50 feet	v_x = 650 feet
v_y = 50 feet	v_y = 650 feet
v_z = 100 feet	v_z = 1200 feet

Table 3.5

ERROR VARIANCE MODEL: $\dot{P}(t) = FP(t) + P(t)F^T + GQG^T$

$P_{11}(0) = 10{,}000 \text{ feet}^2$,	$P_{44}(0) = 10^{-4} \text{ (feet/second)}^2$
$P_{22}(0) = 10{,}000 \text{ feet}^2$,	$P_{55}(0) = 10^{-4} \text{ (feet/second)}^2$
$P33(0) = 10{,}000 \text{ feet}^2$,	

*Initial conditions were obtained from reference [23].

CHAPTER IV. SIMULATION RESULTS AND DISCUSSION

4.1 OVERVIEW

The simulation of the complete system modeled in the preceding sections was performed on Stanford's IBM 360/67 digital computer. Several variations were incorporated in the simulation to provide data in meeting the objectives discussed in Chapter I.

Initially, runs were made with ten discrete measurement updates equally spaced in time (one every second). The equi-time spacing between updates was chosen based on results of Aoki and Li [24]. The Case I configuration used the best information available; i.e., radar measurement noise was limited to 50-feet 1 sigma in the X and Y channels and to 100-feet 1 sigma in the Z channel. These results are shown in Figs. 4.1 through 4.5. The optimal time varying gains were then observed from this data, Figs. 4.6 through 4.10, and were used to mechanize a suboptimal filter with fixed gains. Those results were shown in Figs. 4.11 through 4.14.

Then a simulation was performed, similar in every respect to the previous one except that radar measurements were decreased to 5; i.e., there was a measurement update once every 2 seconds in the 10-second simulated reentry. Again, the optimal gains were computed and then the results were used to mechanize a suboptimal fixed gain filter. These results are shown in Figs. 4.15 through 4.25.

Additionally, a set of data were obtained from the Case II configuration with five measurement updates. Recall Case II used the degraded measurement information in terms of increased covariance errors and measurement noise. The values of 650-feet 1 sigma in the X and Y channel and 1200-feet 1 sigma in the Z channel were used as measurement noise. These results are shown in Figs. 4.32 through 4.38.

There were other sensitivity checks made in this study. Although no graphs were plotted they represent additional results. A case of twenty updates with fixed gains was simulated and several cases with interchanged elements in the Case I and Case II configurations were also obtained and shown as Figs. 4.39 and 4.40. These results are discussed in the following paragraphs of this chapter.

4.2 TEN MEASUREMENT UPDATES, OPTIMAL GAINS, CASE I STATISTICS

The results indicating performance of the filter for this case are shown in Figs. 4.1 through 4.5. Each figure plots the value of ±1 standard deviation from the indicated covariance matrix value. That is, each graph representing one error state of the IMU has the square root of the term in the diagonal of the covariance matrix plotted as a positive and negative 1 sigma value. Because Gaussian statistics are used with zero mean values, the positive standard deviation (plus 1 sigma value) may be interpreted as the root mean square (RMS) error in estimating the applicable state variable. Additionally, each figure shows the difference between the actual state and the best estimate of it ($\delta x - \delta\hat{x}$) which is, in fact, the estimation error of the filter. One way of interpreting the results is to observe that the

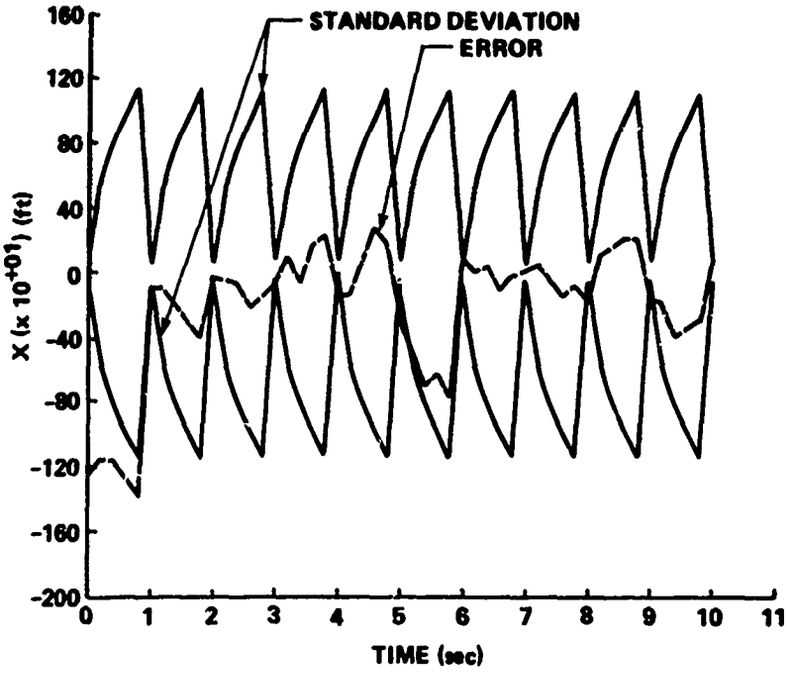

FIG 4.1. FILTER ERROR FOR OPTIMAL ESTIMATION OF THE IMU'S X POSITION ERROR WITH CASE I MEASUREMENT STATISTICS AND TEN UPDATES

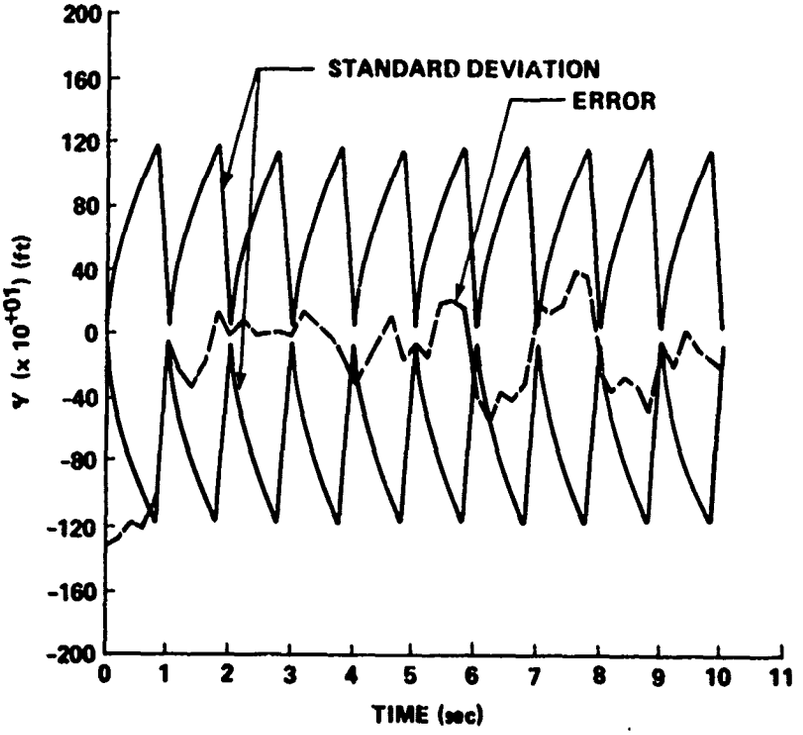

FIG 4.2. FILTER ERROR FOR OPTIMAL ESTIMATION OF THE IMU'S Y POSITION ERROR WITH CASE I MEASUREMENT STATISTICS AND TEN UPDATES

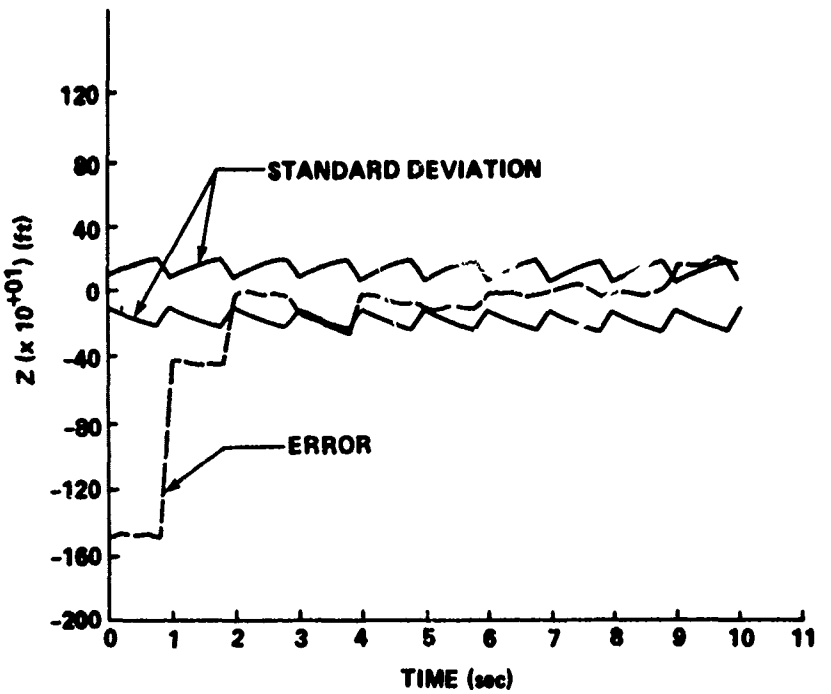

FIG 4.3. FILTER ERROR FOR OPTIMAL ESTIMATION OF THE IMU'S Z POSITION ERROR WITH CASE I MEASUREMENT STATISTICS AND TEN UPDATES

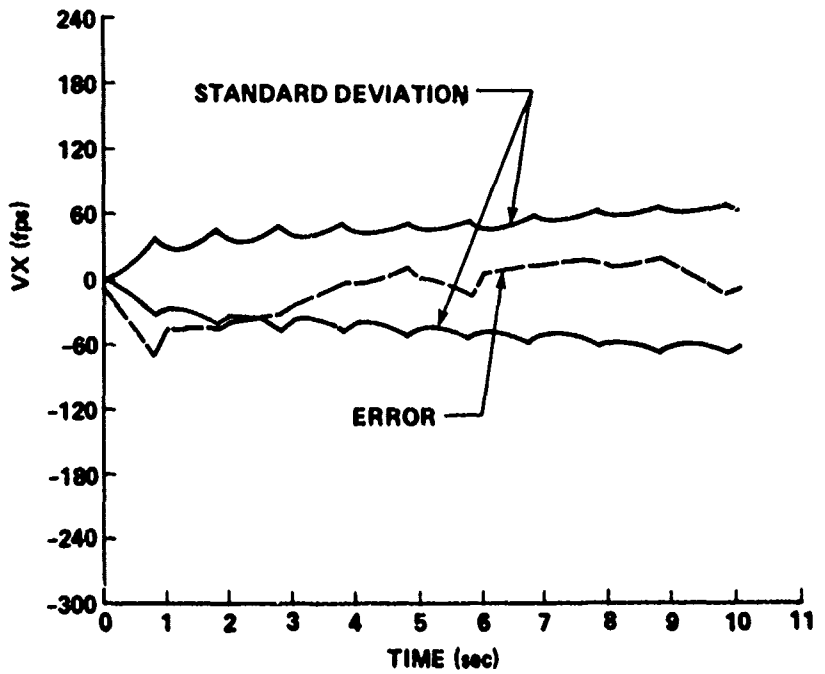

FIG 4.4 FILTER ERROR FOR OPTIMAL ESTIMATION OF THE IMU'S V_x VELOCITY ERROR WITH CASE I MEASUREMENT STATISTICS AND TEN UPDATES

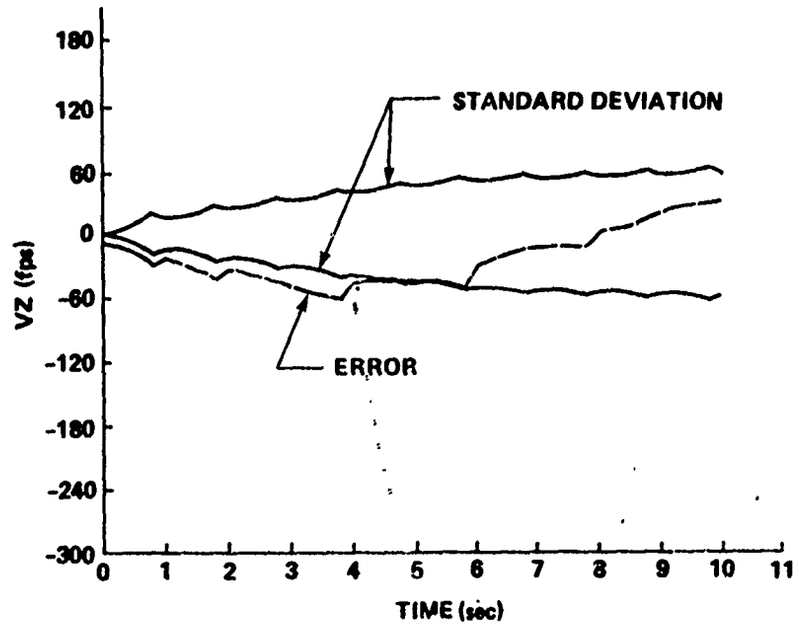

FIG 4.5. FILTER ERROR FOR OPTIMAL ESTIMATION OF THE IMU'S V_z VELOCITY ERROR WITH CASE I MEASUREMENT STATISTICS AND TEN UPDATES

error (the irregular or "noise-like" trace) should be within the ±1 sigma curves approximately 63 percent of the time if the filter is performing properly.

The time optimal gains generated by the filter are shown in Figs. 4.6 through 4.10. These are displayed so that the fixed gains chosen for the suboptimal filter can be readily compared.

4.3 TEN MEASUREMENT UPDATES, FIXED GAINS, CASE I STATISTICS

The fixed gains are chosen to closely approximate the optimal gains. They can not be properly selected without having computed the optimal solution first. For display purposes, the optimal gains are shown with the fixed gains so that a visual comparison can be made. These are also shown in Figs. 4.6 through 4.10.

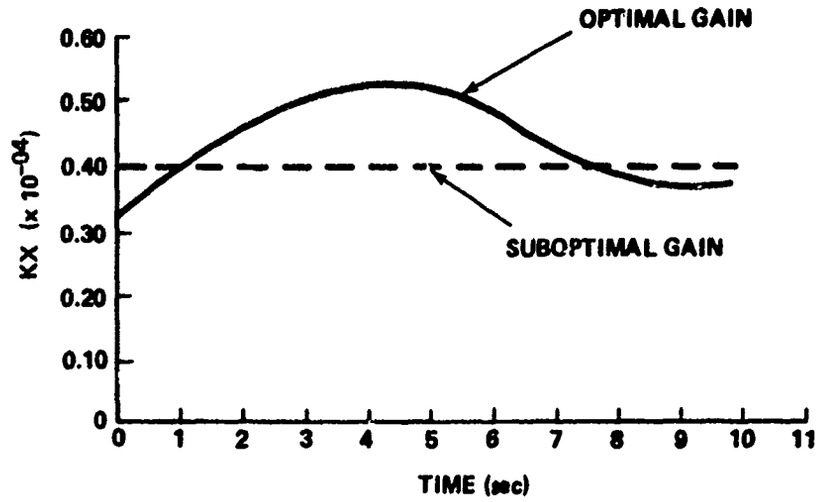

FIG 4.6. COMPARISON OF SUBOPTIMAL AND OPTIMAL TIME VARYING GAIN K_x FOR CASE I MEASUREMENT STATISTICS WITH TEN UPDATES

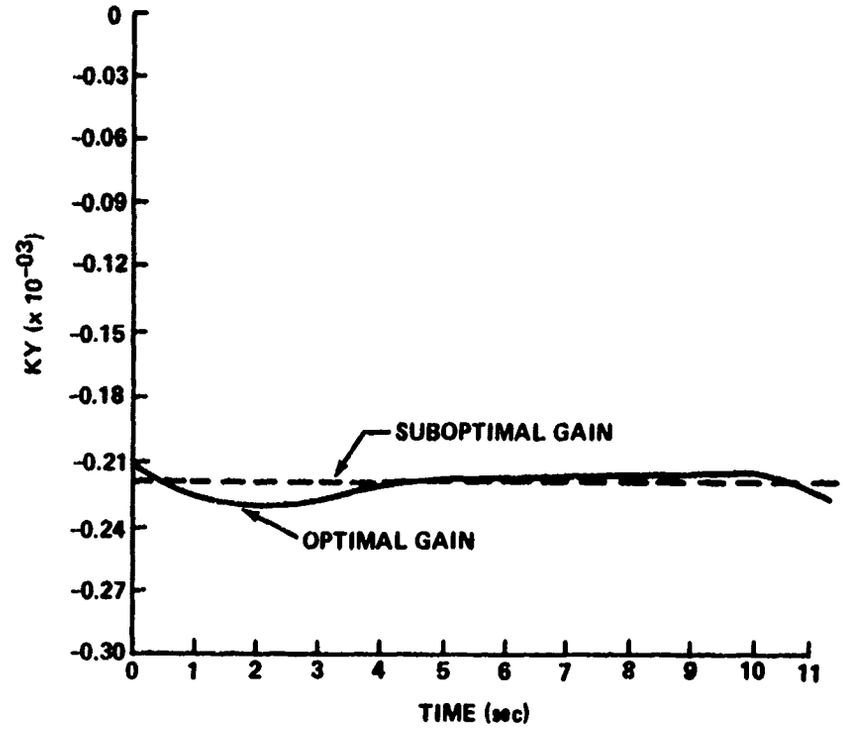

FIG 4.7. COMPARISON OF SUBOPTIMAL AND OPTIMAL TIME VARYING GAIN K_y FOR CASE I MEASUREMENT STATISTICS WITH TEN UPDATES

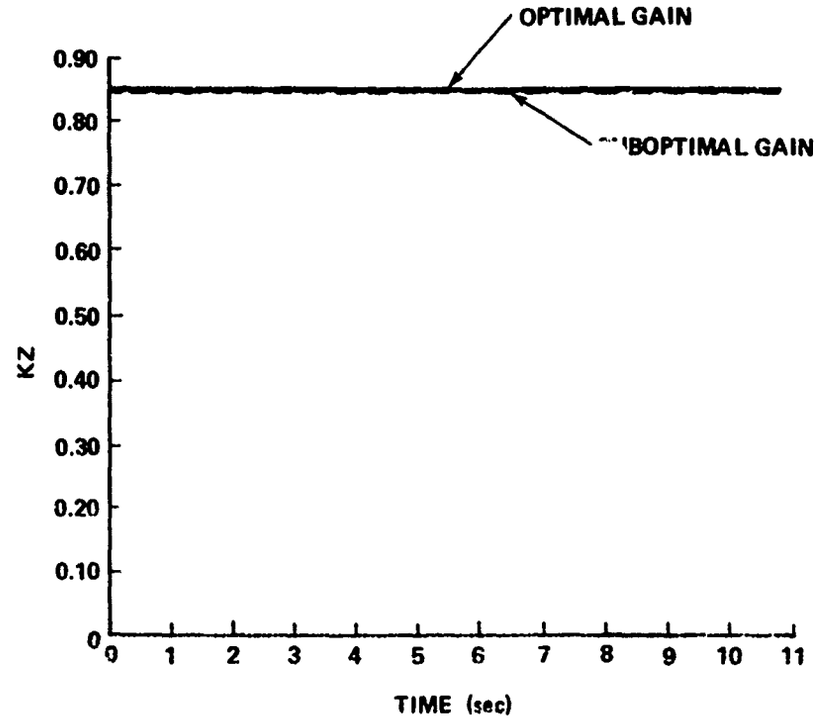

FIG 4.8. COMPARISON OF SUBOPTIMAL AND OPTIMAL TIME VARYING GAIN K_z FOR CASE I MEASUREMENT STATISTICS WITH TEN UPDATES

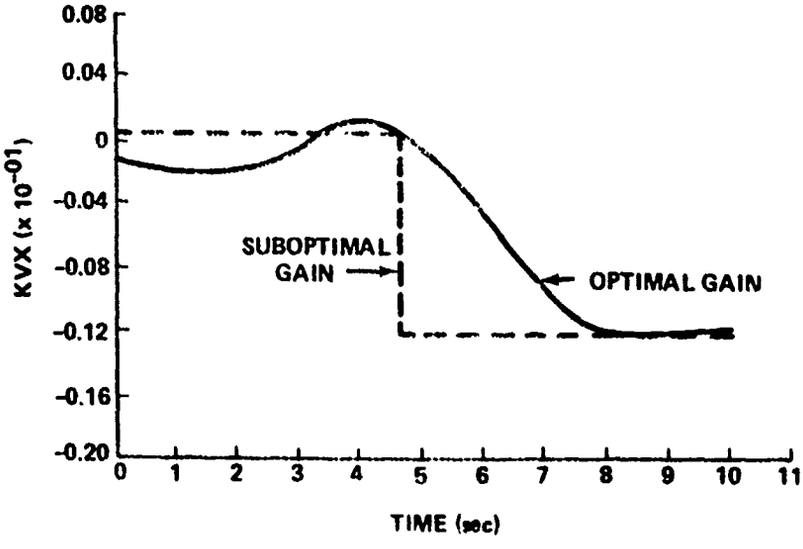

FIG 4.9. COMPARISON OF SUBOPTIMAL AND OPTIMAL TIME VARYING GAIN K_{VX} FOR CASE I MEASUREMENT STATISTICS WITH TEN UPDATES

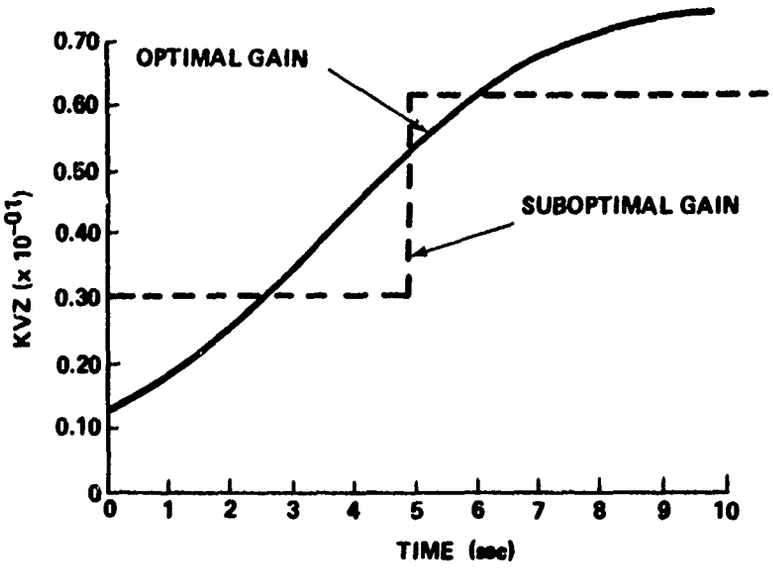

FIG 4.10. COMPARISON OF SUBOPTIMAL AND OPTIMAL TIME VARYING GAIN K_{vz} FOR CASE I MEASUREMENT STATISTICS WITH TEN UPDATES

The error in the filter in attempting to estimate the IMU error, is shown in Figs. 4.11 through 4.14. It is evident that the filter with fixed gains does not estimate the states as well as the filter with optimal gains. It is, in fact, divergent in some cases. Several reasons are available to explain this phenomenon. These are discussed more completely in Chapter 4.9.

4.4 FIVE MEASUREMENT UPDATES, OPTIMAL GAINS, CASE I STATISTICS

The format of the graphical data is similar to the case for ten measurement updates. To minimize data presentation which may appear repetitious (it is not) and to enhance the comparison, the covariance error data represented as the positive standard deviation is plotted in Figs. 4.15 and 4.16. The same comparison is done for the filter's

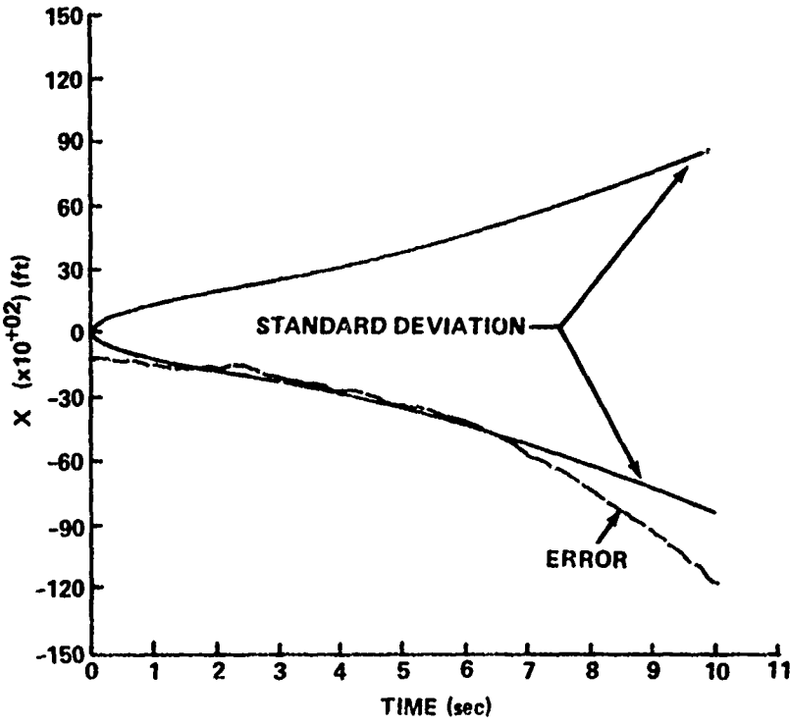

FIG 4.11. FILTER ERROR FOR SUBOPTIMAL ESTIMATION OF THE IMU'S X POSITION ERROR WITH CASE I MEASUREMENT STATISTICS AND TEN UPDATES

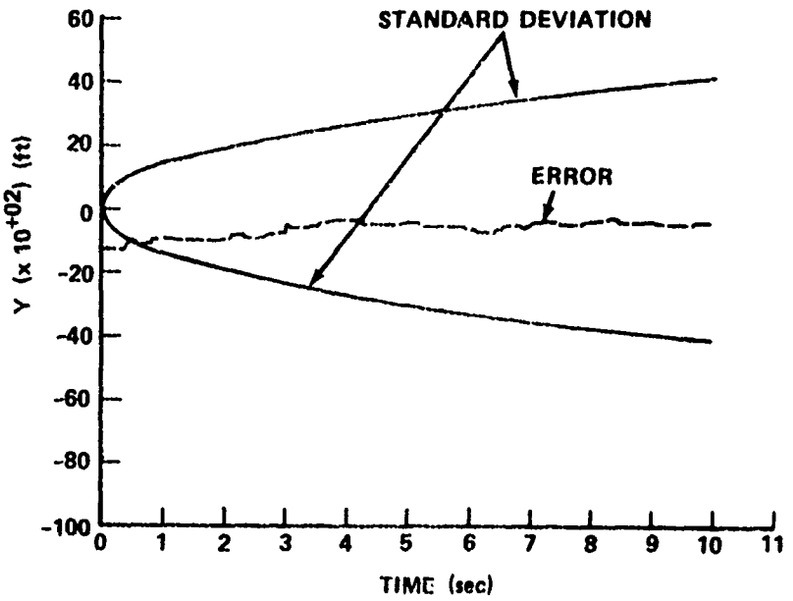

FIG 4.12. FILTER ERROR FOR SUBOPTIMAL ESTIMATION OF THE IMU'S Y POSITION ERROR WITH CASE I MEASUREMENT STATISTICS AND TEN UPDATES

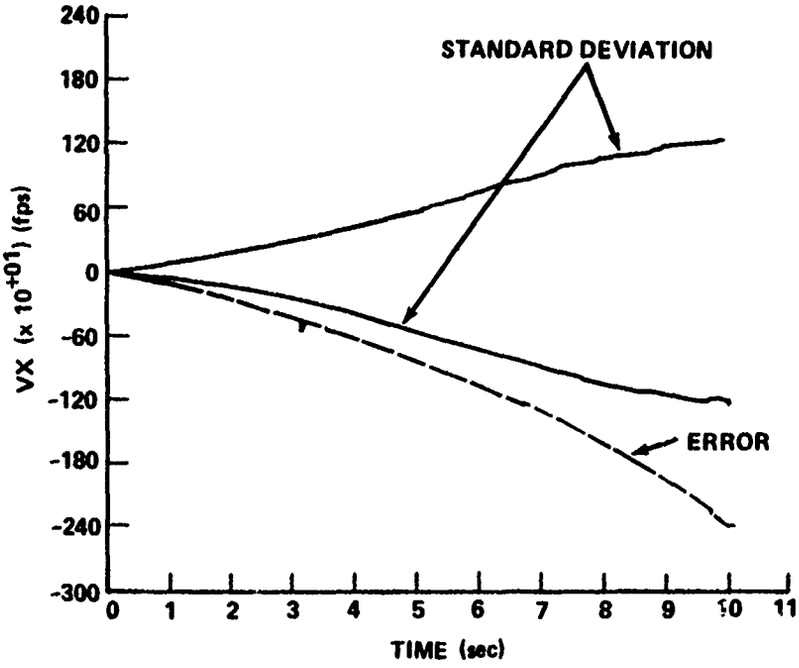

FIG 4.13. FILTER ERROR FOR SUBOPTIMAL ESTIMATION OF THE IMU'S V_x VELOCITY ERROR WITH CASE I MEASUREMENT STATISTICS AND TEN UPDATES

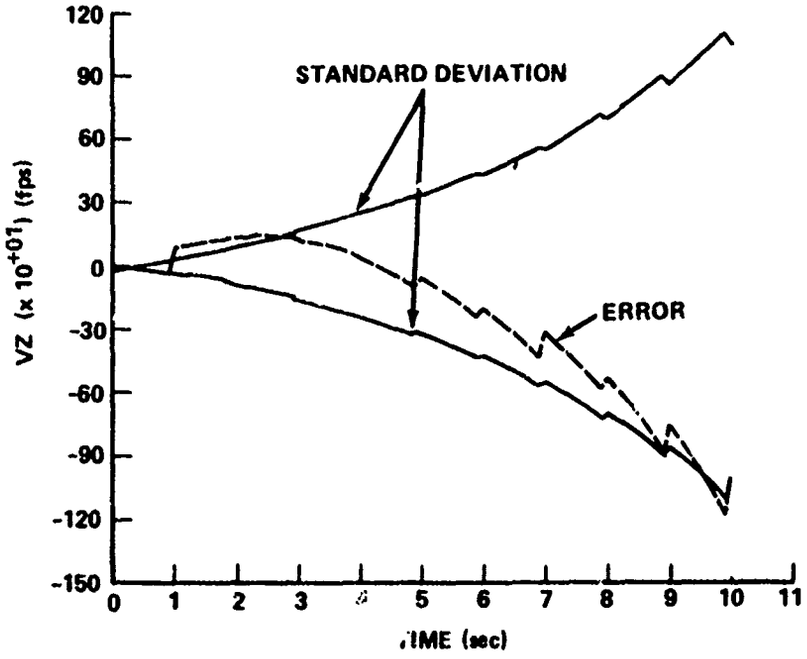

FIG 4.14. FILTER ERROR FOR SUBOPTIMAL ESTIMATION OF THE IMU'S V_z VELOCITY ERROR WITH CASE I MEASUREMENT STATISTICS AND TEN UPDATES

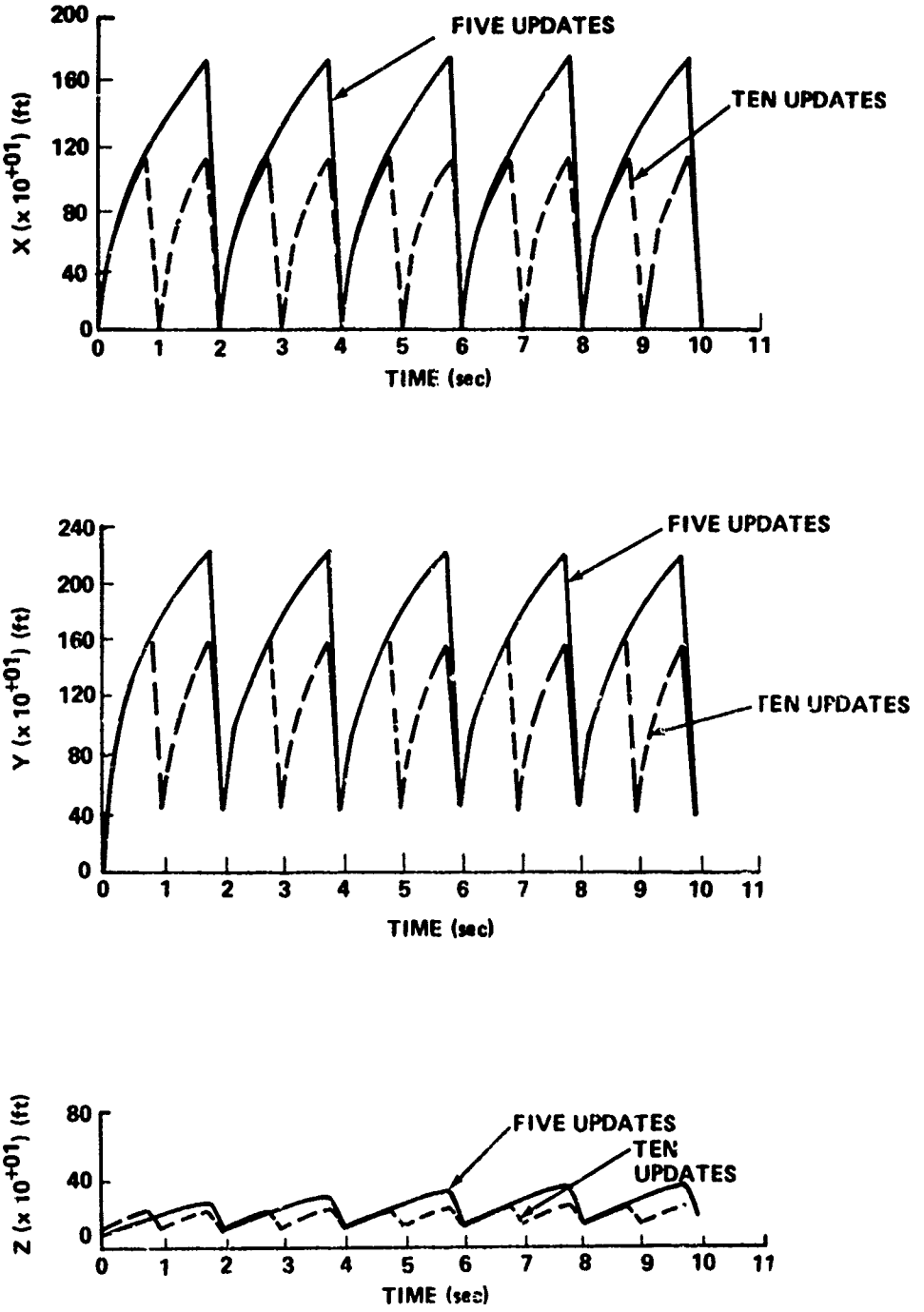

FIG. 4.15. COMPARISON OF IMU'S RMS POSITION ERROR HISTORIES USING OPTIMAL GAINS WITH 10 POSITION FIX ERRORS OF 50-FOOT RMS IN X AND Y AND 100-FOOT RMS IN Z

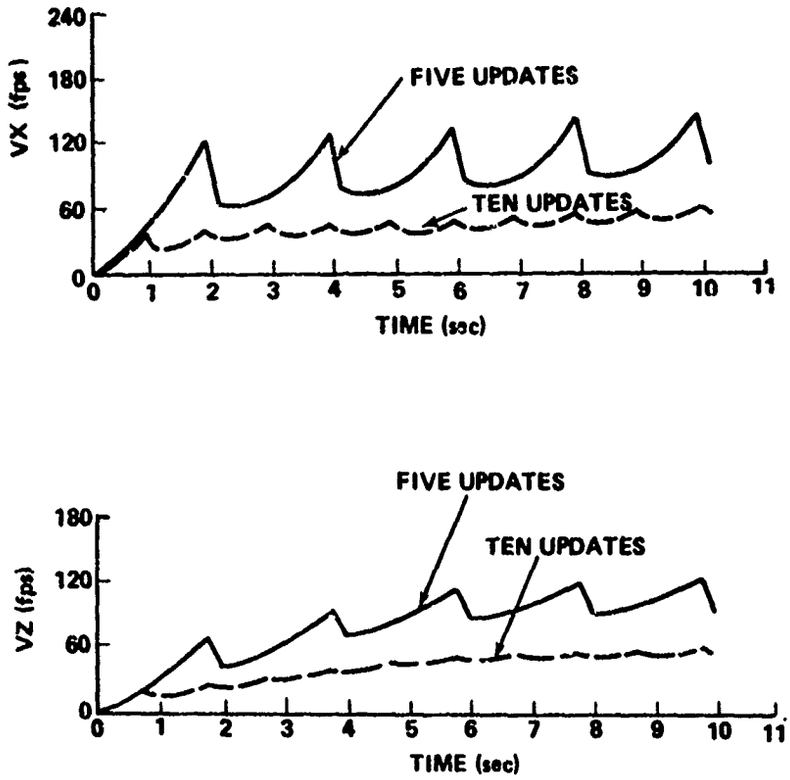

FIG 4.16. COMPARISON OF IMU'S RMS VELOCITY ERROR HISTORIES USING OPTIMAL GAINS WITH TEN POSITION FIX ERRORS OF 50-FOOT RMS IN X AND Y AND 100-FOOT RMS IN Z

error in the estimate of the IMU error states in Figs. 4.17 through 4.20. As can be seen, there is better performance from the filter in the case where ten updates are used.

4.5 FIVE MEASUREMENT UPDATES, FIXED GAINS, CASE I STATISTICS

The fixed gains compared to the optimal gains are given in Figs. 4.21 through 4.25. Because of the change in the graphs' ordinate scale the direct comparison to the ten measurement case is not possible to display. However, again it is noted that the filter performance is poorer when the number of measurements is decreased.

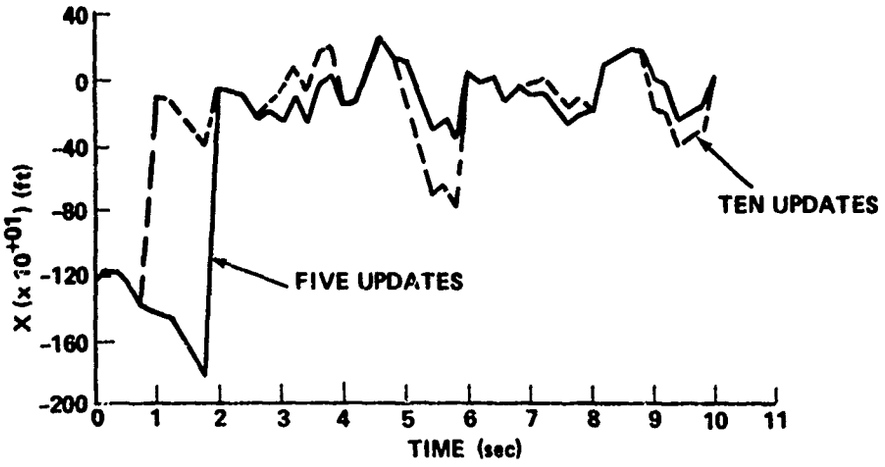

FIG 4.17. COMPARISON OF FILTER ERROR FOR OPTIMAL ESTIMATION OF THE IMU'S X POSITION ERROR WITH CASE I STATISTICS

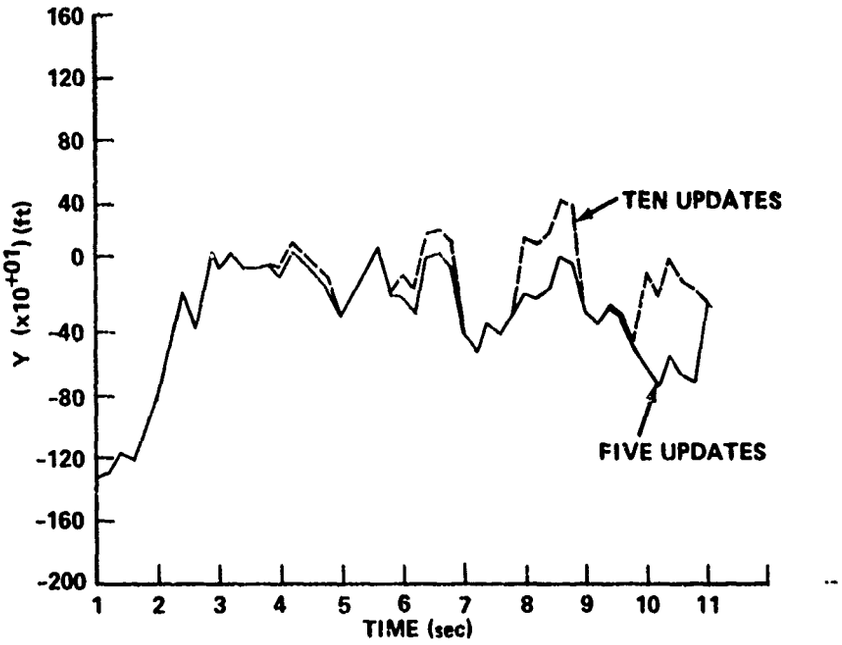

FIG 4.18 COMPARISON OF FILTER ERROR FOR OPTIMAL ESTIMATION OF THE IMU'S Y POSITION ERROR WITH CASE I STATISTICS

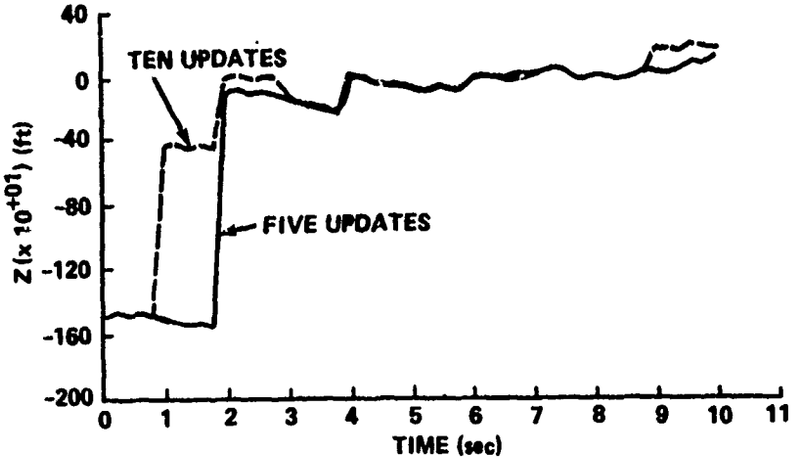

FIG 4.19. COMPARISON OF FILTER ERROR FOR OPTIMAL ESTIMATION OF THE IMU'S Z POSITION ERROR WITH CASE I STATISTICS

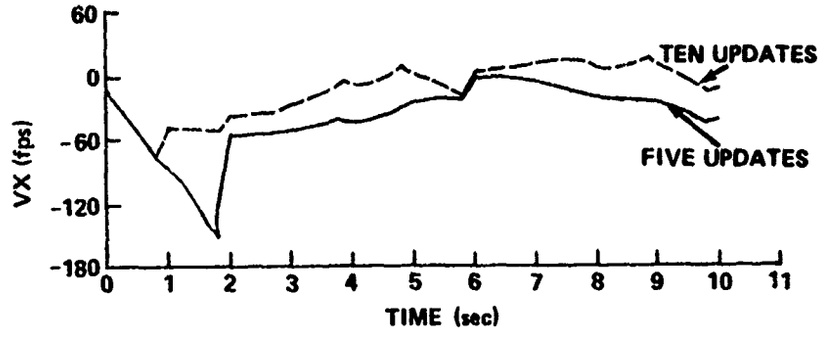

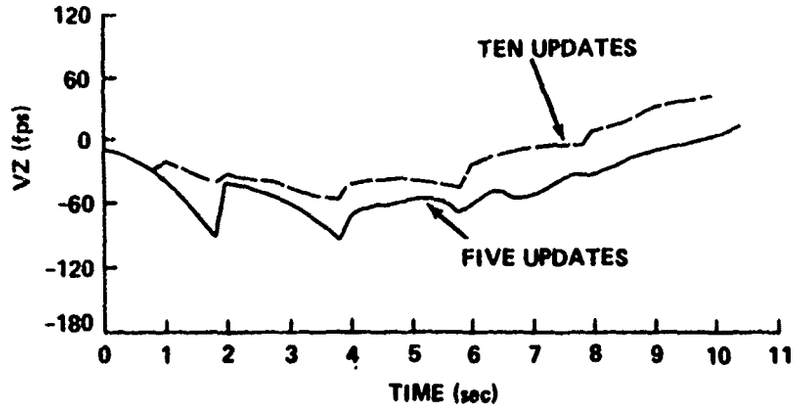

FIG 4.20. COMPARISON OF FILTER ERROR FOR OPTIMAL ESTIMATION OF THE IMU'S V_x AND V_z VELOCITY ERRORS WITH CASE I STATISTICS

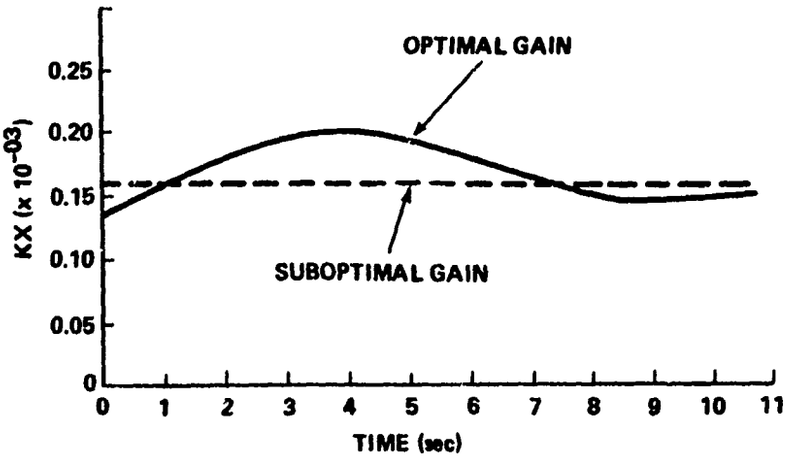

FIG 4.21. COMPARISON OF SUBOPTIMAL AND OPTIMAL TIME VARYING GAIN K_x WITH CASE I MEASUREMENT STATISTICS AND FIVE UPDATES

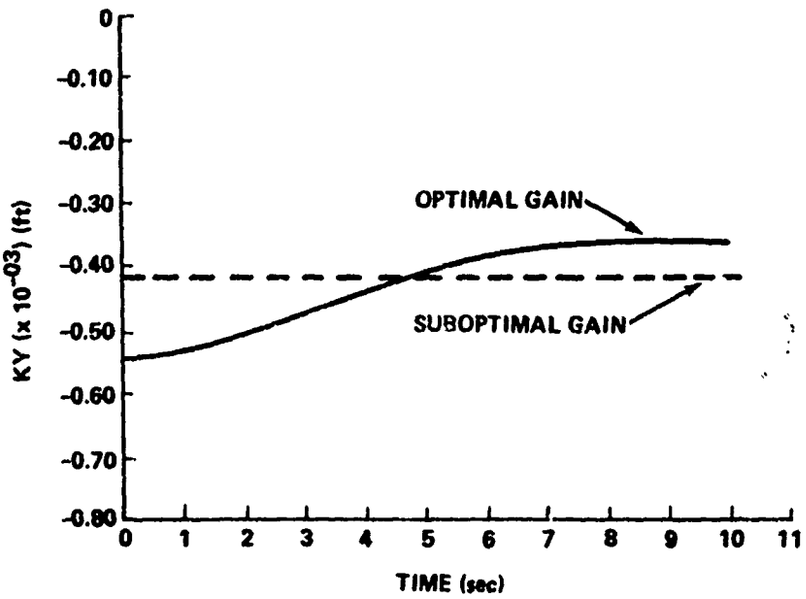

FIG 4.22. COMPARISON OF SUBOPTIMAL AND OPTIMAL TIME VARYING GAIN K_y WITH CASE I MEASUREMENT STATISTICS AND FIVE UPDATES

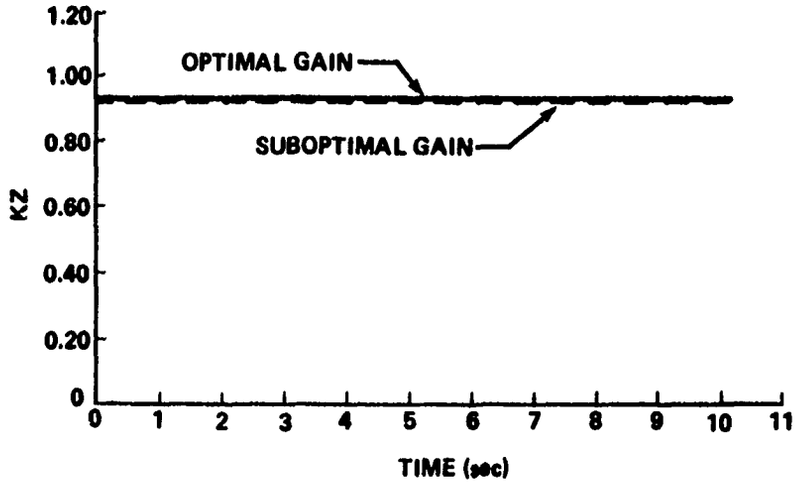

FIG 4.23. COMPARISON OF SUBOPTIMAL AND OPTIMAL TIME VARYING GAIN K_z WITH CASE I MEASUREMENT STATISTICS AND FIVE UPDATES

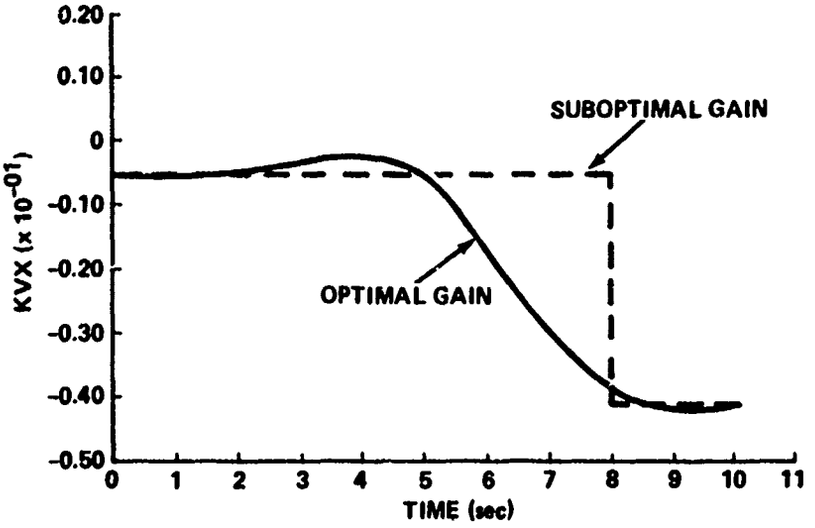

FIG 4.24. COMPARISON OF SUBOPTIMAL AND OPTIMAL TIME VARYING GAIN K_{vx} WITH CASE I MEASUREMENT STATISTICS AND FIVE UPDATES

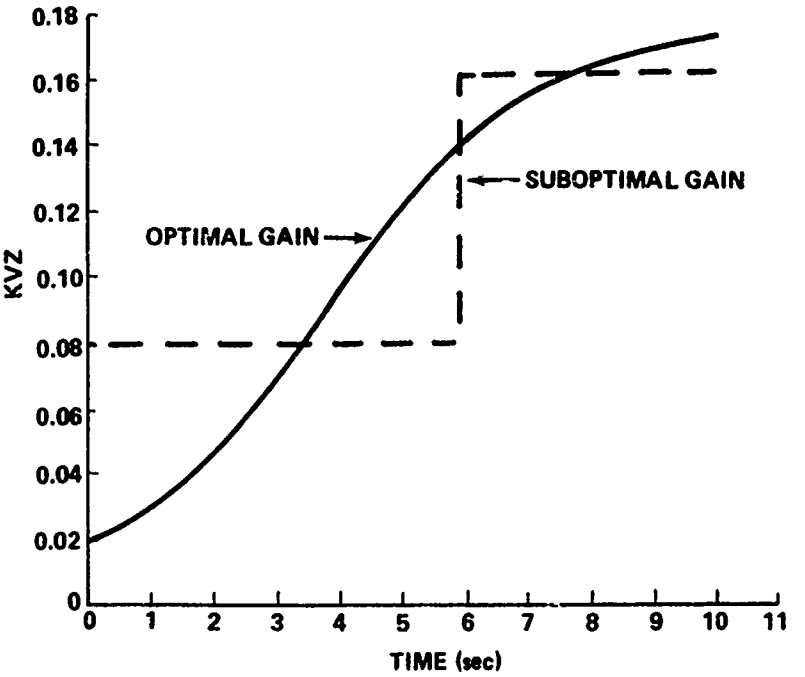

FIG 4.25. COMPARISON OF SUBOPTIMAL AND OPTIMAL TIME VARYING GAIN K_{VZ} WITH CASE I MEASUREMENT STATISTICS AND FIVE UPDATES

The filter errors are shown in Figs. 4.26 through 4.29. They are also seen to diverge and for the same reasons as in the ten measurement fixed gain case.

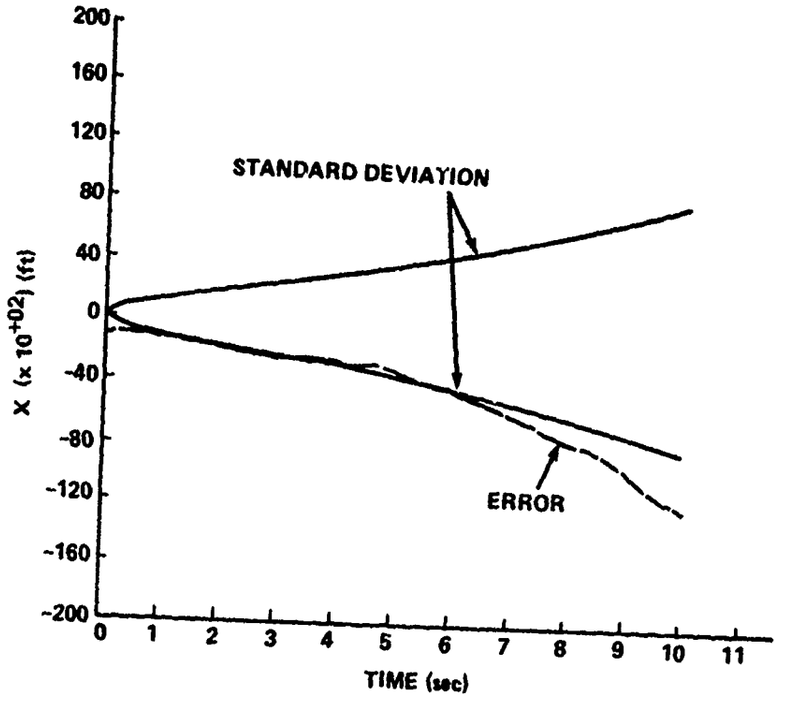

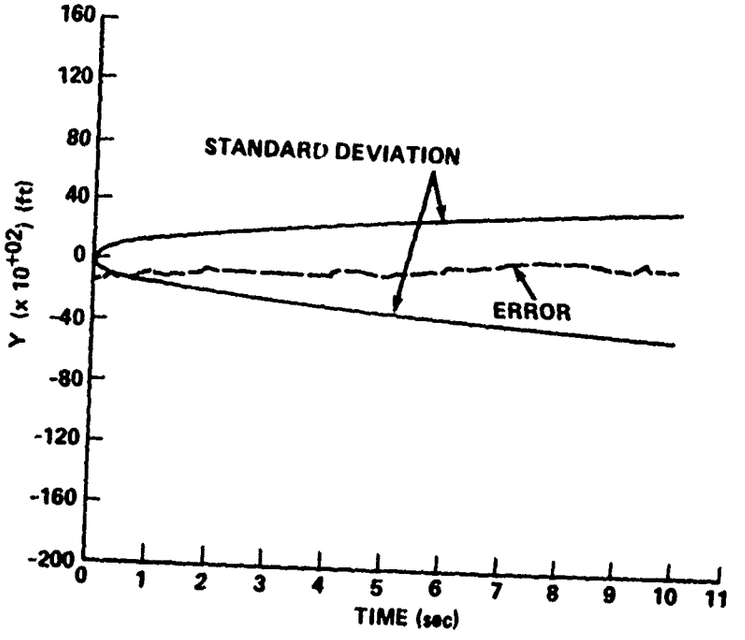

FIG 4.26. FILTER ERROR FOR SUBOPTIMAL ESTIMATION OF THE IMU'S X AND Y POSITION ERRORS WITH CASE I MEASUREMENT STATISTICS AND FIVE UPDATES

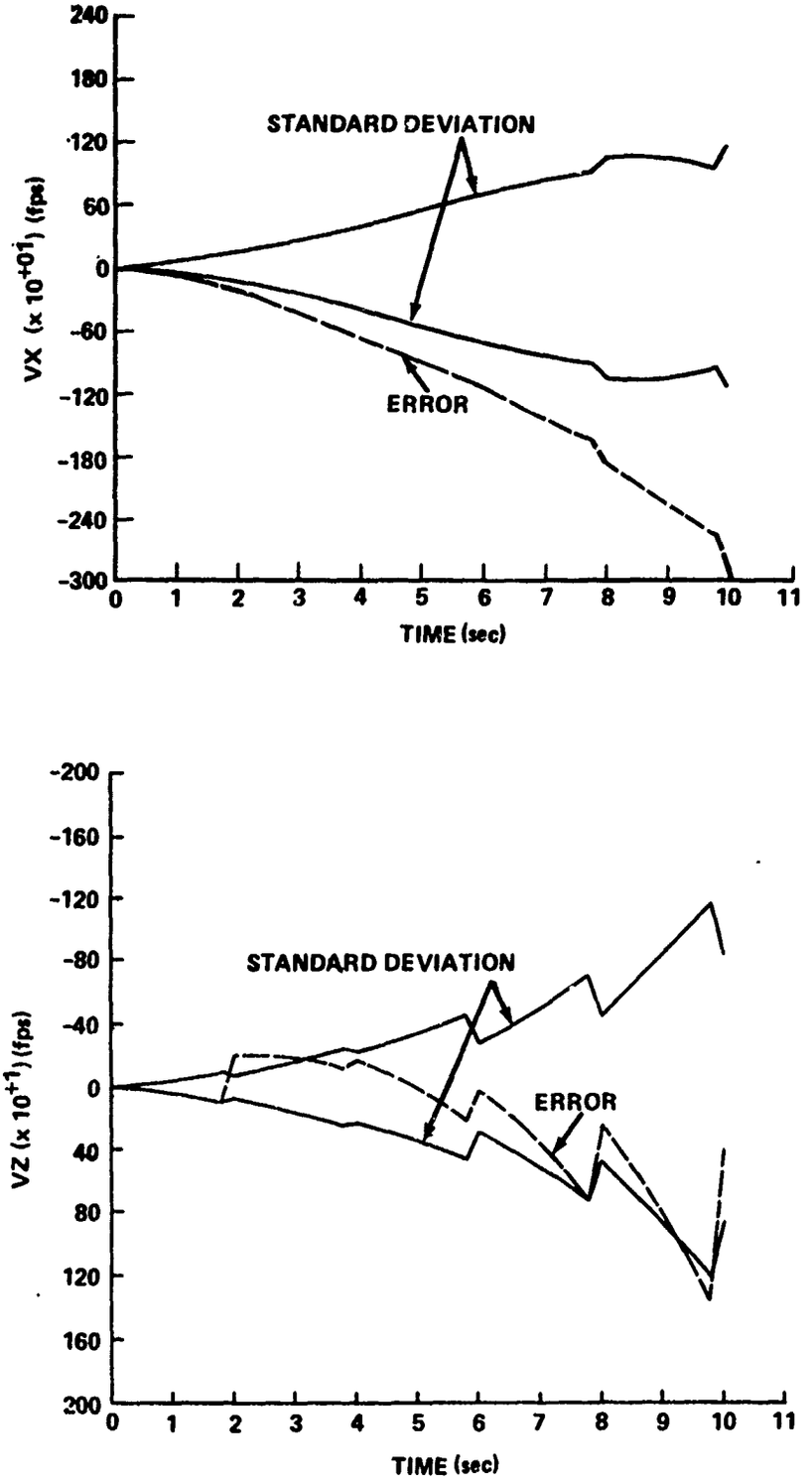

FIG 4.27. FILTER ERROR FOR SUBOPTIMAL ESTIMATION OF THE IMU'S V_x AND V_z VELOCITY ERRORS WITH CASE I MEASUREMENT STATISTICS AND FIVE UPDATES

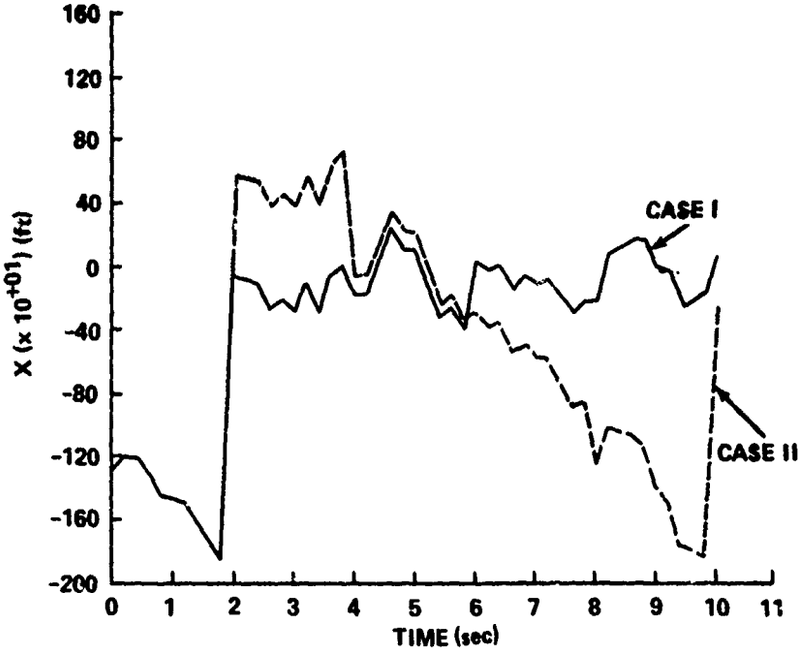

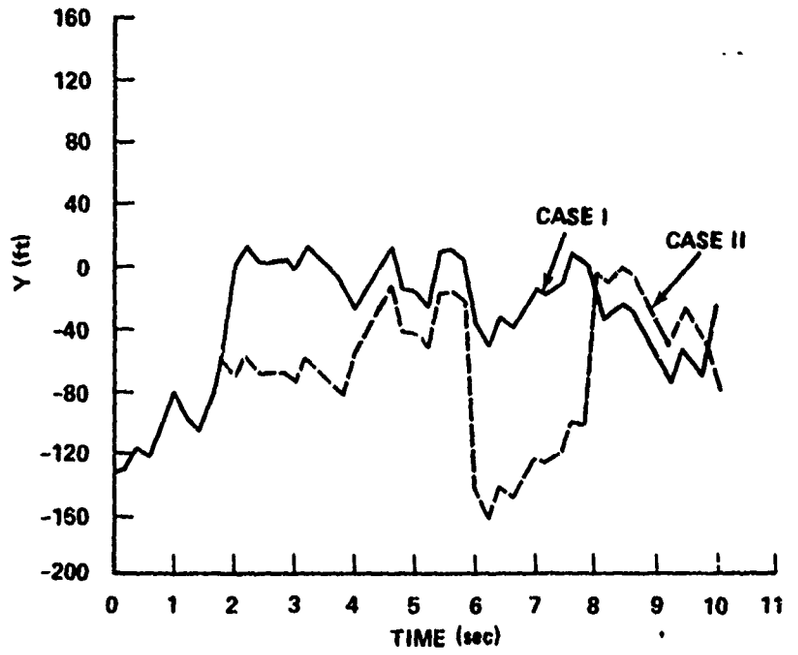

FIG 4.28 COMPARISON OF FILTER ERROR FOR OPTIMAL ESTIMATION OF THE IMU'S X AND Y POSITION ERRORS WITH FIVE UPDATES

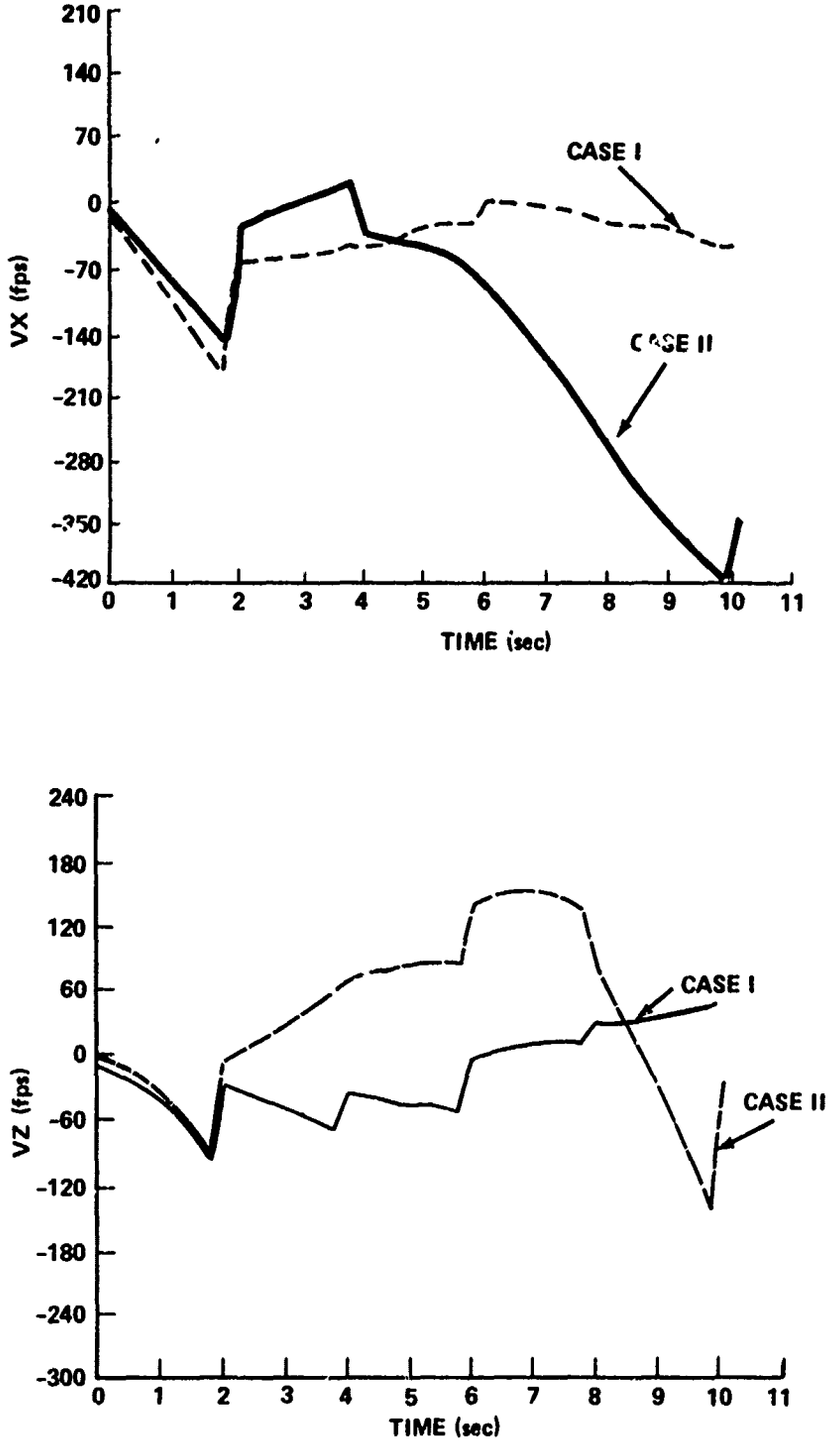

FIG 4.29. COMPARISON OF FILTER ERROR FOR OPTIMAL ESTIMATION OF THE IMU'S V_x AND V_z VELOCITY ERRORS WITH FIVE UPDATES

4.6 FIVE MEASUREMENT UPDATES, OPTIMAL GAINS, CASE II STATISTICS

The filter errors for this case are shown plotted against the filter errors for optimal gains, Case I. Case II differs from Case I in measurement noise parameters. In Case II, V_x and V_y are 650-foot root mean square compared to 50-feet RMS for CASE I. Also, v_z is larger at 1200-foot RMS compared to v_z of Case I which is 100-foot RMS. The increase in measurement error parameters reflect the attempt to include the error caused by radar area correlator time delay that occurs while obtaining a position measurement. The 1100-foot increase in v_z measurement error is used to obtain another set of results by using a fixed error in altitude. In reality, the actual radar altimeter error is 10 percent of the indicated value.

The results shown in Figs. 4.28 and 4.29 verify that the filter errors are smaller without consideration of the time delay; however, care must be taken. The truer more realistic case is given by the larger filter error. There can not be enough emphasis placed on the statement that the filter is only as good, at best, as the model used to describe the real system. Because the model used for this study can never be completely defined to represent an actual system, the filter's performance will vary according to the information mathematically included in its make up.

The ±1 sigma values of the expected error are shown in a comparative display of the Case I and Case II results. Again, as expected, a larger measurement error yields a larger standard deviation. These are shown in Figs. 4.30 and 4.31.

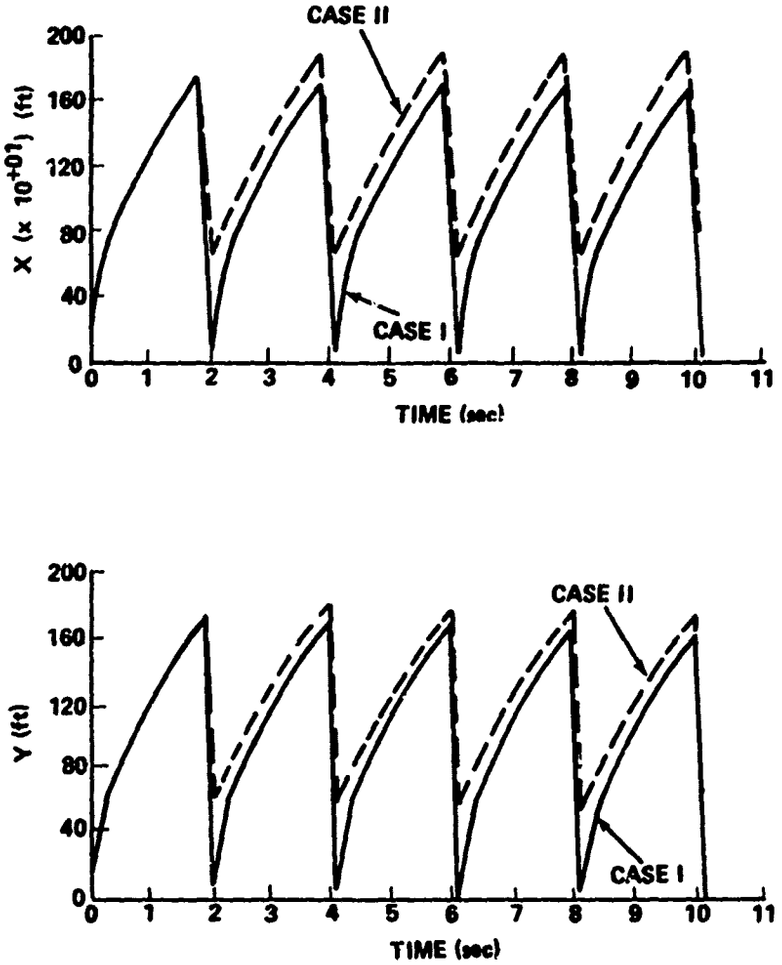

FIG. 4.30. COMPARISON OF IMU'S RMS POSITION ERROR HISTORIES USING OPTIMAL GAINS WITH FIVE POSITION FIX ERRORS OF 650-FOOT RMS IN X AND Y AND 1,200-FOOT RMS IN Z

4.7 FIVE MEASUREMENT UPDATES, FIXED GAINS, CASE II STATISTICS

The gains of the optimal filter are shown with the fixed gains chosen to mechanize the suboptimal filter of Case II. These are given as Figs. 4.32 through 4.36. The Case II optimal gains are shown with them. The results of the Case II fixed gains are plotted with the standard deviations and the filter errors in Figs. 4.37 and 4.38. These errors in estimating the states are larger than the Case I results seen earlier.

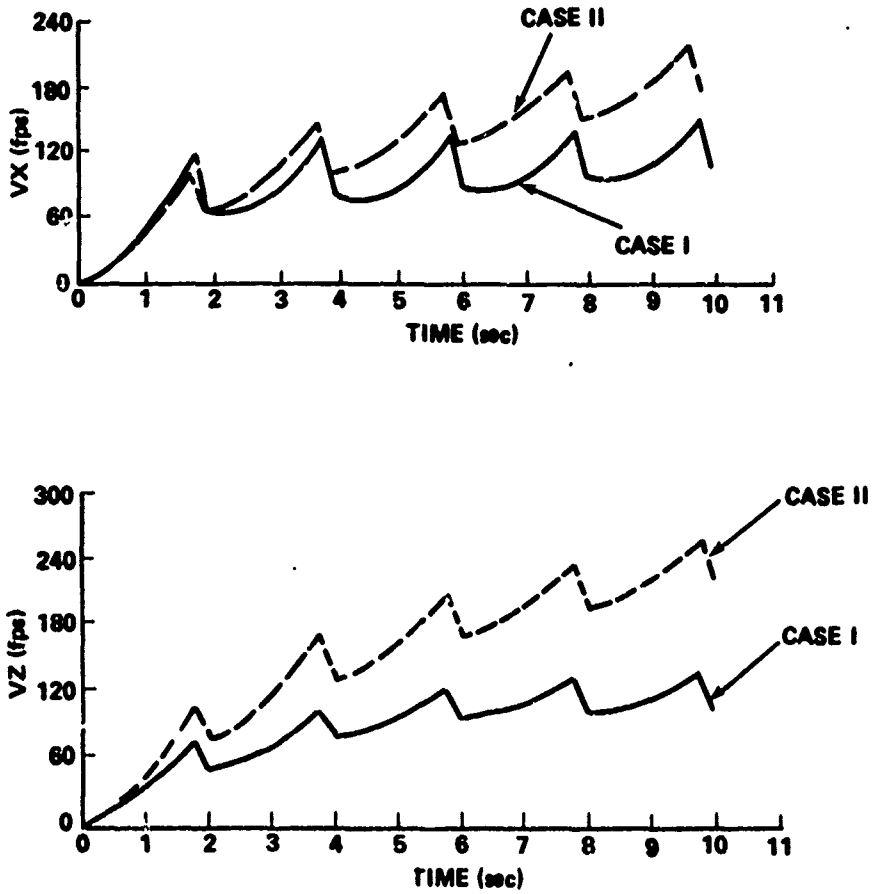

FIG. 4.31. COMPARISON OF IMU'S RMS VELOCITY ERROR HISTORIES USING OPTIMAL GAINS WITH FIVE POSITION FIX ERRORS OF 650-FOOT RMS in X and Y AND 1200-FOOT RMS IN Z

4.8 ADDITIONAL RESULTS

During the course of this study, several changes were made to the model. As was mentioned earlier, the problem of the negative definite error covariance matrix was investigated and corrected with a method that proved successful in obtaining the plots. In one instance, however, a different method of fix was used. The particular simulation was performed with fixed gains obtained from the optimal ten measurement update results. (Recall that only in the fixed gain runs did the

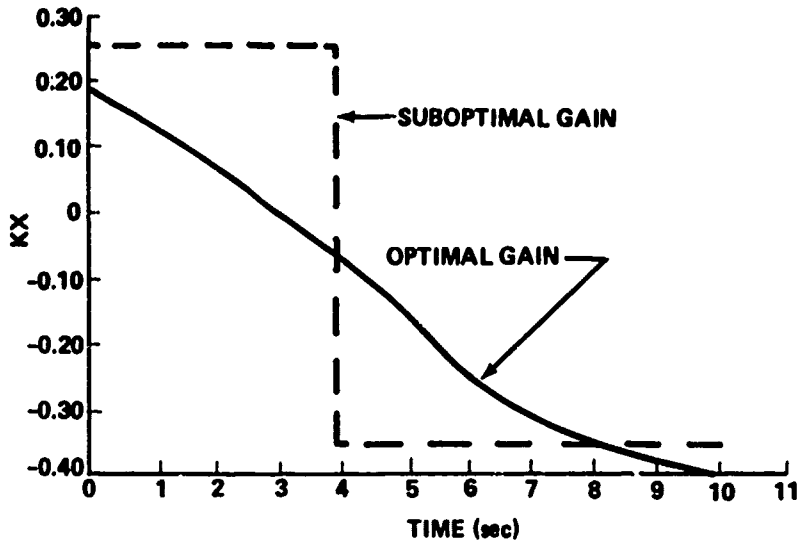

FIG. 4.32. COMPARISON OF SUBOPTIMAL AND OPTIMAL TIME VARYING GAIN K_x WITH CASE II MEASUREMENT STATISTICS AND FIVE UPDATES

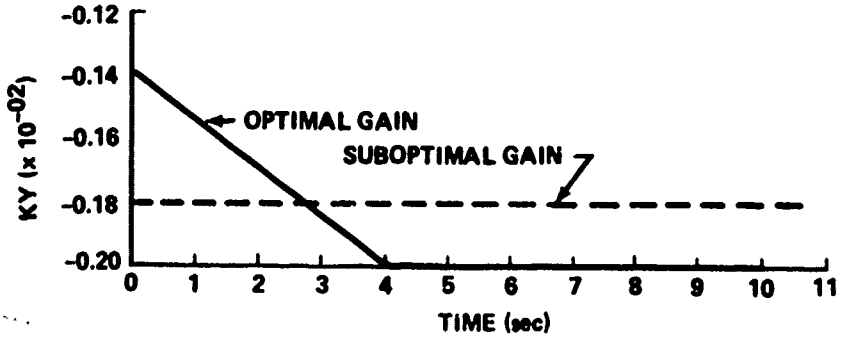

FIG. 4.33. COMPARISON OF SUBOPTIMAL AND OPTIMAL TIME VARYING GAIN K_y WITH CASE II MEASUREMENT STATISTICS AND FIVE UPDATES

negative definite covariance appear.) To overcome the divergence, a smaller integration step size was chosen, 0.05 second compared to 0.2 second, and the number of measurement updates was increased from 10 to 20. Though not displayed here, the results indicated that the covariance matrix become positive semidefinite. The filter error was approximately 10-percent smaller than the fixed five and the fixed ten update

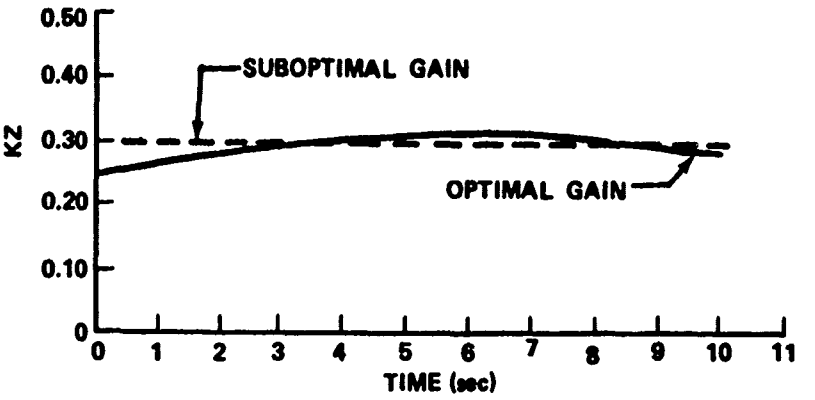

FIG 4.34. COMPARISON OF SUBOPTIMAL AND OPTIMAL TIME VARYING GAIN K_z WITH CASE II MEASUREMENT STATISTICS AND FIVE UPDATES

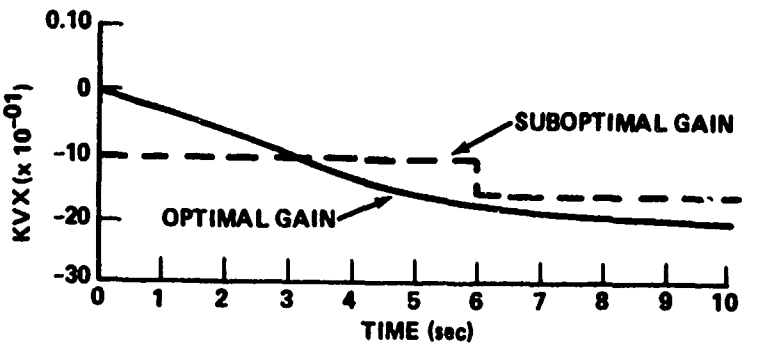

FIG 4.35. COMPARISON OF SUBOPTIMAL AND OPTIMAL TIME VARYING GAIN K_{vx} WITH CASE II MEASUREMENT STATISTICS AND FIVE UPDATES

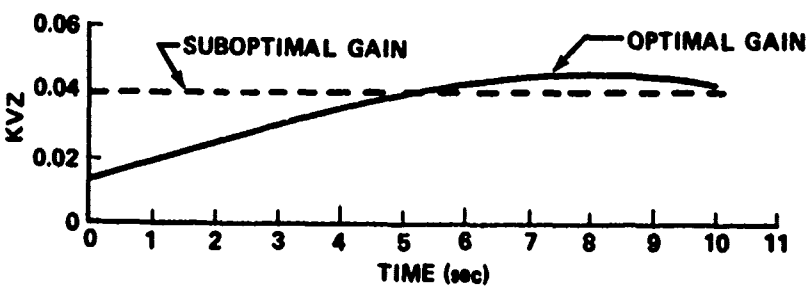

FIG 4.36. COMPARISON OF SUBOPTIMAL AND OPTIMAL TIME VARYING GAIN K_{vz} WITH CASE II MEASUREMENT STATISTICS AND FIVE UPDATES

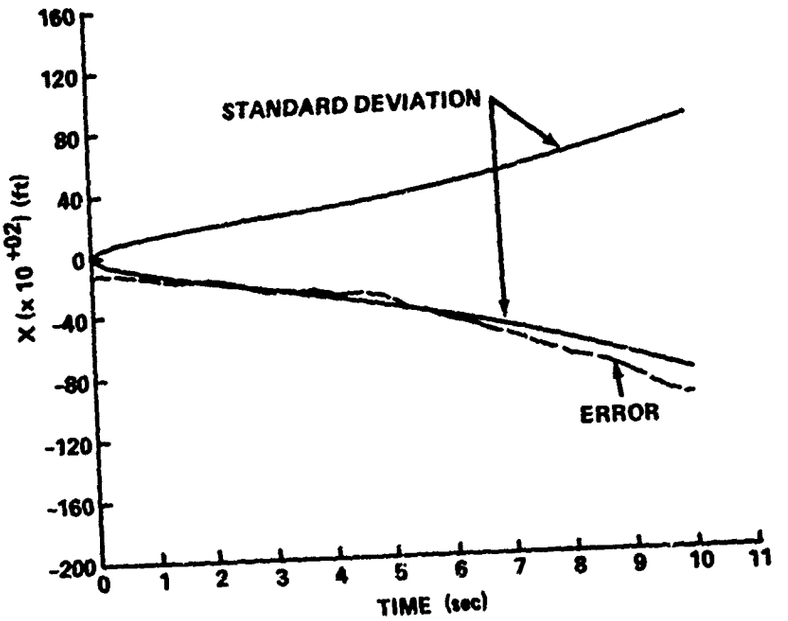

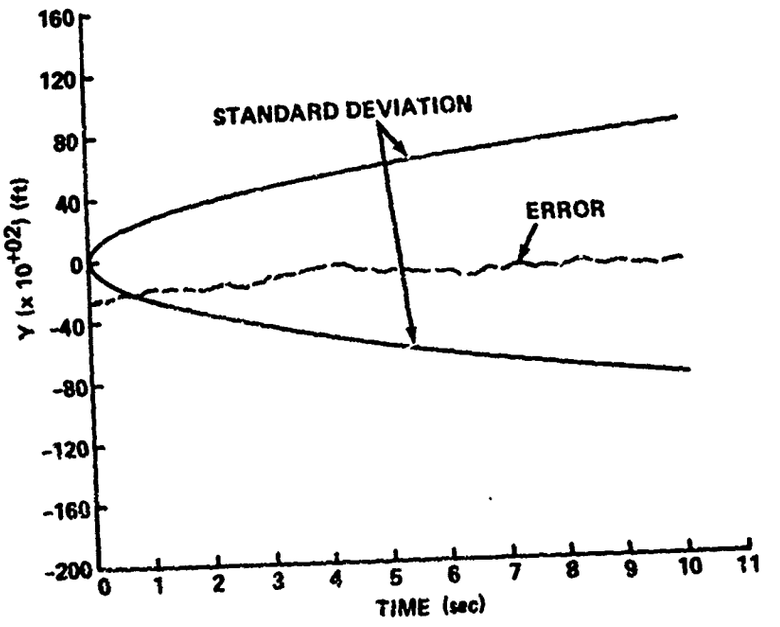

FIG 4.37. FILTER ERROR FOR SUBOPTIMAL ESTIMATION OF THE IMU'S X AND Y POSITION ERRORS WITH CASE II MEASUREMENT STATISTICS AND FIVE UPDATES

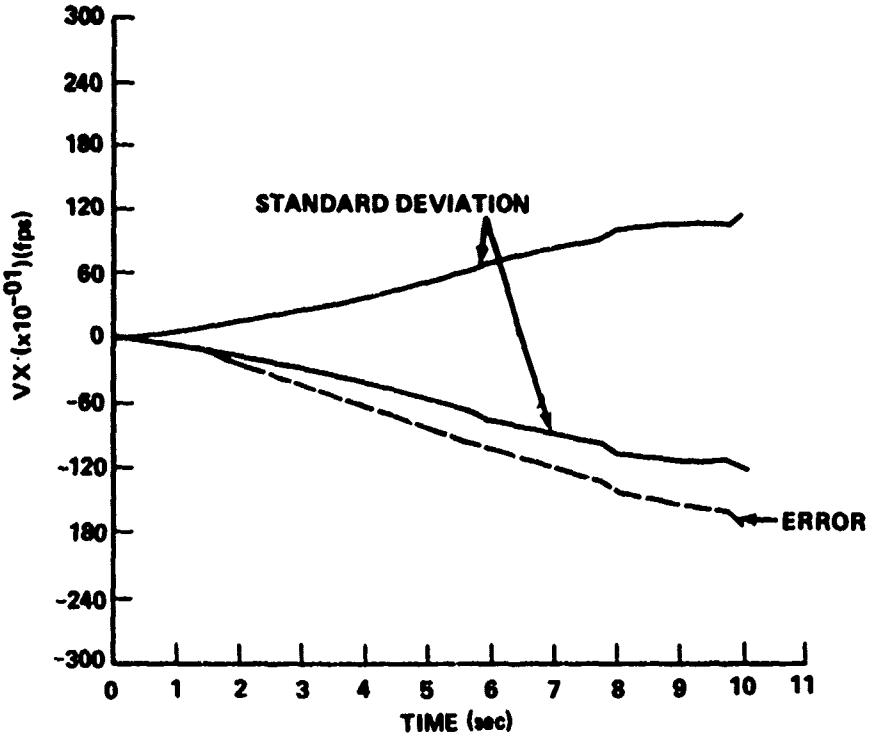

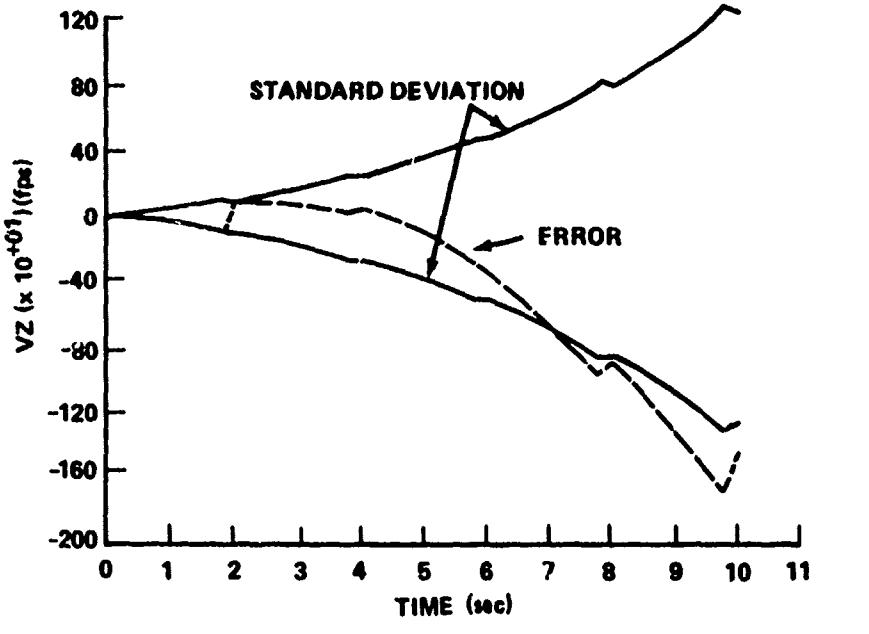

FIG 4.38. FILTER ERROR FOR SUBOPTIMAL ESTIMATION OF THE IMU'S V_x AND V_z VELOCITY ERRORS

cases. However, this filter also began to diverge near the last several seconds in much the same manner as the other fixed gain cases. From the trend observed on several states, a simulated flight of larger than 10 seconds may have eventually resulted in all of the error state estimates diverging.

Another case was run in which the measurement noise was increased to reflect a Case II situation but the R-matrix values were the reduced values of the Case I situation. This was for a five measurement update fixed gains simulation with gains chosen from the Case I results. There was virtually no noticeable change from the straight Case I results in the plots. The results were exactly the same as those displayed in Figs. 4.11 through 4.14.

Pursuing this one more step; additional runs were made but the R-matrix values were increased to fully reflect the Case II situation. Once again, however, the fixed gains were chosen from Case I. Again, the results obtained were almost exactly these of Case I. The conclusion is inescapable, the filter is not sensitive to measurement error and measurement error covariance matrix changes when the gains are fixed. The filter is a function of the gains alone in the fixed gain mode. Different results are obtained when the same simulation is run with the exception that fixed gains, more accurately reflecting Case II, are chosen. Those results are in Figs. 4.39 and 4.40 and are different from the Case I fixed gains with Case II statistics.

4.9 DISCUSSION OF RESULTS

The error of the filter in estimating the IMU error states was shown to be larger in every case where the fixed gains were used. In

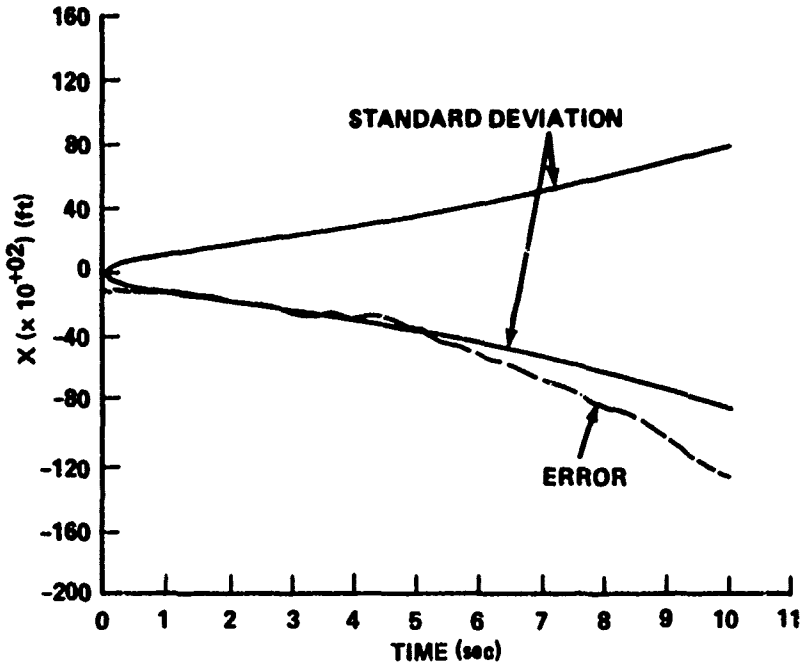

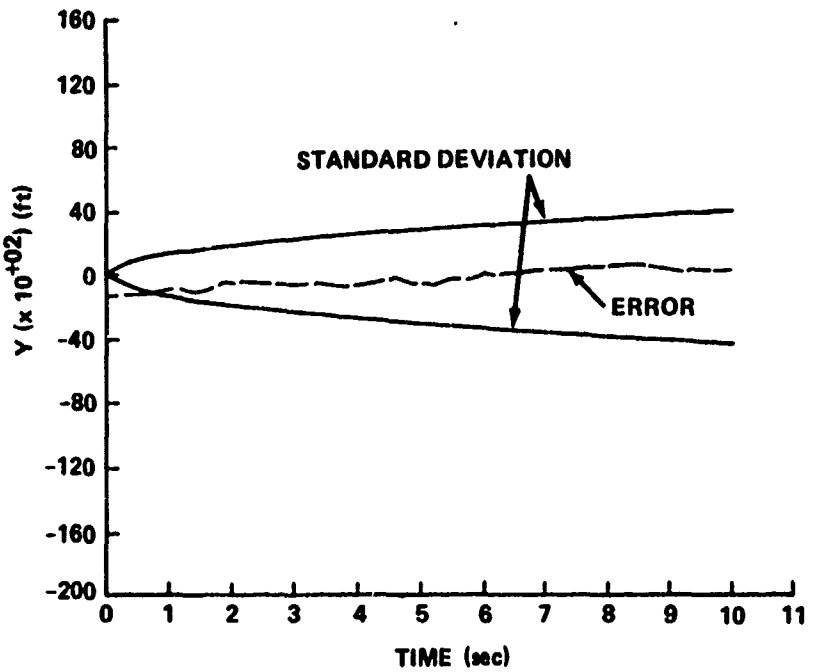

FIG 4.39. FILTER ERROR FOR SUBOPTIMAL ESTIMATION OF THE IMU'S X AND Y POSITION ERRORS WITH CASE II MEASUREMENT STATISTICS AND CASE I FIXED GAINS USING FIVE UPDATES

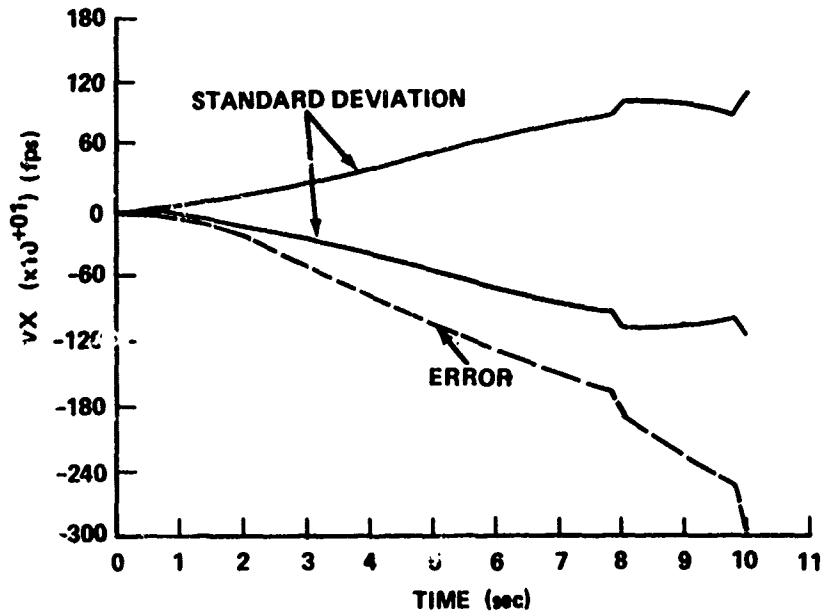

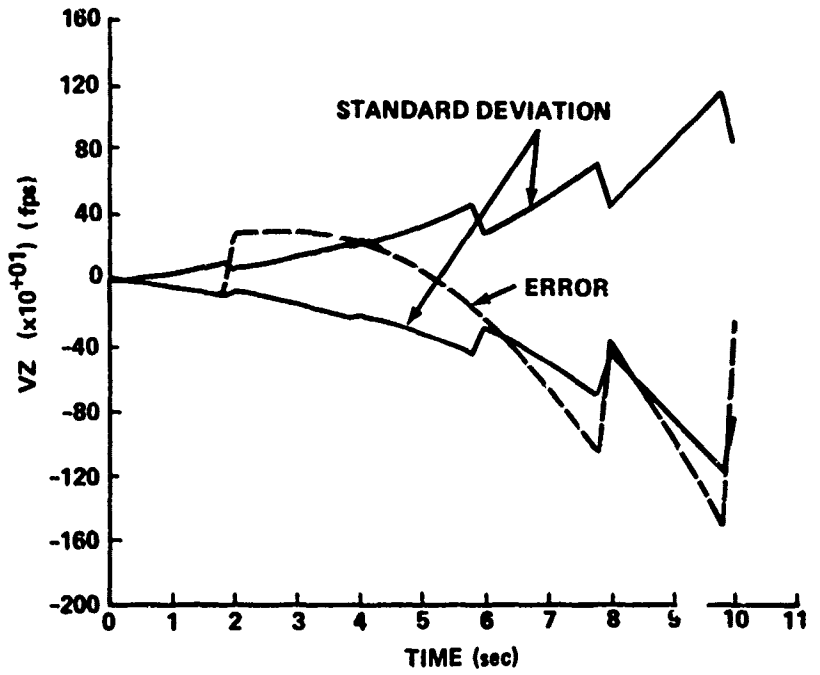

FIG 4.40. FILTER ERROR FOR SUBOPTIMAL ESTIMATION OF THE IMU'S V_x AND V_z VELOCITY ERRORS WITH CASE II MEASUREMENT STATISTICS AND CASE I FIXED GAINS USING FIVE UPDATES

some instances, there were divergent estimates whereas the optimal gains did not exhibit this behavior. Qualitatively, the following argument seems reasonable.

The estimate of the IMU error state depends on the difference in the actual measurement vector (Z) and the knowledge of the measurement matrix (H) with the estimate of the state vector ($\hat{X}$) at the instant the measurements are taken. This difference is multiplied, or weighted, by the optimal gain (K) which, in turn, is a function of terms computed from the covariance differential equation ($\dot{P}$). In the case where the optimal gains are used, the value of K is computed at every measurement update and is a function of the measurement noise, observation matrix, and more importantly, the old covariance values (P_-). The covariance P_- is obtained from a continuing propagation of $\dot{P}$ between measurements. The optimal gain (K) then utilizes all the measurement noise information, as well as process noise information, and may grow or decrease as the equations dictate. The gain values (K) are essentially the ratio between statistical measures of uncertainty of the state estimate and uncertainty in a measurement. If measurement noise is large and state estimate errors are small, the error in the measurement vector is caused chiefly by noise and, therefore, only a small change in the state estimate would be made; i.e., K will be small. However, small measurement noise and large uncertainty in the state estimate indicates that the measurement vector contains a large quantity of information on the errors in the estimates. Thus, the value for K will be large because the difference between the actual measurement and that predicted from $H\hat{X}$ would be used as the basis for a heavily weighted correction to the estimates.

Simply stated, when fixed gains are used, the previously described rationale does not occur. The covariance differential equation is not propagated between measurements (the single most important reason for choosing a set of fixed gains) so that all process noise statistics are ignored. Because K is fixed, there is no dependence update to update, on the measurement matrix (H) nor on noise statistics contained in the R matrix. Little significance is placed on the new incoming data, via the measurements Consequently, when the measurement vector has good data, it may be ignored and the error in the estimated states continues to grow or diverge.

It should be emphasized that on an actual on-board computer utilizing the fixed gains to implement the filter, the covariance matrix Riccati equations ($\dot{P}$) would not be computed. That they are not to be computed on board is the motivation for studying the effects of using fixed gains. In this study however, the plots of the standard deviation calculated from the covariance matrix were computed with fixed gains for comparison purposes. This was done to reinforce the arguments of defining a filter with good performance versus one which tended to diverge. As can be observed from the results presented, as the covariance increases, the filter's error increases.

A final comment on the fixed gain results is worthy of mention. The covariance matrix, which theoretically will be positive semidefinite, became negative definite in the P_{33} or δz term. This is the classic effect of filter divergence discussed in much of the literature. Because there was a need to obtain the square root of

this matrix in the plot subroutine, termination of the program occurred before all the plots could be made. The problem was overcome by not plotting the filter error covariance in the estimate of δz. This occurred in every fixed gain simulation except one when another method was used to correct the problem. This particular case was discussed in Chapter 4.8.

CHAPTER V. CONCLUSIONS AND RECOMMENDATIONS FOR FUTURE STUDY

5.1 CONCLUSIONS

In terms of the objectives specified in Section 1.5, the following conclusions are stated as having been verified during the course of this study.

a) The simplest inertial system mechanization which fulfills the constraint of minimum on-board computer capacity is the tangent plane mechanization.

b) The comparison between results of filters using five measurements updates and ten measurement updates indicate the filter error is smaller with more updates in estimating the state variables. The choice of ten measurement updates giving better results is shown conclusively. Indications are that the maximum of 15 measurements allowable would be the best. The measurements must be equally spaced in time for this application to allow time for processing.

c) The filter should be formulated with no less than five state variables. If the on-board computer has the capacity, the additional three states describing a constant inertial platform tilt would be desirable provided statistics describing IMU tilt can be obtained so that initial conditions can be properly chosen.

d) The complete five state filter studied here should not be formulated with fixed gains in each of the state estimates. The

results do indicate however, that the IMU position errors in X and Y are estimated with only modest filter error. Thus, the X and Y position errors can be derived in a fixed gain formulation. The savings in computer capacity needed to estimate three states with optimal time varying gains, while using fixed gains in estimating the other two states, alone yield a savings of 40 percent in computing the covariance matrix Riccati equation.

e) An excellent reference [17] was obtained which gave a comprehensive table of IMU characteristics required for performance with the statistics used in this study. It is used to specify the IMU and portions of the IMU computer for physical realization. Table 5.1 summarizes the IMU specifications. Specification for the radar area correlation system and radar altimeter are more general. The figure of merit used for the radar area correlation system was its resolution and for the altimeter, its accuracy. These are summarized in Table 5.2.

5.2 RECOMMENDATIONS FOR FUTURE STUDY

There are several problems related to this application which could be pursued further. The first of these would be to include more states in the filter formulation. This would more closely represent the physical situation, though it would require more computer capacity than may be allowed. The purpose would be to investigate the filter error relative to the number of states modeled. It would not imply *a priori* that additional states need be used in the actual system. The

Table 5.1

SPECIFICATIONS FOR THE IMU

Component Specifications	Gyros	Magnitude
	Constant drift rate (degree/hour)	0.3
	Mass unbalance [(degree/hour)/g]	0.2
	End plate drift [(degree/hour)/g]	0.15
	Anisoelasticity [(degree/hour)/g^2]	--
	Accelerometers	Magnitude
	Bias (g)	10^{-4}
	Scale factor (g/g)	81×10^{-6}
	Nonlinearity (g/g^2)	--
Platform Specification	Allowable Misalignment	1 Sigma Error
	X-Y plane level (arc seconds)	26.7
	Azimuth (arc seconds)	32.4
Guidance Computer	Error Source	1 Sigma Error
	In-flight errors (meter/second)	0.15
	Displacement error (meter)	10.0
	Velocity error (meter/second)	0.4

following considerations should also be investigated to observe the effects on the filter error:

a) The radar area correlation system is considered to have measurement noise correlated with the input noise

b) The radar area correlation system's time delay is modeled as a true transport lag

Table 5.2

SPECIFICATIONS FOR THE RADAR

	Error Source	1 Sigma Error
Radar Area Correlation System	X channel resolution (feet)	50
	Y channel resolution (feet)	50
	Correlation processing time of 0.2 seconds	
	Error Source	1 Sigma Error
Radar Altimeter	Inaccuracy of output	10% of indicated altitude

c) The platform tilt errors ($\vec{\psi}$) are modeled

d) The IMU sensors are modeled as an input process noise which is:

1) A random constant

2) A random walk

3) A random walk plus a bias

e) The mechanization of the other two nontangent plane IMU coordinate systems.

The sensitivity of the model to changes in the noise statistics should be investigated for the optimal gain cases with all of the previously listed formulations.

Initially, the purpose of the study was to pick one value of K to be fixed constant throughout the terminal flight phase for each state in a suboptimal filter formulation. However, the results of the optimal filter directed the decision to pick, in some cases, at least two levels of gains. The obvious extension is to investigate the mechanization which uses the optimal values of the gain at each update

without computing the covariance matrix Riccati equation. That is, instead of choosing a two level value of K, choose it to be five level for the five update case and ten level for the ten update case. In the latter for example, storing 50 values of K, 10 for each of the 5 states, would be a savings on the computer required, presuming the filter does not diverge.

An analysis should be performed to determine the sensitivity of the filter to the simplification of using fixed or precomputed gains. It was observed that the accuracy of the filter degraded when the fixed gains were used. This analysis would give the bounds and structure of the error covariance as a function of gain using fixed noise statistics. It would lend some confidence to the greater use of fixed or precomputed gains stored a priori.

A complete trajectory study is characterized by its higher complexity relative to the case presented in this thesis. It includes a full aerodynamic description of the flight vehicle, its inertia properties, autopilot mechanization, and targeting information in addition to the measurement kinematics considered. Then, by appropriate manipulation of initial conditions, the truest figure of merit, the vehicle's miss distance, could be established and compared in cases with and without the filter implemented. The concept would be simulated with a complete inertial system, radar area correlation system, and radar altimeter in the autopilot mechanization. The estimator would still be used to feed back error states to the inertial system for correction of its output to the autopilot actuators. In proper perspective, it should be noted that this entire report would be the basis of only one subroutine (the estimator) in such a simulation.

Needless to say, this type of study is a quantum step up in the hierarchy of analysis and simulation. But by the very virtue of its complexity, it represents the best tool closely approaching actual hardware flight test. The only additional realism would be to include a hardware-in-the-loop simulation. However, the obvious disadvantages of hardware acquisition (caused by high cost and lack of availability) and maintenance, preclude it from serious consideration at this time.

APPENDIX A

DERIVATION OF THE IMU POSITION AND PLATFORM MISALIGNMENT ERROR EQUATIONS

A.1 PLATFORM MISALIGNMENT ERROR EQUATION

It is assumed that the computer mechanization is perfect, i.e., that the equations of motion are solved with accuracy. Thus, the guidance system would operate perfectly if the initial conditions were correct and if there were no component errors. Realistically, there are a host of errors contributed by the gyros, accelerometers, resolvers, torquers, pick-offs, etc. However, this analysis will only consider two major errors that the gyro and accelerometer propagate. The predominant sources of error for the gyro are the drift rate and scale factor, and for the accelerometer the bias and scale factor.

Three coincident coordinate axes are of interest. Each is defined by a set of orthogonal unit vectors in a right handed triad. For a perfectly operating, errorless guidance system, all three bases would coincide. For small angular rotations, a pseudovector may be defined which is the vector angle relating one basis to another. It can therefore be defined by the following:

$$\delta\vec{\psi} = \begin{bmatrix} \delta\psi_x \\ \delta\psi_y \\ \delta\psi_z \end{bmatrix} \triangleq \text{the vector angle between the computer basis and the platform basis.}$$

$$\vec{\delta\phi} = \begin{bmatrix} \delta\varphi_x \\ \delta\varphi_y \\ \delta\varphi_z \end{bmatrix} \triangleq \text{the vector angle between the local basis (which may be in any mechanization) and the platform basis.}$$

$$\vec{\delta\theta} = \begin{bmatrix} \delta\theta_x \\ \delta\theta_y \\ \delta\theta_z \end{bmatrix} \triangleq \text{the vector angle between the local basis and the computer basis.}$$

As mentioned previously, ideally all the bases would coincide; but by the definitions given, it is concluded

$$\dot{\vec{\delta\phi}} = \dot{\vec{\delta\theta}} + \dot{\vec{\delta\psi}} \quad . \tag{A.1}$$

In terms of the notation used throughout this thesis,

$$\dot{\vec{\delta\phi}} \triangleq \vec{\omega}^{P-L}$$

$$\dot{\vec{\delta\theta}} \triangleq \vec{\omega}^{C-L}$$

$$\dot{\vec{\delta\psi}} \triangleq \vec{\omega}^{P-C} \quad .$$

Thus, Eq. (A.1) is rewritten as

$$\vec{\omega}^{P-L} = \vec{\omega}^{P-C} + \vec{\omega}^{C-L} \quad . \tag{A.2}$$

Ideally, it is desired that the platform rotate with the local coordinate basis in inertial space, i.e.,

$$\vec{\omega}^{P-I} = \vec{\omega}^{L-I} \qquad \text{(Ideal)} \quad . \tag{A.3}$$

However, because the gyros are measuring this platform rotation with

respect to the inertial basis and because the gyros are additionally being torqued by signals from the computer to maintain a particular mechanization, the platform conforms to the following actual matrix equation:

$$\underset{P}{\omega}^{P-I} = \left(E_3 + \underset{P}{K}^{g}\right) \underset{C}{\omega}^{C-I} + \underset{P}{\epsilon} \quad , \text{(Actual)} \tag{A.4}$$

where

$$E_3 \triangleq \begin{bmatrix} 1 & 0 & 0 \\ 0 & 1 & 0 \\ 0 & 0 & 1 \end{bmatrix} \quad .$$

To get all terms in the same basis, note that the following transformations hold:

$$\underset{P}{\omega} = T_{P/C} \; \underset{C}{\omega} \tag{A.5}$$

and

$$T_{P/C} = T_{P/C}^{T} \approx E_3 + \Psi \quad , \tag{A.6}$$

where

$$\Psi = \begin{bmatrix} 0 & -\psi_z & \psi_y \\ \psi_z & 0 & -\psi_x \\ -\psi_y & \psi_x & 0 \end{bmatrix} \quad .$$

Thus,

$$\underset{C}{\omega}^{C-I} = \left(E_3 + \Psi\right) \underset{P}{\omega}^{C-I} = \underset{P}{\omega}^{C-I} + \Psi \; \underset{P}{\omega}^{C-I} \quad . \tag{A.7}$$

Putting Eq. (A.7) into Eq. (A.4) yields

$$\omega_P^{P-I} = \left(E_3 + K_g\right)\left(\omega_P^{C-I} + \Psi\ \omega_P^{C-I}\right) + \epsilon_P$$

$$= \omega_P^{C-I} + K_g\ \omega_P^{C-I} + \Psi\ \omega_P^{C-I} + \epsilon_P \quad . \qquad (A.8)$$

Now,

$$\Psi\ \omega_P^{C-I} = \begin{bmatrix} 0 & -\psi_z & \psi_y \\ \psi_z & 0 & -\psi_x \\ -\psi_y & \psi_x & 0 \end{bmatrix} \begin{bmatrix} \omega_x \\ \omega_y \\ \omega_z \end{bmatrix} \quad , \qquad (A.9)$$

thus,

$$\vec{\omega}^{P-I} = \vec{\omega}^{C-I} + \vec{\vec{K}}_g \cdot \vec{\omega}^{C-I} + \psi \times \vec{\omega}^{C-I} + \vec{\epsilon} \quad . \qquad (A.10)$$

But

$$\vec{\omega}^{P-I} - \vec{\omega}^{C-I} = \vec{\omega}^{P-C} \quad ,$$

where from the earlier definitions,

$$\vec{\omega}^{P-C} \triangleq \delta\dot{\vec{\psi}} \quad .$$

It is also noted that

$$\delta\dot{\vec{\psi}} \triangleq \overset{C}{\vec{\psi}} \quad . \qquad (A.11)$$

Combining Eq. (A.10) and Eq. (A.11) yields the following:

$$\overset{C}{\vec{\psi}} = \vec{\vec{K}}_g \cdot \vec{\omega}^{C-I} + \vec{\psi} \times \vec{\omega}^{C-I} + \vec{\epsilon} \quad . \qquad (A.12)$$

Finally, as a minor modification, let $\delta\vec{\theta} = 0$; i.e., let the ideal local frame equal the ideal computer frame. The resulting local frame symbols are

$$\boxed{\overset{L}{\dot{\vec{\Psi}}} = -\vec{\omega}^{L-I} \times \vec{\Psi} + \vec{K}_g \cdot \vec{\omega}^{L-I} + \vec{\epsilon}} \quad . \tag{A.13}$$

Eq. (A.13) is the same as Eq. (2.9) in the text.

A.2 POSITION ERROR EQUATION

Beginning with the set of equations in invariant vector form given as Eqs. (2.8a) and (2.8b), assume that $\delta\theta = 0$; i.e., that the local basis is aligned with the true or computer basis. Thus,

$$\overset{C}{\dot{\vec{r}}} = \vec{V} + \vec{\omega}^{E-C} \times \vec{r} \tag{A.14}$$

and

$$\overset{C}{\dot{\vec{V}}} = \vec{f} + \vec{g} - \left(\vec{\omega}^{E-I} + \vec{\omega}^{C-I}\right) \times \vec{V} \quad . \tag{A.15}$$

Equation (A.15) which is in terms of the gravity field intensity vectors is, when rewritten in terms of the gravitational field intensity vectors,

$$\overset{C}{\dot{\vec{V}}} = \vec{f} + \vec{G} - \left(\vec{\omega}^{E-I} + \vec{\omega}^{C-I}\right) \times \vec{V} - \vec{\omega}^{E-I} \times \left(\vec{\omega}^{E-I} \times \vec{r}\right) \quad . \tag{A.16}$$

Now defining the indicate quantities in the preceding ideal equation composed of a nominal component and an error component, the following variation to first order is resolved:

$$\overset{C}{\dot{\vec{r}}} + \delta\overset{C}{\dot{\vec{r}}} = \vec{V} + \delta\vec{V} - \vec{\omega}^{C-E} \times \vec{r} - \vec{\omega}^{C-E} \times \delta\vec{r} \quad , \tag{A.17}$$

where

$$\vec{\omega}^{C-E} = -\vec{\omega}^{E-C}$$

$$\vec{\omega}^{C-E} = \vec{\omega}^{C-I} - \vec{\omega}^{E-I} \quad ,$$

and $\vec{\omega}^{C-I}$ and $\vec{\omega}^{E-I}$ are known exactly (no perturbation is needed).

Subtracting Eq. (A.14) from Eq. (A.17) yields

$$\overset{C}{\delta\vec{r}} = \delta\vec{V} - \vec{\omega}^{C-E} \times \delta\vec{r} \quad , \tag{A.18}$$

rewritten as

$$\delta\vec{V} = \overset{C}{\delta\vec{r}} + \vec{\omega}^{C-E} \times \delta\vec{r} \quad , \tag{A.19}$$

which is recognized as the Coriolis Law if the following definition is used:

$$\delta\vec{V} \triangleq \overset{E}{\delta\vec{r}} \quad .$$

Thus,

$$\delta\vec{V} = \overset{E}{\delta\vec{r}} = \overset{C}{\delta\vec{r}} + \vec{\omega}^{C-E} \times \delta r \quad . \tag{A.20}$$

Now by straight forward application of the Coriolis Law

$$\overset{I}{\delta\vec{r}} = \overset{E}{\delta\vec{r}} + \vec{\omega}^{E-I} \times \delta\vec{r} \tag{A.21a}$$

$$= \delta\vec{V} + \vec{\omega}^{E-I} \times \delta\vec{r} \quad . \tag{A.21b}$$

Taking another derivative,

$$\overset{II}{\delta\vec{r}} = \overset{I}{\delta\vec{V}} + \vec{\omega}^{E-I} \times \overset{I}{\delta\vec{r}} \tag{A.22a}$$

or

$$\overset{II}{\delta\vec{r}} = \overset{I}{\delta\vec{V}} + \vec{\omega}^{E-I} \times \left(\delta\vec{V} + \vec{\omega}^{E-I} \times \delta\vec{r}\right) \quad . \tag{A.22b}$$

Repeating the same process with Eq. (A.16) yields,

$$\overset{C}{\vec{V}} + \overset{C}{\delta\vec{V}} = \vec{f} + \delta\vec{f} + \vec{G} + \delta\vec{G} - \vec{\omega}^{E-I} \times \left[\vec{\omega}^{E-I} \times (\vec{r} + \delta\vec{r})\right]$$

$$-\left(\vec{\omega}^{E-I} + \vec{\omega}^{C-I}\right) \times \left(\vec{V} + \delta\vec{V}\right) \quad . \tag{A.23}$$

Subtracting Eq. (A.16) from Eq. (A.23) yields

$$\overset{C}{\delta\vec{V}} = \delta\vec{f} + \delta\vec{G} - \vec{\omega}^{E-I} \times \left(\vec{\omega}^{E-I} \times \delta\vec{r}\right)$$

$$-\left(\vec{\omega}^{E-I} + \vec{\omega}^{C-I}\right) \times \delta\vec{V} \quad . \tag{A.24}$$

Again, the Coriolis Law is

$$\overset{I}{\delta\vec{V}} = \overset{C}{\delta\vec{V}} + \vec{\omega}^{C-I} \times \delta\vec{V} \quad . \tag{A.25}$$

Substituting Eq. (A.24) into Eq. (A.25) gives

$$\overset{I}{\delta\vec{V}} = \delta\vec{f} + \delta\vec{G} - \vec{\omega}^{E-I} \times \left(\vec{\omega}^{E-I} \times \delta\vec{r}\right) - \vec{\omega}^{E-I} \times \delta\vec{V} \quad . \tag{A.26}$$

Now derive the terms in $\delta\vec{G}$, which is a function of $\vec{r}$ and of time t.

$$\vec{G} = G(\vec{r}, t) = -\frac{K\vec{r}}{r^3} + \vec{e}(\vec{r}, t) + \vec{\eta}(\vec{r}, t) \quad , \tag{A.27}$$

where

$\vec{e}(\vec{r}, t) \triangleq$ oblateness of earth and sun-moon effects

$\eta(\vec{r}, t) \triangleq$ randomness effects.

Thus,

$$\vec{G} + \delta\vec{G} = \frac{-(K + \delta K)(\vec{r} + \delta\vec{r})}{\left[(r + \delta\vec{r}) \cdot (r + \delta\vec{r})\right]^{\frac{3}{2}}} + \vec{e} + \delta\vec{e} + \vec{\eta} \qquad \text{(A.28a)}$$

$$= \frac{-\vec{r}\delta K}{r^3} - \frac{K(\vec{r} + \delta\vec{r})}{\left(\vec{r}^2 + \delta\vec{r}^2 + 2\vec{r} \cdot \delta\vec{r}\right)^{\frac{3}{2}}} + \vec{e} + \delta\vec{e} + \vec{\eta} \quad . \qquad \text{(A.28b)}$$

Now,

$$\delta r = \hat{r} \times \delta\vec{r} \quad ;$$

i.e., δr is a scalar and $\hat{r}$ is a unit vector in the r direction given by

$$\hat{r} = \frac{\vec{r}}{|r|} \quad .$$

Consequently, performing a binomial expansion on the denominator and neglecting higher order terms yields

$$\vec{G} + \delta\vec{G} = \frac{-\vec{r}\delta K}{r^3} - \frac{K}{r^3}(\vec{r} + \delta\vec{r})\left(1 - \frac{3\vec{r} \cdot \delta\vec{r}}{r^2}\right) + \vec{e} + \delta\vec{e} + \vec{\eta} \quad . \qquad \text{(A.29)}$$

Subtracting Eq. (A.27) from Eq. (A.29),

$$\delta\vec{G} = \frac{-\vec{r}\delta K}{r^3} - \frac{K\delta\vec{r}}{r^3} + \frac{3K\vec{r}}{r^5}(\vec{r} \times \delta\vec{r}) + \delta\vec{e} + \vec{\eta} \quad . \qquad \text{(A.30)}$$

Now defining

$$\omega_s^2 \triangleq \frac{K}{r^3}$$

to be a constant when $r \approx R_{earth}$, and more precisely

$$\delta\vec{e} \triangleq \frac{\partial\vec{e}}{\partial\vec{r}} \cdot \delta\vec{r} \quad ,$$

then

$$\delta\vec{G} = -\omega_s^2 \left[\vec{\vec{1}} - 3\hat{\hat{r}}\hat{r} - \frac{1}{\omega_s^2} \frac{\partial \vec{e}}{\partial \vec{r}} \right] \cdot \delta\vec{r} - \frac{\vec{r}\delta K}{r^3} + \vec{\eta} \quad . \tag{A.31}$$

Deriving the terms in $\delta\vec{f}$ and using a basis viewing that which the computer "sees" from the platform-mounted instruments yields

$$\underset{C}{f} + \underset{C}{\delta f} = \begin{bmatrix} E_3 + K_f \\ \qquad\quad P \end{bmatrix} \underset{P}{f} + \underset{P}{b} \quad . \tag{A.32}$$

Using the transformation

$$T_{P/C} = \left(E_3 - \Psi \right) \quad , \tag{A.33}$$

so that

$$\underset{P}{f} = \left(E_3 - \Psi \right) \underset{C}{f} \quad , \tag{A.34}$$

then

$$\underset{C}{f} + \underset{C}{\delta f} = \left(E_3 - \Psi \right)_C^f + \left(E_3 - \Psi \right)_C^{K_f} \underset{C}{f} + \left(E_3 - \Psi \right)_C^b \quad . \tag{A.35}$$

Subtracting Eq. (A.32) from Eq. (A.35), the matric form is

$$\underset{C}{\delta f} = \underset{C}{K_f} \underset{C}{f} + \underset{C}{b} - \underset{C}{\Psi} \times \underset{C}{f} \quad , \tag{A.36}$$

or in vector form

$$\delta\vec{f} = \vec{\vec{K}}_f \cdot \vec{f} + \vec{b} - \vec{\Psi} \times \vec{f} \quad . \tag{A.37}$$

Substituting Eqs. (A.31) and (A.37) into Eq. (A.26) for $\delta\vec{G}$ and $\delta\vec{f}$ and neglecting the oblateness and random terms, the result is

$$\delta\vec{V}^{I} = \vec{\vec{K}}_f \cdot \vec{f} + \vec{b} - \vec{\psi} \times \vec{f} - \omega_S^2 \left[\vec{\vec{1}} - 3\hat{r}\hat{r}\right] \times \delta\vec{r}$$

$$- \vec{\omega}^{E-I} \times \left(\vec{\omega}^{E-I} \times \delta\vec{r}\right) - \vec{\omega}^{E-I} \times \delta\vec{V} \quad . \qquad \text{(A.38)}$$

Finally, substituting Eq. (A.38) into Eq. (A.22b) yields

$$\boxed{\delta\ddot{\vec{r}}^{II} - \omega_S^2 \left[\vec{\vec{1}} - 3\hat{r}\hat{r}\right] \cdot \delta\vec{r} = \vec{\vec{K}}_f \cdot \vec{f} + \vec{b} - \vec{\psi} \times \vec{f}} \quad , \qquad \text{(A.39)}$$

which corresponds to Eq. (2.10) in the text.

Appendix B

AN OVERVIEW OF RADAR AREA CORRELATION NAVIGATION

B.1 GENERAL

This is a short compendium abstracted primarily from the following authors: Wiley [18], Stauffer [19], Eppler and Willstadter [25], Develet [26], and Diamantides [27]. It is not intended to be a treatise on the subject but rather a convenient, self-contained reference on radars in the navigation application as compared to radar transmitter-receiver design.

It is possible to use an airborne radar to obtain completely automatic navigation by comparison of the image generated by the vehicle's radar in flight with a series of stored reference radar images made by previous reconnaissance. The comparison is made by finding the autocorrelation or cross correlation between the live image and the reference image; this process is called radar area correlation or simply radar map matching.

The radar map-matching process determines the displacement of the live radar image with respect to the position of the reference image. By "position" of an image is meant the geographical location of the radar that will create the image in question. The displacement data, in geographic coordinates, is then fed back to the navigation computer to update computed position. Figure B.1 shows the geometry of the

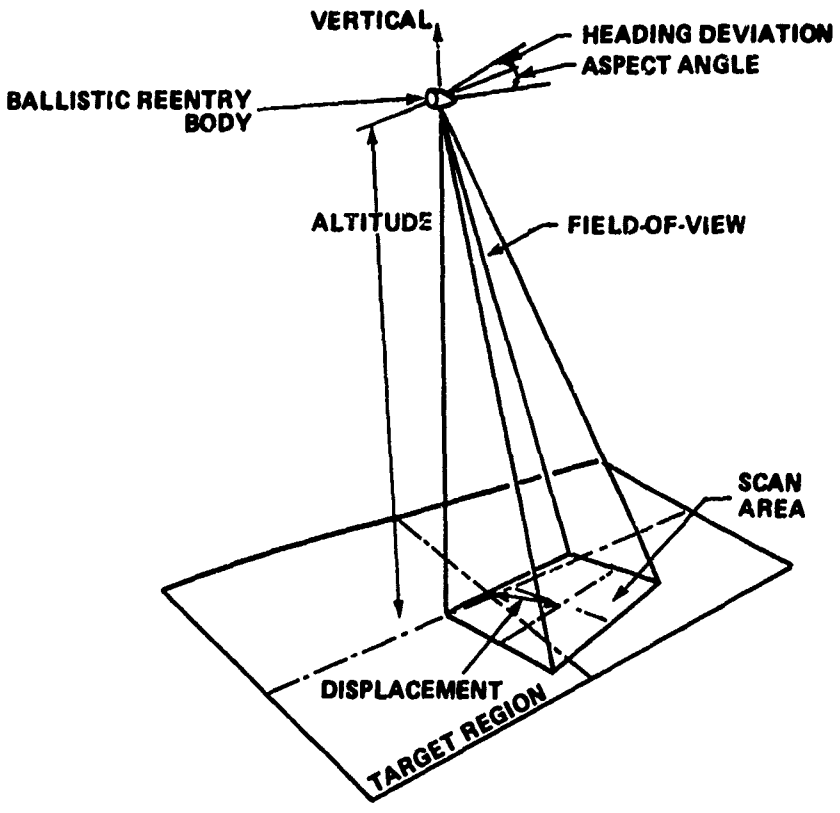

FIG. B.1. TYPICAL PROBLEM GEOMETRY

problem. Because the map matcher can deliver almost continuous error data, it is conceivable that these signals could be used to steer the vehicle directly. However, the area correlation data, although free of error that accumulates with time, contain high-frequency noise resulting from the continuous fluctuations in the radar image. Attempts to smooth out this noise by integration result in area correlation time constants that are too long to control the vehicle in a stable manner. The solution is one of combining a fast-responding, low-noise device that has the disadvantage of accumulating errors causing long-term drift (such as an inertial platform) with a slower,

noisy device without drift, the area correlator. By proper allotment of time constants between the two devices, it is possible to produce a fast-responding system with little noise and no drift.

B.2 PRINCIPLES

The basic principle of an active radar ground mapping system is that it transmits energy and detects the part of it scattered back from a target. However, instead of the usual point target, the target in this case is the ground, which can be considered as an extended array of scatterers. The radar map is obtained by scanning or painting the ground and displaying the return on a cathode ray tube or photographic film. Because the scattering characteristics of the ground will vary from point to point, the map will be in the form of a varying brightness pattern. Variations of intensity in this brightness pattern can be interpreted in terms of the topographical and man-made features of the terrain. For example, the energy back-scattered from a smooth surface such as calm water will be much less than that from a rough surface such as the ground. The degree of correspondence between the brightness pattern and the features of the terrain depends on the characteristics of the antenna beam pattern used to paint the ground.

The antenna beam pattern usually employed in ground mapping systems is narrow in one dimension and has wide angular coverage in the other dimension. This type of beam is known as a fan beam. It is usually oriented so that the narrow dimension is horizontal, thus illuminating a long narrow strip of ground from beneath the vehicle to some maximum range. Thus, for a given pointing direction, the radar

beam illuminates targets at many different ranges and depression angles. Variations in the brightness are therefore functions of range and the angle at which the ground is viewed as well as the reflective properties of the terrain. This condition, if not corrected, would complicate the correlation between the radar image and terrain. To compensate for the effects of range and viewing angle, the vertical gain pattern of a radar ground mapping antenna is designed to be a function of the depression angle at which a given patch of ground is viewed. This type of pattern is as a cosecant-squared beam.

Scanning of the antenna beam is usually accomplished either by rotating the antenna about a vertical axis or by positioning the antenna along the vehicle so that its motion provides the scanning. When the beam is rotated a full 360 degrees about the vertical axis, the image is usually in the form of a plan position map with the vehicle at the center. Most systems employing this type of scan use a sector scan, i.e., less than the full 360 degrees. When the sector is directed forward of the vehicle, the system is known as a forward-looking area correlation radar. Systems employing the velocity scanning technique, where the beam is directed to the side of the vehicle, are known as side-looking radars. The images obtained with this system are in the form of strip maps along each side of the vehicle's track and are especially adapted to the use of photographic techniques to obtain a permanent record. This permanent record or signal storage has led to the consideration of the correlation process as an integral part of radar image matching.

B.3 RADAR IMAGE MATCHING - CORRELATION

Imagery matching is, in essence, a way of measuring the similarity between two displays; its outcome conveys information not only about the displays' structures but also about their relative positions. The former is of value to the problem of quantifying displays of scenes or objects and, subsequently, to the problem of attaching meaningful characteristic numbers to the scenes or objects in question for the purpose of classification. The latter lends itself to position fixing and therefore, if the displays are maps, to automatic navigation and homing guidance.

The study of display matching is essentially a study of the correlation function and inasmuch as a figure, map, or other subject is displayed in two dimensions. The correlation function under consideration is for two dimensions,

$$\phi(\xi, \eta) = \frac{1}{4XY} \int_{-Y}^{Y} \int_{-X}^{X} T(x, y)\, T(x + \xi, y + \eta)\, dxdy \quad , \quad (B.1)$$

where $T(x, y)$ is the display brightness at (x, y) and ξ, η the relative displacements.

In display matching, there is generally a current image which is compared to a memory image, the output of this comparison being the input to a detection system. If the two images are different, the resultant output is mutual property of both image functions and can be ascribed no more to one of the images than to the other. The process, then, is called cross correlation. If, however, an image is correlated with a duplicate of itself, the output is wholly a property of that

image and the process is called autocorrelation. Where cross correlation is executed for functional purposes, autocorrelation is performed for purely analytic reasons. According to one school of thought, the pattern recognition process that occurs when a pilot observes a target scene or when a photo interpreter examines an aerial photograph is similar to the correlation process previously described. The principal difference between the two is that memory and detection are contained within the physiological equipment of a human being.

In some early mechanizations, area correlation was done by projecting the live radar image onto the stored reference image and measuring the total light emerging from the back of the reference image (Fig. B.2). If the two signals are statistically alike, $\phi(\xi, \eta)$ is largest when the images are in register and $\xi = \eta = 0$. As the images move out of register, so that ξ and η are not zero, $\phi(\xi, \eta)$ becomes smaller, decreasing asymptotically to zero for very large displacements, completely destroying any statistical similarity between the image elements in the product.

If one image is rapidly scanned over the other in a small circle, the output light will fluctuate. The major component of this fluctuation will be at the nutation rate because, in the general case, the nutation circle will be closest to the correlation peak at one point in the circle and furthest away (180 degrees) in nutation phase from the instant of maximum light. The phase of the fluctuation will change with respect to the nutation drive if the nutation circle moves around the correlation peak at $\xi, \eta = 0$. One can synchronously demodulate the light fluctuation with respect to the in-phase and quadrature nutation

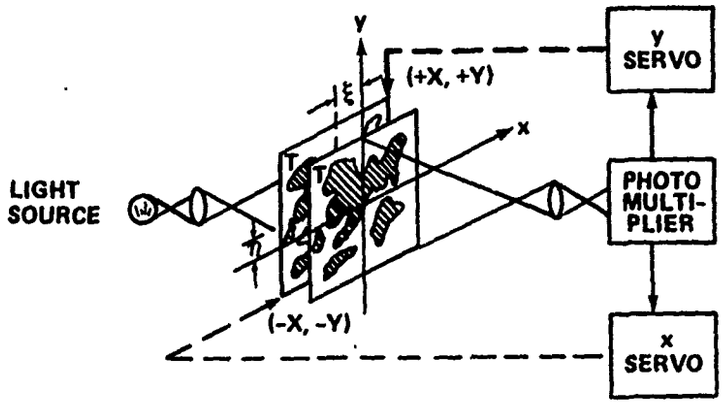

FIG B.2. IMAGE MATCHING MECHANIZATION

drive signals and integrate the demodulator outputs. The integrator outputs are servo-error signals, changing in algebraic sign at ξ, $\eta = 0$ in the correct manner to register the images, when they are applied to servoamplifiers, which move one of the images with respect to the other. In this manner, displacement of one image with respect to the other can be measured. If the radar-image signals were identical, and if the correlator could operate on infinitely large samples of the two signals, then the cross correlation function ϕ (ξ, η) would be a noiseless smoothly varying function of ξ and η and would have a perfectly defined maximum. The correlation tracker could then determine the correlation peak position and, hence, the register point, to any desired accuracy. However, the signals are not identical and the correlator must work with finite samples of the image signals. In general, the two images are not made at the same location; as a result, scintillation, moving shadows, and the like destroy identicality. In addition, there is receiver noise in both images. Even if the signals were identical, the finite signal sample size would produce fluctuations from correlation to correlation.

From both of the previously mentioned cases, then, the value of the cross correlation function generated for a given ξ, η varies unpredictably from one correlation to the next, as does the location of the maximum value. Because the location of the maximum value ($\xi = \eta = 0$) is the output quantity of interest, its variation from correlation to correlation is a fluctuating error in the displacement measurement, which determines the accuracy of the map-matching process. As a rule of thumb, experience has shown that a well-designed system can measure ξ and η to approximately one-half the radar-range resolution if areas ahead and to the side of the vehicle are simultaneously used in the match process. This placement of the matched areas insures reltative motion of the images in the range direction, which is the narrow dimension of the target elements for changes of ξ and η.

B.4 SYSTEM'S CONSIDERATIONS

Some of the most important system considerations for ground image referencing radar systems involve resolution, accuracy, range and operational altitude, and all-weather capability.

As accuracy is the basic measure of navigation systems performance, resolution is the basic measure of performance for radar ground area correlation systems. Resolution, a measure of the system's ability to distinguish between closely spaced objects or to delineate the details of a large area, is usually defined in terms of range resolution and transverse or azimuth resolution. While the ultimate resolution attained by the system is a function of many parameters, the single criterion most commonly used to judge it is the pulse packet size as projected on the ground. The system parameters which determine

the pulse packet size are antenna beamwidth and pulse length, as measured at the half-power points.

Beamwidth is a function of the transmitted wavelength and the dimensions of the antenna being expressed approximately by

$$\theta = \frac{K\lambda}{D} \quad , \tag{B.2}$$

where

θ = beamwidth defined by the half-power points

λ = transmitted wavelength

D = pertinent dimension of the antenna aperture

K = constant dependent on the particular aperture. A typical value for this constant is 70 where θ is expressed in degrees and λ and D are measured in the same units.

The system designer is confronted at once with a compromise in the selection of the transmitted wavelength and the dimensions of the antenna. To narrow the beamwidth, either the wavelength must be decreased or the dimensions of the antenna must be increased. In decreasing the wavelength, the problems of atmospheric attenuation and the generation of large amounts of power become increasingly difficult. The maximum size of the antenna obviously will be limited for airborne installations.

Range resolution may be improved by decreasing the pulse length. Again, there is a minimum limit because the average power transmitted is a direct function of pulse length. Also to be considered in this connection is the altitude at which the system will operate because the length of the pulse, as projected on the ground, is a function of the radar altitude.

Another important area with regard to system resolution concerns the receiver. Here, one of the basic considerations is its dynamic range, i.e., the range of signal amplitudes which it can accommodate without distortion. Because a radar image is a brightness pattern, variations of intensity within the image contribute to the resolution of certain features. The range of signal amplitudes encountered in a given correlation operation may be large. If the receiver or display system cannot accommodate such a range of signal amplitudes without distortion, loss of much detail within the image will occur. If the gain or intensity is set at the noise threshold, strong targets will "bloom", thus obscuring nearby weaker targets. If the gain or intensity is set too high, the weaker targets will not be mapped.

System accuracy is as equally important in many respects as system resolution. Distorted or "smeared" images make it difficult to obtain a true measure of ground distances or to resolve details within the image. Types of errors that can occur are altitude errors, drift errors, and stabilization errors. Errors in the measurement of the altitude of the mapping vehicle can cause distortions in the image because in most systems altitude is used to set in the range scan factor. Angular distortion of the image can occur also if there is no compensation made for drift.

Stabilization errors occur when the antenna is not stabilized for pitch and roll displacements. Such errors produce distortion and smearing of the image. The degree of distortion or smearing that will occur is difficult to define analytically. However, related studies on

airplane motions in turbulent air have indicated that displacements of as little as 1 degree in pitch occur with such frequency as to make stabilization desirable.

B.5 SIGNAL PROCESSING AND A MECHANIZATION SCHEME

The procedure starts with the acquisition of a reference image by e.g., a reconnaissance satellite. The image correlation process is concerned with determining the position offset, with respect to this stored reference image, of terrain whose radar return is scanned by the reentry body. To process the data digitally, the radar and reference images must be sampled in space and quantized in intensity.

By space sampling, it is meant that the radar signal is sampled at particular instants of time and these samples are used to represent areas on the ground. The size of these areas depends on the radar resolution and the signal processing. Intensity quantization means that the amplitude of the radar signal at the sampling instant is represented by one of K discrete values. For the binary case, (K = 2), a sample is stored as a "1" or "0" depending on whether or not its amplitude exceeds a specified threshold.

As a result of space-sampling and amplitude quantization, the radar and reference images can be represented as a matrix in which each element represents the radar return from a particular area of the image. In the binary case, the condition for correlation of an element of the reference image with an element of the radar image is that both elements are alike, i.e., both have the value "1" or both have the

value "0". The image area correlation system must compare reference and radar images element by element and count the number of places in which they agree.

In the correlation process, the radar image is in effect superimposed in each of a matrix of discrete positions over the reference image and a measure of the resultant correlation is obtained for each superposition. Provided it exceeds a predetermined correlation threshold level, the sampled superposition yielding maximum correlation is taken as the best estimate for the true superposition region. The precise best estimate of position within this region is then made by employing interpolation techniques.

To be able to locate the match point with an error less than one-half the distance between samples, it is necessary to use an interpolation procedure. If this were not done, it would be necessary to decrease the distance between samples, thus requiring higher radar resolution, larger computer memory, and longer computation time.

Thus, the area correlation system must perform four operations:

a) Store the space-sampled, amplitude quantized radar signal as a matrix representation of the mapped area.

b) Shift the radar and prestored reference images relative to each other, conceptually as shown in Fig. B.2.

c) Determine the correlation between radar and reference images for each possible offset. For the two-level system, for example, the correlation is obtained by counting the number of elements in which the radar and offset reference matrices coincide.

d) Interpolate between offsets to determine the match point.

Appendix C

OPTIMAL ESTIMATION OF STATES IN A LINEAR SYSTEM WITH CORRELATED PROCESS NOISE AND MEASUREMENT NOISE

C.1 GENERAL

The idea is to estimate the state of a system $x(t)$ from observed or measured data $z(t)$ where x and z are vector quantities. There is a known relationship between the observation and state vectors and there is additive noise present in the observation. These comments can be expressed in the continuous case as

$$\dot{x}(t) = F(t)\, x(t) + G(t)\, u(t) \tag{C.1}$$

and

$$z(t) = H(t)\, x(t) + v(t) \quad , \tag{C.2}$$

where

$x(t) \triangleq n \times 1$ vector of state variables

$u(t) \triangleq n \times 1$ vector of input noise

$F(t) \triangleq n \times n$ matrix representing linear dynamics

$G(t) \triangleq m \times n$ matrix representing the effect of the input on dynamics

$z(t) \triangleq p \times 1$ vector of system outputs (observations)

$H(t) \triangleq p \times n$ matrix relating x and z

$V(t) \triangleq p \times 1$ vector of noise in the measurement.

Furthermore, $u(t)$ and $V(t)$ are Gaussian white noise random variables with zero mean and auto-covariance matrices

$$E\left\{u(t)\ u^T(t)\right\} = Q(t)\ \delta(t - \tau) \qquad (C.3)$$

$$E\left\{v(t)\ v^T(t)\right\} = R(t)\ \delta(t - \tau) \quad . \qquad (C.4)$$

Also, for the case where the two noises are correlated, the cross-covariance matrix is

$$E\left\{u(t),\ v^T(\tau)\right\} = S(t)\ \delta(t - \tau) \quad . \qquad (C.5)$$

The symbol E{ } denotes the expected value of the quantity in the brackets, A^T denotes the transpose of matrix A, and the quantity $\delta(t - \tau)$ is the Dirac δ-function.

C.2 PROBLEM AND PURPOSE

The problem is to derive the main results of the Kalman-Bucy filter [8] with the extension, not originally considered in their paper, that correlated input and process measurement noise is to be expected. The purpose is to develop familiarity with the techniques of their classic paper, obtain useful results for further applications, and have a basis for discussion of their work as a self-contained item in this report.

C.3 SOLUTION

With no pretense of originality, the solution begins with the results given in the paper by Kalman and Bucy [8] as Eq. (38). Their Eq. (38) states, in essence, that the Weiner-Hopf equation yields a necessary and sufficient condition for a minimum variance estimator of

$$\left[x(t),\ x\left(t_1\right)\right] \quad ,$$

i.e.,

$$\text{cov}\left[x(t_1),\ z(\sigma)\right] = \int_0^t A(t_1,\ \tau)\ \text{cov}\left[z(\tau), z(\sigma)\right] d\tau,\ \forall\ 0<\sigma<t\ . \quad \text{(C.6)}$$

Continuing the development, let $t_1 = t$ for simplicity in the development and differentiate the left side of Eq. (C.6) with $0 < \sigma < t$.

Then,

$$\begin{aligned}
\frac{d}{dt}\ \text{cov}\left[x(t),\ z(\sigma)\right] &= \text{cov}\left[\dot{x}(t),\ z(\sigma)\right] + \text{cov}\left[x(t),\ \dot{z}(\sigma)\right] \\
&= \text{cov}\left[F(t)\,x(t) + G(t)\,u(t),\ z(\sigma)\right] \\
&= \text{cov}\left[F(t)\,x(t),\ z(\sigma)\right] + \text{cov}\left[G(t)\,u(t),\ z(\sigma)\right] \\
&= F(t)\ \text{cov}\left[x(t),\ z(\sigma)\right] + G(t)\,\text{cov}\left[u(t),\ H(\sigma)\,x(\sigma) + v(\sigma)\right] \\
&= F(t)\,\text{cov}\left[x(t),\ z(\sigma)\right] + G(t)\,H(\sigma)\,\text{cov}\left[u(t),\ x(\sigma)\right] \\
&\quad + G(t)\left[\text{cov}\ u(t),\ v(\sigma)\right]\ . \qquad \text{(C-7)}
\end{aligned}$$

Now differentiating the right side of Eq. (C.6) using Liebnitz's rule,

$$\frac{\partial}{\partial t}\int_0^t A(t,\ \tau)\ \text{cov}[z(\tau),\ z(\sigma)]d\tau = -0 + A(t,\ t)\ \text{cov}[z(t),\ z(\sigma)]$$

$$+ \int_0^t \frac{\partial}{\partial t} A(t,\ \tau)\ \text{cov}[z(\sigma),\ z(\tau)]d\tau\ , \qquad \text{(C.8)}$$

where

$$\begin{aligned}
\text{cov}[z(t),\ z(\sigma)] &= \text{cov}[H(t)\,x(t) + v(t),\ z(\sigma)] \\
&= H(t)\,\text{cov}[x(t),\ z(\sigma)] + \text{cov}[v(t),\ z(\sigma)], \qquad \text{(C.9)}
\end{aligned}$$

and

$$H(t)\ \underset{\text{(C-6)}}{\text{cov}}[x(t),\ z(\sigma)] = H(t)\int_0^t A(t,\tau)\ \text{cov}[z(\tau),\ z(\sigma)]\ d\tau\ . \quad \text{(C.10)}$$

From Eqs. (C.6), (C.7), and (C.8)

$$\frac{d}{dt}\left\{\text{cov}[x(t),\, z(\sigma)] = \int_0^t A(t,\, \tau)\ \text{cov}[z(\sigma),\, z(\tau)]\,d\tau\right\} \Longrightarrow$$

$$F(t)\ \text{cov}[x(t),\, z(\sigma)] + G(t)\ H(\sigma)\ \text{cov}[u(t)\ x(\sigma)] + G(t)\ \text{cov}[u(t),\, v(\sigma)]$$

$$= A(t,\, t)\ H(t)\ \text{cov}[x(t),\, z(\sigma)] + A(t,\, t)\ \text{cov}[v(t),\, z(\sigma)]$$

$$+\int_0^t \frac{\partial}{\partial t} A(t,\, \tau)\ \text{cov}[z(\sigma),\, z(\tau)]\,d\tau, \quad \forall\, 0<\sigma<t \quad . \quad \text{(C.11)}$$

Noting also in Eq. (C.11) that

$$A(t,\, t)\ \text{cov}[v(t),\, z(\sigma)] = A(t,\, t)\ \text{cov}[v(t),\, H(\sigma)\ x(\sigma) + v(\sigma)]$$

$$= A(t,\, t)\ H(\sigma)\ \text{cov}[v(t), x(\sigma)] + A(t,\, t)$$

$$\text{cov}[v(t), v(\sigma)], \qquad \text{(C.12)}$$

and putting it in the integral form of Eq. (C.6) where appropriate, Eq. (C.11) becomes $\forall\ 0 < \sigma < t$,

$$F(t)\int_0^t A(t, \tau)\ \text{cov}[z(\sigma), z(\tau)]\,d\tau - A(t, t)\ H(t)\int_0^t A(t, \tau)\ \text{cov}[z(\sigma), z(\tau)]\,d\tau$$

$$-\int_0^t \frac{\partial}{\partial t} A(t, \tau)\ \text{cov}[z(\sigma), z(\tau)]\,d\tau + G(t)\ H(\sigma)\ \text{cov}[u(t), x(\sigma)] + G(t)\ \text{cov}[u(t), v(t)]$$

$$- A(t, t)\ H(\sigma)\ \text{cov}[v(t), x(\sigma)] + A(t, t)\ \text{cov}[v(t), v(\sigma)] = 0 \quad . \quad \text{(C.13)}$$

The last four terms in Eq. (C.13) can be rationalized to zero as follows:

$G(t)\, H(\sigma)\, \text{cov}\,[u(t), x(\sigma)] = 0$ because present noise measurement is uncorrelated with previous condition of state

$G(t)\, \text{cov}\,[u(t), v(\sigma)] = 0$ because present noise measurement is uncorrelated with previous condition of state

$H(\sigma)\, \text{cov}[v(t), x(\sigma)] = 0$ for the time $\sigma < \tau$

$\text{cov}[v(t), v(\sigma)] = 0$ because past noise does not influence present noise measurement.

Thus Eq. (C.13) becomes,

$$\int_0^t \left[F(t)\, A(t,\tau) - A(t,t)\, H(t)\, A(t,\tau) - \frac{\partial A}{\partial t}(t,\tau)\right] \text{cov}\left[z(\sigma), z(\tau)\right] d\tau = 0 \quad \text{(C.14)}$$

This is satisfied if $A(t, \tau)$ is a solution of the equation. Therefcre,

$$\frac{\partial A}{\partial t}(t, \tau) = F(t)\, A(t, \tau) - A(t, t)\, H(t)\, A(t, \tau) \quad . \quad \text{(C.15)}$$

Deriving a differential equation for $\hat{x}(t)$ commences with

$$\hat{x}(t|t) = \int_0^t A(t, \tau)\, z(\tau)\, d\tau \quad . \quad \text{(C.16)}$$

Thus,

$$\dot{\hat{x}}(t|t) = \frac{d}{dt}\int_0^t A(t, \tau)\, z(\tau)\, d\tau = A(t, t)\, z(t) + \int_0^t \frac{\partial A(t, \tau)}{\partial t}\, z(\tau)\, d\tau \,. \quad \text{(C.17)}$$

Putting Eq. (C.15) into Eq. (C.17) gives

$$\dot{\hat{x}}(t|t) = A(t, t)\, z(t) + \int_0^t [F(t)\, A(t, \tau) - A(t, t)\, H(t)\, A(t, \tau)\, z(\tau)\, d\tau \quad \text{(C.18)}$$

$$= [F(t) - A(t, t)\, H(t)] \int_0^t A(t, \tau)\, z(\tau)\, d\tau + A(t, t)\, z(t) \quad \text{(C.19)}$$

or finally,

$$\boxed{\dot{\hat{x}}(t|t) = F(t)\,\hat{x}(t|t) + A(t,\,t)\,[z(t) - H(t)\,x(t|t)] \quad , \quad \forall\ 0 < \sigma < t} \qquad (C.20)$$

Now solve for the optimum gain, noting that $A(t,\,t) \triangleq K(t)$, by using Eq. (C.6) again,

$$\mathrm{cov}\left[x(t_1),\, z(\sigma)\right] = \int_0^t A(t_1,\,\tau)\ \mathrm{cov}[z(\tau),\, z(\sigma)]\ d\tau, \quad \forall\ \ 0 < \sigma < t \quad . \qquad (C.21))$$

Rewrite by letting $t_1 = t$ to obtain

$$\mathrm{cov}[x(t),\, y(\sigma) + v(\sigma)] = \int_0^t A(t,\,\tau)\ \mathrm{cov}[y(\tau) + v(\tau),\, y(\sigma) + v(\sigma)]d\tau \quad . \qquad (C.22)$$

Expanding the left side of Eq. (C.22) yields

$$\begin{aligned}\mathrm{cov}[x(t),\, y(\sigma) + v(\sigma)] &= \mathrm{cov}[x(t),\, y(\sigma)] + \mathrm{cov}\left[x(t),\, v^T(\sigma)\right] \\ &= \mathrm{cov}\left[x(t),\, x^T(\sigma)\ H^T(\sigma)\right] + \mathrm{cov}\left[x(t),\, v^T(\sigma)\right] \\ &= \mathrm{cov}\left[x(t),\, x^T(\sigma)\right] H^T(\sigma) + \mathrm{cov}\left[x(t),\, v^T(\sigma)\right]. \qquad (C.23)\end{aligned}$$

At time $\sigma = t$,

$$\mathrm{cov}\left[x(t),\, y(t) + v(t)\right] = \mathrm{cov}\left[x(t),\, x^T(t)\right] H^T(t) + \mathrm{cov}\left[x(t),\, v^T(t)\right] . \qquad (C.24)$$

Now,

$$x(t) = \Phi(t,\,0)\ x(0) + \int_0^t \Phi(t,\,\tau)\ G(\tau)\ u(\tau)\ d\tau \quad , \qquad (C.25)$$

therefore,

$$\text{cov}\left[x(t),\ v^T(t)\right] = \int_0^t \Phi(t,\ \tau)\ G(\tau)\ \text{cov}\left[u(\tau),\ v^T(t)\right] d\tau \quad , \qquad (C.26)$$

because $x(0)$ is independent of $v(t)$, $t \geq 0$.

But,

$$\text{cov}\left[u(\tau),\ v^T(t)\right] = S(t)\ \delta(t - \tau) \qquad (C.27)$$

so that Eq. (C.26) is

$$\text{cov}\left[x(t),\ v^T(t)\right] = G(t)\ S(t) \quad , \qquad (C.28)$$

and finally the left side of Eq. (C.21) becomes

$$\text{cov}\left[x(t),\ z^T(t)\right] = \text{cov}\left[x(t),\ x^T(t)\right] H^T(t) + G(t)\ S(t) \qquad (C.29)$$

Now under the integral sign in Eq. (C.21),

$$\text{cov}\left[z(\tau), z^T(\sigma)\right] = \text{cov}\left[z(\tau), z^T(t)\right] \quad \text{at } \sigma = t \quad . \qquad (C.30)$$

Therefore,

$$\begin{aligned}
\text{cov}\left[z(\tau)\ z^T(\sigma)\right] &= \text{cov}\left[z(\tau),\ H(t)\ x(t) + v(\tau)^T\right] \qquad (C.31)\\
&= \text{cov}\left[z(\tau),\ x^T(t)\right] H^T(t) + \text{cov}\left[z(\tau),\ v^T(t)\right]\\
&= \text{cov}\left[z(\tau),\ x^T(t)\right] H^T(t) + \text{cov}\left[H(\tau)\ x(\tau) + v(\tau), v^T(t)\right]\\
&= \text{cov}\left[z(\tau),\ x^T(t)\right] H^T(t) + H(\tau)\ \text{cov}\left[x(\tau),\ v^T(t)\right]\\
&\qquad + \text{cov}\left[v(\tau),\ v^T(t)\right]\\
&= \text{cov}\left[z(\tau),\ x^T(t)\right] H^T(t) + H(\tau)\ \text{cov}\left[x(\tau),\ v^T(t)\right]\\
&\qquad + R(t)\ \delta(t - \tau). \qquad (C.32)
\end{aligned}$$

Putting Eqs. (C.29) and (C.30) into Eq. (C.21) gives

$$\mathrm{cov}\left[x(t),\, x^T(t)\right] H^T(t) + G(t)\, S(t) - \int_0^t A(t,\, \tau)\, \mathrm{cov}\left[z(\tau),\, x^T(t)\right] H^T(t)\, d\tau$$

$$- \int_0^t A(t,\, \tau)\, H(\tau) \left[\mathrm{cov}\, x(\tau),\, v^T(t)\right] d\tau - \int_0^t A(t,\tau)\, R(t)\, \delta(t-\tau)\, d\tau = 0 \qquad \text{(C.33)}$$

Now,

$$\int_0^t A(t,\, \tau)\, H(\tau)\, \mathrm{cov}\left[x(\tau),\, v^T(t)\right] d\tau = 0 \quad , \qquad \text{(C.34)}$$

because

$$\mathrm{cov}\left[x(\tau),\, v^T(t)\right] = \begin{cases} 0 & , \quad t \neq \tau \\ \\ G(t)\, S(t), & t = \tau \end{cases} .$$

Except for the infinitesimal instant when $t = \tau$, the integral in Eq. (C.34) is zero. Also,

$$\int_0^t A(t,\, \tau)\, R(t)\, \delta(t-\tau) d\tau = A(t,\, t)\, R(t) \triangleq K(t)\, R(t) \quad .$$

Therefore Eq. (C.33) becomes

$$\mathrm{cov}\left[x(t),\, x^T(t)\right] H^T(t) + G(t)\, S(t) - \int_0^t A(t,\, \tau)\, \mathrm{cov}\left[z(\tau),\, x^T(t)\right] H^T(t)\, d\tau$$

$$- K(t)\, R(t) = 0 \quad . \qquad \text{(C.35)}$$

Now appealing to mathematical formalities of continuity, differentiality, etc., which are necessary to interchange the integral and covariance operations,

$$\operatorname{cov}\left[x(t) - \int_0^t A(t, \tau)\, z(\tau) d\tau,\ x^T(t)\right] H^T(t) + G(t)\, S(t) = K(t)\, R(t), \tag{C.36}$$

but from Eq. (C.16)

$$\int_0^t A(t, \tau)\, z(\tau)\, d\tau = x(t|t) \triangleq x(t) \quad .$$

Therefore, Eq. (C.36) becomes

$$\operatorname{cov}\left[x(t) - \hat{x}(t),\ x^T(t)\right] H^T(t) + G(t)\, S(t) = K(t)\, R(t) \tag{C.37}$$

or

$$\operatorname{cov}\left[\tilde{x}(t),\ x^T(t)\right] H^T(t) + G(t)\, S(t) = K(t)\, R(t) \quad . \tag{C.38}$$

Now,

$$\begin{aligned} \operatorname{cov}\left[\tilde{x}(t),\ x^T(t)\right] &= \operatorname{cov}\left[\tilde{x}(t),\ \tilde{x}^T(t) + \hat{x}^T(t)\right] \\ &= \operatorname{cov}\left[\tilde{x}(t),\ \tilde{x}^T(t)\right] + \operatorname{cov}\left[\tilde{x}(t),\ \hat{x}^T(t)\right] \\ &= \operatorname{cov}\left[\tilde{x}(t),\ \tilde{x}^T(t)\right] \triangleq \Sigma(t) \quad , \end{aligned} \tag{C.39}$$

where the last covariance term is zero because the error is perpendicular to its estimate [7]. Now, putting Eq. (C.39) into Eq. (C.38),

$$\Sigma(t)\, H^T(t) + G(t)\, S(t) = K(t)\, R(t) \quad , \tag{C.40}$$

so that the optimal gain is

$$\boxed{K(t) = \left[\Sigma(t)\, H(t) + G(t)\, S(t)\, R(t)^{-1}\right]} \, . \tag{C.41}$$

For the covariance Riccati equation it is noted

$$\Sigma(t) = \mathrm{cov}\left[\tilde{x}(t), \tilde{x}(t)\right] \quad , \tag{C.42}$$

$$\dot{\Sigma}(t) = \mathrm{cov}\left[\dot{\tilde{x}}(t), \tilde{x}(t)\right] + \mathrm{cov}\left[\tilde{x}(t), \dot{\tilde{x}}(t)\right] \quad . \tag{C.43}$$

Defining

$$\tilde{x}(t) \triangleq x(t) - \hat{x}(t) \quad , \tag{C.44}$$

$$\dot{\tilde{x}}(t) \triangleq \dot{x}(t) - \dot{\hat{x}}(t) \quad , \tag{C.45}$$

then,

$$\begin{aligned}
\dot{\tilde{x}}(t) &= F(t)\, x(t) + G(t)\, u(t) - F(t)\, \hat{x}(t) - K(t)\left[z(t) - H(t)\, \hat{x}(t)\right] \\
&= F(t)\, x(t) + G(t)\, u(t) - F(t)\, \hat{x}(t) - K(t)\left[H(t)\, x(t) + v(t) - H(t)\, \hat{x}(t)\right] \\
&= F(t)\left[x(t) - \hat{x}(t)\right] - K(t)\, H(t)\left[x(t) - \hat{x}(t)\right] + G(t)\, U(t) - K(t)\, v(t) \quad .
\end{aligned}$$

Thus,

$$\dot{\tilde{x}}(t) = \left[F(t) - K(t)\, H(t)\right] \tilde{x}(t) + G(t)\, u(t) - K(t)\, v(t) \quad . \tag{C.46}$$

The solution to this differential equation is

$$\tilde{x}(t) = \Phi(t, 0)\, \tilde{x}(0) + \int_0^t \Phi(t, \tau)\left[G(\tau)\, u(\tau) - K(\tau)\, v(\tau)\right] d\tau \quad . \tag{C.47}$$

Next, put Eq. (C.46) and (C.48) into Eq. (C.43) noting again,

$$\text{cov}\left[u(t),\ u^T(\tau)\right] = Q(t)\ \delta(t-\tau)$$

$$\text{cov}\left[v(t),\ v^T(\tau)\right] = R(t)\ \delta(t-\tau)$$

$$\text{cov}\left[u(t),\ v^T(\tau)\right] = S(t)\ \delta(t-\tau)\ .$$

To simplify the notation, drop the arguments henceforth

$$\dot{\Sigma} = \text{cov}\left[(F-KH)\tilde{x} + Gu - Kv,\ \tilde{x}\right] + \text{cov}\left[\tilde{x},\ (F-KH)\tilde{x} + Gu - Kv\right]$$

$$= F\,\text{cov}\left[\tilde{x},\ \tilde{x}\right] - KH\,\text{cov}\left[\tilde{x},\ \tilde{x}\right] + G\,\text{cov}\left[u,\ \tilde{x}\right] - K\,\text{cov}\left[v,\ \tilde{x}\right]$$

$$+ \text{cov}\left[\tilde{x},\ \tilde{x}\right]F^T - \text{cov}\left[\tilde{x},\ \tilde{x}\right]H^T K^T + \text{cov}\left[\tilde{x},\ u\right]G^T - \text{cov}\left[\tilde{x},\ v\right]K^T\ , \qquad (C.48)$$

$$\dot{\Sigma} = F\Sigma - KH\Sigma + \frac{1}{2}GQG^T - KRK - \Sigma F^T - \Sigma H^T K^T + \frac{1}{2}GQG^T - GSK^T - KS^T G^T\ . \qquad (C.49)$$

$$\dot{\Sigma} = F\Sigma + \Sigma F^T - K\left[\Sigma H^T + GS\right]^T - \left[\Sigma H^T + GS\right]K^T + KRK^T + GQG^T\ . \qquad (C.50)$$

Using Eq. (C.41) for K in Eq. (C.50),

$$\dot{\Sigma} = F\Sigma + \Sigma F^T - \left[\Sigma H + GS\right]R^{-1}\left[H\Sigma^T + S^T G^T\right] - \left[\Sigma H^T + GS\right]\left\{\left[\Sigma H + GS\right]R^{-1}\right\}^T$$

$$+ \left[\Sigma H + GS\right]R^{-1}R\left\{\left[\Sigma H + GS\right]R^{-1}\right\}^T + GQG^T,$$

or

$$\boxed{\dot{\Sigma} = F\Sigma + \Sigma F^T - \left(\Sigma H^T + GS\right)R^{-1}\left(\Sigma H^T + GS\right)^T + GQG^T}\ . \qquad (C.51)$$

C.4 SUMMARY

The results of the Kalman-Bucy paper have been extended to include

the case wherein there is correlation between the input process noise and the measurement noise. The equations of interest are shown in Table C.1.

Table C.1

SUMMARY OF KALMAN-BUCY ESTIMATOR WITH CORRELATED INPUT-MEASUREMENT NOISE

Message model	$\dot{x}(t) = F(t)\, x(t) + G(t)\, u(t)$
Observation model	$z(t) = H(t)\, x(t) + v(t)$
A priori statistics	$E\{u(t)\} = 0$ $E\{u(t),\, u^T(\tau)\} = Q\delta(t-\tau)$ } Process noise $E\{v(t)\} = 0$ $E\{v(t),\, v^T(\tau)\} = R\delta(t-\tau)$ } Measurement noise $E\{u(t),\, v^T(\tau)\} = S\delta(t-\tau)$ Correlated process and measurement noise
Filter algorithm	$\dot{\hat{x}}(t) = F(t)\, \hat{x}(t) + K(t)[z(t) - H(t)\, \hat{x}(t)]$
Optimal gain algorithm	$K(t) = [\Sigma(t)\, H^T(t) + G(t)\, S(t)]\, R^{-1}(t)$
Error variance algorithm	$\dot{\Sigma}(t) = F(t)\, \Sigma(t) + \Sigma(t)\, F^T(t) - [\Sigma(t)\, H^T(t) + G(t)\, S(t)]\, R^{-1}(t)[\Sigma(t)\, H^T(t) + G(t)\, S(t)]^T + G(t)\, Q(t)\, G(t)$
Initial conditions	$\hat{x}(0) = E\{x(t_o)\} = \mu_x(o)$ $\Sigma(0) = E\{[x(t_o) - \hat{x}(t_o)][x(t_o) - \hat{x}(t_o)]^T\} = \sigma_x(o)$ $x(0) = x(t_o)$

Appendix D

COMPUTER PROGRAM LISTING AND SAMPLE OUTPUT

The listing is given for the five measurement, Case II, with fixed gains. The program is written in Fortran IV using double precision arithmetic.

The MAIN program defines the initial conditions on the states and the constant values. It then establishes the covariance matrix Riccati equation as well as temporary storage locations for the flow of data when the program commences. The measurement matrix (H), is established as a set of three row vectors to give a sequential updating. Though not a savings in this case, it is established for future studies wherein correlated input-measurement noise is to be investigated. After the measurement update sequence is completed, the updated states and covariances are used as new initial conditions for the differential equations propagated in subroutine DIFFEQ. The output is formatted for the printout and finally the plot routine is prepared to accept data for storage on tape for later graphing off line.

Subroutine DIFFEQ is the subroutine which specifies the form of the differential equations. It computes elements of the F matrix about the current estimate rather than about a nominal trajectory because the latter is undefined. The random noise injected into the system equations is also defined in this subroutine. It uses random numbers

generated with a uniform distribution in subroutine RANDU to obtain random numbers with a Gaussian distribution using the Box-Müller transformation.

Subroutine RUK is a fourth-order Runga-Kutta quaterature routine which integrates the differential equations.

Subroutine SORT is a matrix conditioner to prepare the measurement matrix for call into the update sequencing. Again, though it is not necessary in this case, it is available for future studies when the rows of H are no longer merely a single constant, unity, and a list of zeros.

Subroutine RANDU is a random number generator. It generates random numbers with a uniform distribution in the closed set [0, 1].

The subroutine BLOCK DATA sets up initial conditions throughout the program prior to any computations in the algorithms. It is an efficient way to initialize constants which are common to many subroutines.

The computer printout shown in the last two pages of text are representative of the data obtained. The last page is the printout at time t = 10 seconds into the simulated flight. The page previous to it indicates the initial conditions at time t = 0 second.

```
C*****************
C      ESTIMATION OF INERTIAL SYSTEM ERRORS
C  USING TERMINAL GUIDANCE POSITION MEASUREMENTS
C         VIA A RADAR MAP MATCHING SYSTEM
C*****************
C  THIS PROGRAM GENERATES A CONSTANT VELOCITY DESCENT TRAJECTORY,
C  COMMENCING AT 30,000 FT. FOR A RE-ENTRY BODY.  AN EXTENSION OF THE
C  KALMAN-BUCY FILTER ESTIMATES THE ERROR IN AN INERTIAL SYSTEM.  THE
C  EQUATIONS MODELLING THE SYSTEM HAVE BEEN LINEARIZED ABOUT THE CUR-
C  RENT ESTIMATE.  A MONTE CARLO TECHNIQUE IS USED TO GENERATE THE
C  NOISE IN THE MEASUREMENTS SIMULATED AS A RADAR MAP-MATCHING SYSTEM,
C  AND TO SIMULATE THE NOISE IN THE INPUT PROCESS.  A PLOT ROUTINE
C  LOCATED AT THE END OF MAIN PROGRAM GENERATES THE OUTPUT GRAPHS.
C**************
C  DEFINITIONS OF THE DIMENSIONED VARIABLES
C**************
C      X(I)            STATES OF THE SYSTEM
C      DX(I)           DIFFERENTIALS OF THE STATES
C      SAAV(I,J)        A STATE ARRAY SAVED FOR EACH INCREMENT OF TIME
C      SAAVUP(I,J)     TEMPORARY STORE FOR ALL THE STATES
C      XSAAV(I)            "       "    "      THE INS STATES
C      PSAAV(I)            "  VECTOR    "   " THE COVARIANCE ELEMENTS
C      P(I,J)              "  MATRIX    "   "    "       "       "
C      HROW1(I,J)      A ROW VECTOR OF MEASUREMENT OBSERVATIONS
C      HROW2(I,J)      " "   "    "    "      "           "
C      HROW3(I,J)      " "   "    "    "      "           "
C      H(I)            THE MEASUREMENT VALUES
C      STO(I)          STORAGE OF MEASUREMENTS AND GAINS
C      RKOP(I,J)       STORAGE OF OPTIMAL GAINS FOR THE ENTIRE RUN
C      PPLUS9I)        STORAGE OF COVARIANCE AFTER A MEASUREMENT UPDATE
C      XMSAV(I)          "     "   STATES    "   "      "       "
C      ERRX(I)         DIFFERENCE BETWEEN ACTUAL AND ESTIMATED STATES AFTER
C                      A MEASUREMENT UPDATE
C      ERRXM(I)        DIFFERENCE BETWEEN ACTUAL AND ESTIMATED STATES
C                      BEFORE A MEASUREMENT UPDATE
C      F(I,J)          DYNAMIC SYSTEM F MATRIX
C      FP(I,J)         MULTIPLIED F AND P MATRICES
C      DQDT(I,J)       MULTIPLIED D,Q,AND D TRANSPOSE MATRICES
C**************
C  DEFINITIONS OF THE NONDIMENSIONED VARIABLES
C**************
C      X1       X-POSITION ERROR OF INS AS A STATE
C      Y2       Y-POSITION  "    "  "  "  "  "
C      Z3       Z-POSITION  "    "  "  "  "  "
C      XP6      X1 STATE PERTURBED WITH NOISE
C      YP7      Y2  "      "        "    "
C      ZP8      Z3  "      "        "    "
C      RX       SPECTRAL DENSITY OF MEASUREMENT NOISE IN X
C      RY         "          "   "       "          "  " Y
C      RZ         "          "   "       "          "  " Z
C      QX         "          "   "  PROCESS         "  " X
C      QY         "          "   "       "          "  " Y
C      QZ         "          "   "       "          "  " Z
C      OMEGA    EARTH'S ANGULAR VELOCITY IN AN INERTIAL BASIS
C      DEG      DEGREE
C      GE       EARTH'S ACCELERATION OF GRAVITY
C      RE       EARTH'S RADIUS
C      ELAT     LATITUDE
C      PI       CONSTANT IN RADIANS
C      IUPDAT   THE NUMBER OF MEASUREMENT OBSERVATIONS
C      IX       RANDOM NUMBER FOR THE MONTE CARLO SIMULATION
C      DT       INTEGRATION STEP SIZE
```

```
C**************
C  NOTE:  ALL OTHER VARIABLES ARE USED TO SHORTEN THE
C  ALGEBRAIC EXPRESSIONS AND HENCE ARE SELF EXPLANATORY.
C**************
C  MAIN PROGRAM FOLLOWS
C**************
      IMPLICIT REAL*8 (A-H,O-Z)
      REAL*8 X(26),DX(26)
      COMMON/ARRAY1/SAAV(26,58),SAAVUP(26),XSAAV(5),
     1 PSAAV(15),P(5,5)
      COMMON/ARRAY2/HROW1(1,5),HROW2(1,5),HROW3(1,5),H(5),ST9(5),
     1 RKOPT(5,58),PPLUS(25),XMSAV(5)
      COMMON/ARRAY3/ERRX(5),ERRXM(5)
      COMMON/ARRAY4/F(5,5),FP(5,5),DQDT(5,5)
      COMMON/B1/X1,Y2,Z3,XP6,YP7,ZP8,RX,RY,RZ
      COMMON/C1/OMEGA,ELAT,DEG,GE,RE,PI,T,DELTAT,ICOUNT,IMAX,IUPDAT,NS
      COMMON/C2/IX,LIM
      EXTERNAL RANDU
C
C  CONSTANTS INITIALIZED IN THIS BLOCK.
C
      OMEGA=15.04107D0
      DEG=0.0174532900
      GE=32.1740D0
      RE=6378388.D0*3.28100
      ELAT=45.D0
      PI=3.141592653600
      IUPDAT=10
      LIM=51
      NS=26
      IX=4000
      DT=0.200
C
C  THESE ARE ADDITIONAL NON ZERO IC .
C  NOMINAL STATE ON FIRST PASS,ESTIMATED STATE THEREAFTER.
C
       DO 1011 J=1,NS
1011   X(J)=0.D0
       DO 1012 J=1,NS
1012   DX(J)=0.00
C
C  ACTUAL STATE IC.
C
      X(6)=1253.00
      X(7)=1317.00
      X(8)=1500.00
      X(9)=10.00
      X(10)=10.00
C
C  STATE ERROR COVARIANCE IC, UPPER TRIANGLE ONLY.
C
      X(11)=10000.00
      X(13)=10000.00
      X(16)=10000.00
      X(20)=0.0000100
      X(25)=0.0000100
C
C  INTEGRATION OF MAIN EQUATIONS
C
C  RMAX AND IMAX EQUAL TOTAL OF FLIGHT,T,DIVIDED BY INTEGRATION
C  STEP SIZE DELTA-T. K10 AND I10 ARE VARIED ACCORDING TO THE
C  NUMBER OF INTEGRATION STEPS AND DELTA-T SIZE.
```

```
125:  C
126:        RMAX=50.DO
127:        IMAX=IDINT(RMAX)
128:  C     K10=IMAX/IUPDAT
129:        K10=11
130:        ICOUNT=1
131:        DO 125 M5=1,NS
132:        DO 125 N5=1,56
133:  125   SAAV(M5,N5)=0.DO
134:        DO 1000 I10=1,6
135:  119   DO 120 J1=1,NS
136:        NS1=NS
137:  120   SAAV(J1,ICOUNT)=X(J1)
138:        ICOUNT=ICOUNT+1
139:  C
140:  122   CALL RUK(X,DT,NS1)
141:  C
142:        IF (ICOUNT-K10) 119,200,200
143:  200   CONTINUE
144:        DO 124 M4=1,NS
145:  124   SAAV(M4,ICOUNT)=X(M4)
146:  C
147:  C  GET READY FOR THE MEASUREMENT UPDATE.  THE H-MATRIX IS
148:  C  TREATED AS 3 SEPARATE ROWS OF H IN ORDER TO SAVE ON MATRIX
149:  C  MULTIPLICATION.  EACH INTEGRATION INTERVAL IS STORED IN ARRAY
150:  C  NAMED SAAV.
151:        DO 150 K=1,NS
152:  150   SAAVJP(K)=0.DO
153:        DO 151 I=1,NS
154:  151   SAAVJP(I)=SAAV(I,ICOUNT)
155:  C
156:  C  XHAT MINUS IS TAKEN FROM SAAVUP AND PLACED IN TEMPORARY STORAGE.
157:  C
158:        DO 152 J=1,5
159:  152   XSAAV(J)=0.DO
160:        DO 153 K=1,5
161:  153   XSAAV(K)=SAAVUP(K)
162:  C
163:  C  P MINUS IS TAKEN FROM SAAVJP AND PLACED IN ANOTHER TEMPORARY STORAGE.
164:  C
165:        DO 154 J=1,15
166:  154   PSAAV(J)=0.DO
167:        M1=0
168:        DO 155 K=11,25
169:        M1=M1+1
170:  155   PSAAV(M1)=SAAVJP(K)
171:  C
172:  C  PLACE P MINUS INTO 5X5 MATRIX FOR MEASUREMENT UPDATE.
173:  C
174:        DO 156 I=1,5
175:        DO 156 J=1,5
176:  156   P(I,J)=0.DO
177:        K1=0
178:        DO 157 M=1,5
179:        DO 157 N=1,M
180:        K1=K1+1
181:        P(N,M)=PSAAV(K1)
182:  157   P(M,N)=P(N,M)
183:  C
184:  C  DEFINE H AS A SET OF ROW VECTORS INSTEAD OF A SINGLE MATRIX.
185:  C  THESE ARE ITS IC.
186:  C
```

```
187:        HR9W1(1,1)=1.D0
188:        HR9W2(1,2)=1.D0
189:        HR9W3(1,3)=1.D0
190: C
191: C  MEASUREMENT ERR0R MATRIX IN C0LJMN F9RM.
192: C
193:        ERR0R1=XP6+RX-1.D0*X1
194:        ERR0R2=YP7+RY-1.D0*Y2
195:        ERR0R3=ZP8+RZ-1.D0*Z3
196: C
197: C  EXPECTED VALJE 0F MEASJREMENT N0ISE.
198: C
199:        SIGRX=50.D0
200:        PR9D1=SIGRX*SIGRX
201:        SIGRY=50.D0
202:        PR9D2=SIGRY*SIGRY
203:        SIGRZ=100.D0
204:        PR9D3=SIGRZ*SIGRZ
205: C
206: C  THIS IS FIRST INCREMENT 0F THE MEAsJREMENT UPDATE SEQJENCE.
207: C
208:        D0 105  LL1=1,5
209: 105    H(LL1)=0.D0
210:        D0 101 L1=1,5
211: 101    H(L1)=HR9W1(1,L1)
212:        CALL S9RT(P,H,ST9,5,5,1,5,2,25,5,5)
213:        CALL S9RT(H,ST9,HPHT,1,5,5,1,1,5,5,1)
214:        IF (HPHT.EQ.0) HPHT=1.D-15
215:        HPHT=HPHT+PR9D1
216:        D0 30 I=1,5
217: C  F0R THE FIXED GAINS CASE, H(I) IS BYPASSED WITH A
218: C  C0MMENT AND THE C0NSTANTS ARE INSERTED.  THE SAME
219: C  IS TRJE F0R THE 2ND AND 3RD INCREMENTS 9F JPDATES.
220: C  THE CASE HERE IS F0R THE 5 JPDATE SEQJENCE.
221: C      H(I)=ST9(I)/HPHT
222:        H(1)=0.16D-03
223:        H(2)=-0.40D-03
224:        H(3)=0.93D0
225:        H(4)=-0.05D-01
226:        IF(IC9UNT.GE.41)  H(4)=-0.4D-01
227: 300    H(5)=0.08D0
228:        IF(IC9JNT.GE.31)  H(5)=+0.16D0
229: 310    CONTINJE
230:        XSAAV(I)=XSAAV(I)+H(I)*ERR9R1
231:        D0 30 J=1,5
232: 30     P(I,J)=P(I,J)-H(I)*ST9(J)
233: C
234: C  THIS IS SEC9ND INCREMENT 9F THE MEASJREMENT JPDATE SEQJENCE.
235: C
236:        D0 102 L2=1,5
237: 102    H(L2)=HR9W2(1,L2)
238:        CALL S9RT(P,H,ST9,5,5,1,5,2,25,5,5)
239:        CALL S9RT(H,ST9,HPHT,1,5,5,1,1,5,5,1)
240:        IF (HPHT.EQ.0) HPHT=1.D-15
241:        HPHT=HPHT+PR9D2
242:        D0 31 I=1,5
243: C      H(I)=ST9(I)/HPHT
244:        H(1)=0.16D-03
245:        H(2)=-0.40D-03
246:        H(3)=0.93D0
247:        H(4)=-0.05D-01
248:        IF(IC9UNT.GE.41)  H(4)=-0.4D-01
```

```
      320   H(5)=0.0800
            IF(ICOUNT.GE.31)  H(5)=+0.1600
      330   CONTINUE
            XSAAV(I)=XSAAV(I)+H(I)*ERROR2
            DO 31 J=1,5
      31    P(I,J)=P(I,J)-H(I)*STO(J)
C
C  THIS IS THIRD INCREMENT OF THE MEASUREMENT UPDATE SEQUENCE.
C
            DO 103 L3=1,5
      103   H(L3)=HROW3(1,L3)
            CALL SORT(P,H,STO,5,5,1,5,2,25,5,5)
            CALL SORT(H,STO,HPHT,1,5,5,1,1,5,5,1)
            IF (HPHT.EQ.0) HPHT=1.0-15
            HPHT=HPHT+PROD3
            DO 32 I=1,5
C           H(I)=STO(I)/HPHT
            H(1)=0.160-03
            H(2)=-0.400-03
            H(3)=0.9300
            H(4)=-0.050-01
            IF(ICOUNT.GE.41)  H(4)=-0.400-01
      340   H(5)=0.0800
            IF(ICOUNT.GE.31)  H(5)=+0.1600
      350   CONTINUE
            RKOPT(I,ICOUNT)=H(I)
            XSAAV(I)=XSAAV(I)+H(I)*ERROR3
            DO 32 J=1,5
      32    P(I,J)=P(I,J)-H(I)*STO(J)
            DO 106 K2=1,25
      106   PPLUS(K2)=0.00
            K3=10
            DO 104 I3=1,5
            DO 104 J3=1,I3
            K3=K3+1
      104   PPLUS(K3)=P(J3,I3)
C
C  AT THIS POINT THE MEASUREMENT UPDATE SEQUENCE IS COMPLETED.
C  THE VALUE FOR X HAT PLUS IS STORED IN THE LAST XSAAV(I), THE VALUES
C  P PLUS ARE STORED IN THE LAST PPLUS(I), AND THE OPTIMAL GAINS ARE
C  IN KOPT(I).
C
C  GET THE UPDATED STATES AND COVARIANCES BACK INTO A FORMAT
C  SUITABLE AS THE NEW IC'S FOR TIME PROPOGATION VIA INTEGRATION OF THE
C  DIFFERENTIAL EQUATIONS.
C
C  THIS IS FOR XHAT PLUS.
C
            DO 162 K11=1,5
      162   X(K11)=XSAAV(K11)
C
C  THIS COLLECTS X PERTURBED
C
            DO 164 M11=6,10
      164   X(M11)=SAAVUP(M11)
C
C  THIS IS COVARIANCE PLUS.
C
            DO 163 LII=11,25
      163   X(LII)=PPLUS(LII)
C
C  THIS IS TIME
```

```
311:  C
312:  165   X(26)=SAAVJP(26)
313:  C
314:  C  THIS BLOCK FORMATS THE OUTPUT.
315:  C
316:        M=1
317:        IF (K10.NE.11) M=K10-10
318:  701   FORMAT('1',/,5X,'T=',D12.4,2X,'SAAV INDEX=',I4,/)
319:        WRITE(6,701)  SAAV(26,M),M
320:  C
321:  702   FORMAT(' ',5X,'THE ACTUAL ERROR IN THE INERTIAL NAVIGATOR ,IE,',
322:       1 'THE PERTURBED STATE :')
323:        WRITE(6,702)
324:  C
325:  703   FORMAT(' ',5X,'XP =',D17.10,2X,'YP =',D17.10,2X,'ZP =',D17.10,2X,
326:       1 'VXP=',D17.10,2X,'VZP=',D17.10,///)
327:        WRITE(6,703)  SAAV(6,M),SAAV(7,M),SAAV(8,M),SAAV(9,M),SAAV(10,M)
328:  C
329:  704   FORMAT(' ',5X,'THE ESTIMATED INERTIAL NAVIGATOR ERROR (STATE)'
330:       1 ' BEFORE A MEASUREMENT UPDATE :')
331:        WRITE(6,704)
332:  C
333:  705   FORMAT(' ',5X,'XE =',D17.10,2X,'YE =',D17.10,2X,'ZE =',D17.10,2X,
334:       1 'VXE=',D17.10,2X,'VZE=',D17.10,///)
335:        WRITE(6,705)  SAAV(1,M),SAAV(2,M),SAAV(3,M),SAAV(4,M),SAAV(5,M)
336:  C
337:  5051  FORMAT(' ',5X,'THE ESTIMATED INERTIAL NAVIGATOR ERROR (STATE)',
338:       1 ' AFTER A MEASUREMENT UPDATE :')
339:        WRITE(6,5051)
340:  C
341:  5052  FORMAT(' ',5X,'XE =',D17.10,2X,'YE =',D17.10,2X,'ZE =',D17.10,2X,
342:       1 'VXE=',D17.10,2X,'VZE=',D17.10,///)
343:        WRITE(6,5052) XSAAV(1),XSAAV(2),XSAAV(3),XSAAV(4),XSAAV(5)
344:  C
345:  506   FORMAT(' ',5X,'THE FILTER ERROR IN ESTIMATED STATE BEFORE',
346:       1 ' THE MEASUREMENT UPDATE :')
347:        WRITE(6,506)
348:  C
349:        DO 601 L=1,5
350:        N=L+5
351:  601   ERRX(L)=SAAV(L,M)-SAAV(N,M)
352:  507   FORMAT(' ',5X,'ERRX=',D17.10,2X,'ERRY=',D17.10,2X'ERRZ=',D17.10,
353:       1 2X,'ERRVX=',D17.10,2X,'ERRVZ=',D17.10,///)
354:        WRITE(6,507)  ERRX(1),ERRX(2),ERRX(3),ERRX(4),ERRX(5)
355:  C
356:  508   FORMAT(' ',5X,'THE FILTER ERROR IN ESTIMATED STATE',
357:       1 '  AFTER THE MEASUREMENT UPDATE :')
358:        WRITE(6,508)
359:  C
360:        KK=0
361:        DO 602 L=6,10
362:        KK=KK+1
363:  602   XMSAV(KK)=SAAVUP(L)
364:        DO 603 N=1,5
365:  603   ERRXM(N)=XSAAV(N)-XMSAV(N)
366:  C
367:  509   FORMAT(' ',5X,'ERRX=',D17.10,2X,'ERRY=',D17.10,2X,'ERRZ=',D17.10,
368:       1 2X,'ERRVX=',D17.10,2X,'ERRVZ=',D17.10,///)
369:        WRITE(6,509)  ERRXM(1),ERRXM(2),ERRXM(3),ERRXM(4),ERRXM(5)
370:  C
371:  710   FORMAT(' ',5X,'THE ERROR COVARIANCE MATRIX BEFORE',
372:       1 '  A MEASUREMENT UPDATE :')
```

```
      WRITE(6,710)
C
711   FORMAT(' ',5X,'P11 =',D17.10,2X,'P12 =',D17.10,2X,'P13 =',D17.10,
     1 2X,'P14 =',D17.10,2X,'P15 =',D17.10)
      WRITE(6,711)  SAAV(11,M),SAAV(12,M),SAAV(14,M),SAAV(17,M),
     1 SAAV(21,M)
C
712   FORMAT(' ',29X,'P22 =',D17.10,2X,'P23 =',D17.10,2X,'P24 =',D17.10,
     1 2X,'P25 =',D17.10)
      WRITE(6,712)  SAAV(13,M),SAAV(15,M),SAAV(18,M),SAAV(22,M)
C
713   FORMAT(' ',53X,'P33 =',D17.10,2X,'P34 =',D17.10,2X,'P35 =',D17.10)
      WRITE(6,713)  SAAV(16,M),SAAV(19,M),SAAV(23,M)
C
714   FORMAT(' ',77X,'P44 =',D17.10,2X,'P45 =',D17.10)
      WRITE(6,714)  SAAV(20,M),SAAV(24,M)
C
715   FORMAT(' ',101X,'P55 =',D17.10,///)
      WRITE(6,715)  SAAV(25,M)
C
516   FORMAT(' ',5X,'THE ERROR COVARIANCE MATRIX AFTER',
     1 '  A MEASUREMENT UPDATE :')
      WRITE(6,516)
C
517   FORMAT(' ',5X,'P11 =',D17.10,2X,'P12 =',D17.10,2X,'P13 =',D17.10,
     1 2X,'P14 =',D17.10,2X,'P15 =',D17.10)
      WRITE(6,517)  PPLUS(11),PPLUS(12),PPLUS(14),PPLUS(17),PPLUS(21)
C
518   FORMAT(' ',29X,'P22 =',D17.10,2X,'P23 =',D17.10,2X,'P24 =',D17.10,
     1 2X,'P25 =',D17.10)
      WRITE(6,518)  PPLUS(13),PPLUS(15),PPLUS(18),PPLUS(22)
C
519   FORMAT(' ',53X,'P33 =',D17.10,2X,'P34 =',D17.10,2X,'P35 =',D17.10)
      WRITE(6,519)  PPLUS(16),PPLUS(19),PPLUS(23)
C
520   FORMAT(' ',77X,'P44 =',D17.10,2X,'P45 =',D17.10)
      WRITE(6,520)  PPLUS(20),PPLUS(24)
C
521   FORMAT(' ',101X,'P55 =',D17.10,///)
      WRITE(6,521)  PPLUS(25)
C
522   FORMAT(' ',5X,'THE OPTIMAL TIME-VARYING FILTER GAINS :')
      WRITE(6,522)
C
523   FORMAT(' ',5X,'KX =',D17.10,2X,'KY =',D17.10,2X,'KZ =',D17.10,
     1 2X,'KVX=',D17.10,2X,'KVZ=',D17.10,/)
      WRITE(6,523)  RKOPT(1,M),RKOPT(2,M),RKOPT(3,M),RKOPT(4,M),
     1 RKOPT(5,M)
      K10=K10+10
1000  CONTINUE
500   CONTINUE
C
C  THE NEXT BLOCK SETS UP THE PLOT ROUTINE FOR GRAPHING.
C
C
C  DATA FOR THE FIRST GRAPH (X-POSITION) FOLLOWS.
C
      DO 41 I=1,51
      X(I)=SAAV(26,I)
      Y=(SAAV(1,I)-SAAV(6,I))
      CALL POINT1(1,X,Y)
      Y=DSQRT(SAAV(11,I))
```

```
435:       CALLP9INT1(2,X,Y)
436:       Y=-Y
437:       CALL P9INT1(3,X,Y)
438: 41    CONTINUE
439:       CALL CURVE1(1,1,0)
440:       CALL CURVE1(2,1,0)
441:       CALL CURVE1(3,1,0)
442:       CALL P9INT1(4,0.,2.E4)
443:       CALL P9INT1(4,11.,-2.E4)
444:       CALL CURVE1(4,0,3)
445:       CALL TITLE2(43,'FILTER ERROR & VARIANCE: X(FT) VS TIME(SEC)')
446:       CALL GRAPH1(11.,'TIME',10.,'  X ')
447: C
448: C  DATA FOR THE SECOND GRAPH (Y-POSITION) FOLLOWS.
449: C
450:       DO 42 I=1,51
451:       X(I)=SAAV(26,I)
452:       Y=(SAAV(2,I)-SAAV(7,I))
453:       CALL P9INT1(1,X,Y)
454:       Y=DSQRT(SAAV(13,I))
455:       CALLP9INT1(2,X,Y)
456:       Y=-Y
457:       CALL P9INT1(3,X,Y)
458: 42    CONTINUE
459:       CALL CURVE1(1,1,0)
460:       CALL CURVE1(2,1,0)
461:       CALL CURVE1(3,1,0)
462:       CALL P9INT1(4,0.,2.E4)
463:       CALL P9INT1(4,11.,-2.E4)
464:       CALL CURVE1(4,0,3)
465:       CALL TITLE2(43,'FILTER ERROR & VARIANCE: Y(FT) VS TIME(SEC)')
466:       CALL GRAPH1(11.,'TIME',10.,'  Y ')
467: C
468: C  DATA FOR THE THIRD GRAPH (Z-POSITION) FOLLOWS.
469: C
470:       GO TO 430
471: 431   DO 43 I=1,51
472:       X(I)=SAAV(26,I)
473:       Y=(SAAV(3,I)-SAAV(8,I))
474:       CALL P9INT1(1,X,Y)
475:       Y=DSQRT(SAAV(16,I))
476:       CALLP9INT1(2,X,Y)
477:       Y=-Y
478:       CALL P9INT1(3,X,Y)
479: 43    CONTINUE
480:       CALL CURVE1(1,1,0)
481:       CALL CURVE1(2,1,0)
482:       CALL CURVE1(3,1,0)
483:       CALL P9INT1(4,0.,10.E3)
484:       CALL P9INT1(4,11.,-10.E3)
485:       CALL CURVE1(4,0,3)
486:       CALL TITLE2(43,'FILTER ERROR & VARIANCE: Z(FT) VS TIME(SEC)')
487:       CALL GRAPH1(11.,'TIME',10.,'  X ')
488: 430   CONTINUE
489: C
490: C  DATA FOR THE FOURTH GRAPH (X-VELOCITY) FOLLOWS.
491: C
492:       DO 44 I=1,51
493:       X(I)=SAAV(26,I)
494:       Y=(SAAV(4,I)-SAAV(9,I))
495:       CALL P9INT1(1,X,Y)
496:       Y=DSQRT(SAAV(20,I))
```

```
      CALLPOINT1(2,X,Y)
      Y=-Y
      CALL POINT1(3,X,Y)
44    CONTINUE
      CALL CURVE1(1,1,0)
      CALL CURVE1(2,1,0)
      CALL CURVE1(3,1,0)
      CALL POINT1(4,0.,3.E3)
      CALL POINT1(4,11.,-3.E3)
      CALL CURVE1(4,0,3)
      CALL TITLE2(45,'FILTER ERROR & VARIANCE: VX(FPS) VS TIME(SEC)')
      CALL GRAPH1(11.,'TIME',10.,' VX ')
C
C  DATA FOR THE FIFTH GRAPH (Z-VELOCITY) FOLLOWS.
C
      DO 45 I=1,51
      X(I)=SAAV(26,I)
      Y=(SAAV(5,I)-SAAV(10,I))
      CALL POINT1(1,X,Y)
      Y=DSQRT(SAAV(25,I))
      CALLPOINT1(2,X,Y)
      Y=-Y
      CALL POINT1(3,X,Y)
45    CONTINUE
      CALL CURVE1(1,1,0)
      CALL CURVE1(2,1,0)
      CALL CURVE1(3,1,0)
      CALL POINT1(4,0.,2.E3)
      CALL POINT1(4,11.,-2.E3)
      CALL CURVE1(4,0,3)
      CALL TITLE2(45,'FILTER ERROR & VARIANCE: VZ(FPS) VS TIME(SEC)')
      CALL GRAPH1(11.,'TIME',10.,' VZ ')
C
C  DATA FOR THE SIXTH GRAPH (KX OPTIMAL) FOLLOWS.
C
      DO 46 I=1,51
      X(I)=SAAV(26,I)
      Y=RKOPT(1,I)
      CALL POINT1(1,X,Y)
46    CONTINUE
      CALL CURVE1(1,1,0)
      CALL POINT1(2,0.,10.E-04)
      CALL POINT1(2,11.,0.E0)
      CALL CURVE1(2,0,3)
      CALL TITLE2(32,'SUBOPTIMAL GAIN: KX VS TIME(SEC)')
      CALL GRAPH1(11.,'TIME',10.,' KX ')
C
C  DATA FOR THE SEVENTH GRAPH (KY OPTIMAL) FOLLOWS.
C
      DO 47 I=1,51
      X(I)=SAAV(26,I)
      Y=RKOPT(2,I)
      CALL POINT1(1,X,Y)
47    CONTINUE
      CALL CURVE1(1,1,0)
      CALL POINT1(2,0.,-10.0E-04)
      CALL POINT1(2,11.,0.E0)
      CALL CURVE1(2,0,3)
      CALL TITLE2(32,'SUBOPTIMAL GAIN: KY VS TIME(SEC)')
      CALL GRAPH1(11.,'TIME',10.,' KY ')
C
C  DATA FOR THE EIGHTH GRAPH (KZ OPTIMAL) FOLLOWS.
```

```
559:  C
560:        DO 48 I=1,51
561:        X(I)=SAAV(26,I)
562:        Y=RKOPT(3,I)
563:        CALL POINT1(1,X,Y)
564:  48    CONTINUE
565:        CALL CURVE1(1,1,0)
566:        CALL POINT1(2,0.,20.E-01)
567:        CALL POINT1(2,11.,0.E0)
568:        CALL CURVE1(2,0,3)
569:        CALL TITLE2(32,'SUBOPTIMAL GAIN: <Z VS TIME(SEC)')
570:        CALL GRAPH1(11.,'TIME',10.,' <Z ')
571:  C
572:  C  DATA FOR THE NINTH GRAPH (<VX OPTIMAL) FOLLOWS.
573:  C
574:        DO 49 I=1,51
575:        X(I)=SAAV(26,I)
576:        Y=RKOPT(4,I)
577:        CALL POINT1(1,X,Y)
578:  49    CONTINUE
579:        CALL CURVE1(1,1,0)
580:        CALL POINT1(2,0.,5.0E-02)
581:        CALL POINT1(2,11.,-5.0E-02)
582:        CALL CURVE1(2,0,3)
583:        CALL TITLE2(33,'SUBOPTIMAL GAIN: <VX VS TIME(SEC)')
584:        CALL GRAPH1(11.,'TIME',10.,' <VX')
585:  C
586:  C  DATA FOR THE TENTH GRAPH (<VZ OPTIMAL) FOLLOWS.
587:  C
588:        DO 50 I=1,51
589:        X(I)=SAAV(26,I)
590:        Y=RKOPT(5,I)
591:        CALL POINT1(1,X,Y)
592:  50    CONTINUE
593:        CALL CURVE1(1,1,0)
594:        CALL POINT1(2,0.,20.0E-02)
595:        CALL POINT1(2,11.,0.E0)
596:        CALL CURVE1(2,0,3)
597:        CALL TITLE2(33,'SUBOPTIMAL GAIN: <VZ VS TIME(SEC)')
598:        CALL GRAPH1(11.,'TIME',10.,' <VZ')
599:        RETURN
600:        END
```

```
C
C
C
C
C
      SUBROUTINE DIFFEQ(X,DX,DT)
      IMPLICIT REAL*8 (A-H,O-Z)
       REAL*8 X(26),DX(26)
      COMMON/ARRAY1/SAAV(26,5),SAAVJP(26),XSAAV(5),
     1 PSAAV(15),P(5,5)
      COMMON/ARRAY2/WR0W1(1,5),WR0W2(1,5),WR0W3(1,5),W(5),ST0(5),
     1 RK0PT(5,58),PPLUS(25),XMSAV(5)
      COMMON/ARRAY3/ERRX(5),ERRXM(5)
      COMMON/ARRAY4/F(5,5),FP(3,5),DQDT(5,5)
      COMMON/B1/X1,Y2,Z3,XP6,YP7,ZP8,RX,RY,RZ
      COMMON/C1/OMEGA,ELAT,DEG,GE,RE,PI,T,DELTAT,ICOUNT,IMAX,IUPDAT,NS
      COMMON/C2/IX,LIM
C
C  THESE ARE SOME CONSTANTS FOR THIS RUN.
C
       WS=GE/RE
       WX1=0.00
       WY1=OMEGA*DEG*DCOS(ELAT*DEG)
       WZ1=OMEGA*DEG*DSIN(ELAT*DEG)
C
C  FOR SIMPLICITY IN THIS SIMULATION,CHOOSE THE OMEGA VECTOR AND ELAT
C  TO BE CONSTANT. LET ELAT BE  45 DEGREES NORTH.
C  THEY ARE AS FOLLOWS.
      WX=WX1
      WY=WY1
      WZ=WZ1
C
C  THUS, THEIR TIME DERIVATIVES ARE ZERO,IE.WXDOT=WYDOT=WZDOT=0
C  FOR THIS CASE.
C
       F41=-WS+(WY*WY+WZ*WZ)
       F42=-WX*WY
       F43=-WX*WZ
       F51=-WX*WZ
       F52=-WY*WZ
       F53=2.00*WS+(WX*WX+WY*WY)
       X1=X(1)
       Y2=X(2)
       Z3=X(3)
       VX4=X(4)
       VZ5=X(5)
C
C  THESE ARE NOMINAL STATE EQUATIONS WHICH ARE USED AS THE CURRENT
C  ESTIMATED STATE EQUATIONS AFTER THE FIRST PASS THROUGH THE
C  TIME INTEGRATION SEQUENCE.
C
       DX(1)=VX4*DT
       DX(2)=0.00*DT
       DX(3)=VZ5*DT
       DX(4)=(F41*X1+F42*Y2+F43*Z3+2.00*WY*VZ5)*DT
       DX(5)=(F51*X1+F52*Y2+F53*Z3+2.00*WY*VX4)*DT
C
C  NOW FORMULATE THE RANDOM NOISE GENERATED IN SUBROUTINE RANDU
C  THIS NOISE IS PUT INTO THE DRIVING NOISE TERMS Q AND IN THE
C  MEASUREMENTS  NOISE TERMS R.
C
      CALL RANDU(IX,IY,RNDM1)
```

```
      CALL RANDU(IY,IX,RNDM2)
      CALL RANDU(IX,IY,RNDM3)
      CALL RANDU(IY,IX,RNDM4)
      CALL RANDU(IX,IY,RNDM5)
      CALL RANDU(IY,IX,RNDM6)
      CALL RANDU(IX,IY,RNDM7)
      CALL RANDU(IY,IX,RNDM8)
      CALL RANDU(IX,IY,RNDM9)
      CALL RANDU(IY,IX,RNDM10)
      CALL RANDU(IX,IY,RNDM11)
      CALL RANDU(IY,IX,RNDM12)
      CALL RANDU(IX,IY,RNDM13)
      CALL RANDU(IY,IX,RNDM14)
      CALL RANDU(IX,IY,RNDM15)
      CALL RANDU(IY,IX,RNDM16)
C
      QX=1253.DD*DSQRT(-2.DD*DLOG(RNDM1))*DCOS(2.DD*PI*RNDM2)
      QY=1317.DD*DSQRT(-2.DD*DLOG(RNDM3))*DCOS(2.DD*PI*RNDM4)
      QZ= 210.DD*DSQRT(-2.DD*DLOG(RNDM5))*DCOS(2.DD*PI*RNDM6)
      QVX= 1.2DD*DSQRT(-2.DD*DLOG(RNDM7))*DCOS(2.DD*PI*RNDM8)
      QVZ= 1.4DD*DSQRT(-2.DD*DLOG(RNDM9))*DCOS(2.DD*PI*RNDM10)
      RX=  50.DD*DSQRT(-2.DD*DLOG(RNDM11))*DCOS(2.DD*PI*RNDM12)
      RY=  50.DD*DSQRT(-2.DD*DLOG(RNDM13))*DCOS(2.DD*PI*RNDM14)
      RZ= 100.DD*DSQRT(-2.DD*DLOG(RNDM15))*DCOS(2.DD*PI*RNDM16)
C
C  THESE ARE THE PERTURBED VARIABLES,IE, THEY WILL INCLUDE NOISE.
C
      XP6=X(6)
      YP7=X(7)
      ZP8=X(8)
      VXP9=X(9)
      VZP10=X(10)
C
C  THESE ARE ACTUAL STATE EQUATIONS,IE, THEY ARE PERTURBED WITH NOISE.
C
      DX(6)=(VXP9+QX)*DT
      DX(7)=(0.DD+QY)*DT
      DX(8)=(VZP10+QZ)*DT
      DX(9)=(F41*XP6+F42*YP7+F43*ZP8-2.DD*WY*VZP10+QVX)*DT
      DX(10)=(F51*XP6+F52*YP7+F53*ZP8+2.DD*WY*VXP9+QVZ)*DT
C
C  THIS IS THE F-MATRIX COMPOSED OF PARTIALS EVALUATED ABOUT
C  THE CURRENT ESTIMATE.  THAT IS, XHAT = XNOM+VARIATION XHAT.
C
      DO 97 I3=1,5
      DO 97 J3=1,5
97    F(I3,J3)=0.DD
      F(1,4)=1.DD
      F(3,5)=1.DD
      F(4,1)=F41
      F(4,2)=F42
      F(4,3)=F43
      F(4,5)=-2.DD*WY
      F(5,1)=F51
      F(5,2)=F52
      F(5,3)=F53
      F(5,4)=+2.DD*WY
C
C  COLLECT THE COVARIANCE MATRIX ELEMENTS FROM THE STATE VECTOR.
C
      DO 98 I2=1,5
      DO 98 J2=1,5
```

```
125:  98    P(I2,J2)=0.DD
126:        K1=10
127:        DO 12 I=1,5
128:        DO 12 J=1,I
129:        K1=K1+1
130:        P(J,I)=X(K1)
131:  12    P(I,J)=P(J,I)
132:  C
133:  C  FORM MATRIX FP.
134:  C
135:        DO 99 I1=1,5
136:        DO 99 J1=1,5
137:  99    FP(I1,J1)=0.DD
138:        DO 100 I=1,5
139:        DO 100 J=1,5
140:        DO 100 K=1,5
141:  100   FP(I,J)=FP(I,J)+F(I,K)*P(K,J)
142:  C
143:  C  FORM MATRIX ELEMENTS OF D*Q*DTRANSPOSE
144:  C
145:        DO 96 I4=1,5
146:        DO 96 J4=1,5
147:  96    DQDT(I4,J4)=0.DD
148:        Q1=1253.DD
149:        Q11=Q1*Q1
150:        DQDT(1,1)=Q11
151:        Q2=1317.DD
152:        Q22=Q2*Q2
153:        DQDT(2,2)=Q22
154:        Q3=210.DD
155:        Q33=Q3*Q3
156:        DQDT(3,3)=Q33
157:        Q4=1.2DD
158:        Q44=Q4*Q4
159:        DQDT(4,4)=Q44
160:        Q5=1.4DD
161:        Q55=Q5*Q5
162:        DQDT(5,5)=Q55
163:  C
164:  C  COLLECT THE ERROR COVARIANCE EQUATION FOR INTEGRATION IN
165:  C  THE STATE VARIABLE COLUMN.
166:  C
167:        K2=10
168:        DO 106 M=1,5
169:        DO 106 N=1,M
170:        K2=K2+1
171:  106   DX(K2)=(FP(M,N)+FP(N,M)+DQDT(M,N))*DT
172:  C
173:  C  THE LAST STATE IS TIME NEEDED FOR THE INTEGRATION SUBROUTINE.
174:  C
175:        DX(26)=1.DD*DT
176:        RETURN
177:        END
```

```
C
C
C
C
C
      SUBROUTINE RUK(XR,DT,N)
      IMPLICIT REAL*8 (A-H,O-Z)
      DOUBLE PRECISION DT
      DIMENSION XR(26),U1(26),F1(26),D1(26)
      COMMON/ARRAY1/SAAV(26,5R),SAAVJP(26),XSAAV(5),
     1 PSAAV(15),P(5,5)
      COMMON/ARRAY2/HR0W1(1,5),HR0W2(1,5),HR0W3(1,5),H(5),ST0(5),
     1 RK0PT(5,58),PPLUS(25),XMSAV(5)
      COMMON/ARRAY3/ERRX(5),ERRXM(5)
      COMMON/ARRAY4/F(5,5),FP(5,5),DDDT(5,5)
      COMMON/B1/X1,Y2,Z3,XP6,YP7,ZP8,RX,RY,RZ
      COMMON/C1/OMEGA,ELAT,DEG,GE,RE,PI,T,DELTAT,ICOUNT,IMAX,IUPDAT,NS
      COMMON/C2/IX,LIM
      CALL DIFFEQ(XR,D1,DT)
      DO 110 I=1,N
110   U1(I)=XR(I)+0.5D0*D1(I)
      CALL DIFFEQ(U1,F1,DT)
      DO 111 I=1,N
      D1(I)=D1(I)+2.DO*F1(I)
111   U1(I)=XR(I)+0.5D0*F1(I)
      CALL DIFFEQ(U1,F1,DT)
      DO 112 I=1,N
      D1(I)=D1(I)+2.DO*F1(I)
112   U1(I)=XR(I)+F1(I)
      CALL DIFFEQ(U1,F1,DT)
      DO 113 I=1,N
113   XR(I)=XR(I)+(D1(I)+F1(I))/6.DO
      RETURN
      END
```

```
C
C
C
C
C
      SUBROUTINE SORT(A,B,C,NRA,NCA,NRB,NCB,J,NNA,NNB,NNC)
      IMPLICIT REAL*8 (A-H,O-Z)
      DIMENSION A(NNA),B(NNB),C(NNC)
      COMMON/ARRAY1/SAAV(26,58),SAAVJP(26),XSAAV(5),
     1 PSAAV(15),P(5,5)
      COMMON/ARRAY2/HROW1(1,5),HROW2(1,5),HROW3(1,5),H(5),ST0(5),
     1 RKOPT(5,58),PPLUS(25),XMSAV(5)
      COMMON/ARRAY3/ERRX(5),ERRXM(5)
      COMMON/ARRAY4/F(5,5),FP(5,5),DDDT(5,5)
      COMMON/B1/X1,Y2,Z3,XP6,YP7,ZP8,RX,RY,RZ
      COMMON/C1/OMEGA,ELAT,DEG,GE,RE,PI,T,DELTAT,ICOUNT,IMAX,IUPDAT,NS
      COMMON/C2/IX,LIM
C
C  WHERE J=1 => C=AB
C        J=2 => C=ABT
C        J=3 => C=ATB
C
      GO TO (1,2,3),J
3     MA=NCA
      MB=NCB
      MC=NRA
      MD=1
      ME=1
      GO TO 16
2     MB=NRB
      MD=NRB
      GO TO 15
1     MB=NCB
      MD=1
15    MA=NRA
      MC=NCA
      ME=NRA
16    DO 20 I=1,MA
      NC=I-MA
      NB=0
      DO 20 K=1,MB
      NC=NC+MA
      C(NC)=0.DO
      NA=I-MA
      IF (J.EQ.3) NA=(I-1)*MC
      IF (J.EQ.2) NB=K-MB
      DO 20 L=1,MC
      NA=NA+ME
      NB=NB+MD
20    C(NC)=C(NC)+A(NA)*B(NB)
      RETURN
      END
```

```
C
C
C
C
C
      SUBROUTINE RANDU(IX,IY,YFL)
      REAL*8 YFL
      IY=IX*65539
      IF (IY) 5,6,6
5     IY=IY+2147483647+1
6     YFL=IY
      YFL=YFL*.4656613E-9
      RETURN
      END
```

```
C
C
C
C
C
      BLOCK DATA
      IMPLICIT REAL*8 (A-H,O-Z)
      COMMON/ARRAY1/SAAV(26,58),SAAVUP(26),XSAAV(5),
     1 PSAAV(15),P(5,5)
      COMMON/ARRAY2/HRAW1(1,5),HRAW2(1,5),HRAW3(1,5),H(5),STR(5),
     1 RKOPT(5,58),PPLUS(25),XMSAV(5)
      COMMON/ARRAY3/ERRX(5),ERRXM(5)
      COMMON/ARRAY4/F(5,5),FP(5,5),DQDT(5,5)
      COMMON/B1/X1,Y2,Z3,XP6,YP7,ZP8,RX,RY,RZ
      COMMON/C1/OMEGA,ELAT,DEG,GE,RE,PI,T,DELTAT,ICOUNT,IMAX,IUPDAT,NS
      COMMON/C2/IX,LIM
      DATA SAAV/1508*0.D0/,F/25*0.D0/,P/25*0.D0/,FP/25*0.D0/,
     1 DQDT/25*0.D0/,HRAW1/5*0.D0/,HRAW2/5*0.D0/,
     2 SAAVUP/26*0.D0/,XSAAV/5*0.D0/,PSAAV/15*0.D0/,PPLUS/25*0.D0/,ERRX/
     3 5*0.D0/,ERRXM/5*0.D0/,STR,RKOPT/5*0.D0,290*0.D0/,HRAW3/5*0.D0/
     4 ,XMSAV/5*1.D0/
      END
```

```
T=  0.0          SAAV INDEX=    1

 THE ACTUAL ERROR IN THE INERTIAL NAVIGATOR ,IE,THE PERTURBED STATE :
XP = 0.12530000000D 04  YP = 0.13170000000D 04  ZP = 0.15000000000D 04  VXP= 0.10000000000D 02  VZP= 0.10000000000D 02


 THE ESTIMATED INERTIAL NAVIGATOR ERROR (STATE) BEFORE A MEASUREMENT UPDATE :
XE = 0.0                YE = 0.0                ZE = 0.0                VXE= 0.0                VZE= 0.0


 THE ESTIMATED INERTIAL NAVIGATOR ERROR (STATE) AFTER A MEASUREMENT UPDATE :
XE = 0.73333814320 00   YE =-0.78222735270 01   ZE = 0.39111367640 04  VXE=-0.48889209550 02  VZE= 0.19555683820 03


 THE FILTER ERROR IN ESTIMATED STATE BEFORE THE MEASUREMENT UPDATE :
ERRX=-0.12530000000D 04  ERRY=-0.13170000000D 04  ERRZ=-0.15000000000D 04  ERRVX=-0.10000000000D 02  ERRVZ=-0.10000000000D 02


 THE FILTER ERROR IN ESTIMATED STATE  AFTER THE MEASUREMENT UPDATE :
ERRX=-0.19129585170 04  ERRY=-0.62391696690 03  ERRZ= 0.26546834280 04  ERRVX=-0.23016626270 03  ERRVZ= 0.90944589750 02


 THE ERROR COVARIANCE MATRIX BEFORE  A MEASUREMENT UPDATE :
P11 = 0.10000000000D 05  P12 = 0.0                P13 = 0.0                P14 = 0.0                P15 = 0.0
                         P22 = 0.10000000000D 05  P23 = 0.0                P24 = 0.0                P25 = 0.0
                                                  P33 = 0.10000000000D 05  P34 = 0.0                P35 = 0.0
                                                                           P44 = 0.10000000000D-04  P45 = 0.0
                                                                                                    P55 = 0.10000000000D-04


 THE ERROR COVARIANCE MATRIX AFTER  A MEASUREMENT UPDATE :
P11 = 0.34487915930 07  P12 = 0.14381265920 05  P13 = 0.79313489980 04  P14 = 0.22769536900 06  P15 = 0.56271127220 05
                        P22 = 0.34844420900 07  P23 =-0.71179462420 05  P24 = 0.29982354940 05  P25 =-0.11589637240 06
                                                P33 = 0.95744722220 06  P34 =-0.21299918720 06  P35 = 0.77714609890 05
                                                                        P44 = 0.22204382710 05  P45 = 0.30641289710 04
                                                                                                P55 = 0.92052020840 04


 THE OPTIMAL TIME-VARYING FILTER GAINS :
KX = 0.0                KY = 0.0                KZ = 0.0                KVX= 0.0                KVZ= 0.0
```

T= 0.1000D 02 SAAV INDEX= 51

THE ACTUAL ERROR IN THE INERTIAL NAVIGATOR ,IE,THE PERTURBED STATE :
XP = 0.3380966091D 04 YP =-0.3532110175D 03 ZP = 0.8851966261D 04 VXP=-0.5664438046D 03 VZP= 0.1577521346D 04

THE ESTIMATED INERTIAL NAVIGATOR ERROR (STATE)' BEFORE A MEASUREMENT UPDATE :
XE =-0.6851898282D 04 YE =-0.3070404599D 02 ZE = 0.1779542467D 05 VXE=-0.2273140683D 04 VZE= 0.1418906752D 03

THE ESTIMATED INERTIAL NAVIGATOR ERROR (STATE) AFTER A MEASUREMENT UPDATE :
XE =-0.1252128914D 05 YE =-0.4200922306D 02 ZE = 0.2299813915D 05 VXE=-0.3520608051D 04 VZE=-0.4559215935D 03

THE FILTER ERROR IN ESTIMATED STATE BEFORE THE MEASUREMENT UPDATE :
ERRX=-0.9932864372D 04 ERRY= 0.3225069715D 03 ERRZ= 0.8743458405D 04 ERRVX=-0.1706696878D 04 ERRVZ=-0.1435630670D 04

THE FILTER ERROR IN ESTIMATED STATE AFTER THE MEASUREMENT UPDATE :
ERRX=-0.1327047953D 05 ERRY= 0.1863770289D 03 ERRZ= 0.1193687003D 05 ERRVX=-0.2035936388D 04 ERRVZ=-0.1988705531D 04

THE ERROR COVARIANCE MATRIX BEFORE A MEASUREMENT UPDATE :

P11 = 0.6862836638D 08	P12 = 0.8196009130D 07	P13 = 0.1642075447D 08	P14 = 0.8153278014D 07	P15 = 0.1329333832D 08
	P22 = 0.1744225837D 08	P23 =-0.4935807795D 07	P24 = 0.3045803751D 07	P25 =-0.5060325005D 06
		P33 =-0.3439089428D 07	P34 =-0.8897505618D 07	P35 =-0.1057463327D 08
			P44 = 0.1381296131D 07	P45 = 0.1814763731D 07
				P55 = 0.1572826739D 07

THE ERROR COVARIANCE MATRIX AFTER A MEASUREMENT UPDATE :

P11 = 0.6850948425D 14	P12 = 0.2424841109D 15	P13 =-0.1211167846D 18	P14 = 0.2271011788D 16	P15 =-0.6055795873D 16
	P22 = 0.8621656922D 15	P23 =-0.4306374565D 18	P24 = 0.8074708558D 16	P25 =-0.2153171875D 17
		P33 = 0.2153187282D 21	P34 =-0.4037354277D 19	P35 = 0.1076585938D 20
			P44 = 0.7570039269D 17	P45 =-0.2018598633D 18
				P55 = 0.5382929688D 18

THE OPTIMAL TIME-VARYING FILTER GAINS :
KX =-0.4500000000D-03 KY =-0.1600000000D-02 KZ = 0.8000000000D 00 KVX=-0.1500000000D-01 KVZ= 0.4000000000D-01

REFERENCES

1. Broxmeyer, C., "Damping an Inertial System," ARS Guidance and Control Conference, Stanford University, Stanford, California, 7-9 August 1961.

2. Duncan, D. B., "Combined Doppler Radar and Inertial Navigation Systems," Proc. National Electronics Conference, Vol. 14, 1958.

3. Dworetsky, L. H., and Edwards, A., "Principles of Doppler-Inertial Guidance, ARS Journal, Vol. 29, No. 12, December 1959, pp. 967-972.

4. Friedman, A. L., "The Use of Speed and Position Fix Information in Inertial Navigators," ARS Guidance, Control, and Navigation Conference, Stanford University, Stanford, California, 7-9 August 1961.

5. Broxmeyer, C., Inertial Navigation Systems, McGraw-Hill Book Company, New York, 1964.

6. Sorenson, H. W., "Least-Squares Estimation: From Gauss to Kalman," IEEE Spectrum, July 1970.

7. Kalman, R. E., "A New Approach to Linear Filtering and Prediction Problems," Journal of Basic Engineering, Vol. 82D, 1960, pp. 35-45.

8. Kalman, R. E., and Bucy, R. S., "New Results in Linear Filtering and Prediction Theory," Journal of Basic Engineering, Vol. 83D, 1961, pp. 95-108.

9. Sutherland, A. F., Jr., and Gelb, A., Application of the Kalman Filter to Aided Inertial Systems, The Analytical Sciences Corporation, October 1967, Report No. TR-134-1.

10. O'Donnell, C. F., Editor, Inertial Navigation Analysis and Design, McGraw-Hill Book Company, New York, 1964.

11. Pitman, G. R., Editor, Inertial Guidance, John Wiley and Sons, Inc., New York, 1962.

12. Fernandez, M. and Macomber, G. R., Inertial Guidance Engineering, Prentice-Hall, Inc., Englewood Cliffs, New Jersey, 1962.

13. Markey, W. R., and Hovorka, J., The Mechanics of Inertial Position and Heading Indication, John Wiley and Sons, Inc., New York, 1961.

14. Lange, B., Inertial Guidance Systems, Stanford University, Stanford, California, Spring 1967 (Class notes in Course AA 272b).

15. Pinson, J. C., "Inertial Guidance for Cruise Vehicles," Guidance and Control of Aerospace Vehicles, Chapter 4, C. J. Leondes - Editor, McGraw-Hill Book Company, New York, 1963.

16. Brock, L. D., and Schmidt, G. T., "General Questions on Kalman Filtering in Navigation Systems," Theory and Applications of Kalman Filtering, C. T. Leondes - Editor, AGARD, No. 139, February 1970.

17. Martin-Marietta Corporation, Tactical PERSHING Accuracy Analysis, Report No. OR 9195-1, April 1968.

18. Wiley, C. A., "Airborne Radar Navigation," Avionics Navigation Systems, Chapter 8, M. Kayton and W. Fried - Editors, John Wiley and Sons, Inc., New York, 1969.

19. Stauffer, F., "Airborne Navigation and Ground Surveillance," Airborne Radar, Chapter 14, G. Merrill - Editor, D. Van Nostrand Company, Inc., New York, 1961 (In the series Principles of Guided Missile Design).

20. DeBra, D. B., Private Communication, July 1971.

21. Bryson, A. E., Jr., Optimal Estimation and Control Logic in the Presence of Noise, Stanford University, Stanford, California, Winter 1971 (Class notes in Course AM 235b).

22. Bryson, A. E., Jr., and Ho, Y. C., Applied Optimal Control, Blasdell Publishing Company, Waltham, Massachusetts, 1969.

23. Kaminsky, P. T., and Doerer, H. T., A Simplified Derivation and Engineering Application of the Kalman Predictor, Filter, and Smoother, Air Force Missile Development Center Working Paper, MDSC EP-69-2, November 1969.

24. Aoki, M., and Li, M. T., "Optimal Discrete-Time Control System with Cost for Observation," IEEE Transactions, Vol. AC 14, No. 2, April 1969.

25. Eppler, W., and Willstadter, R., "A Simulation of Map Correlation for Ballistic or Orbital Weapons Terminal Correction," Transactions of the Seventh Symposium on Ballistic Missile and Space Technology, Vol. II, U. S. Air Force Academy, Colorado Springs, Colorado, 13-16 August 1962.

26. Develet, J. A., Jr., "Performance of a Synthetic-Aperture Mapping Radar System, IEEE Transactions, Vol. ANE-11, No. 3, September 1964.

27. Diamantides, N. D., "Quantization, Statistics, and Matching of Maps and Pictures," IEEE Transactions, Vol. ANE-11, No. 3, September 1964.